NUREG/CR-6707
SAND2001/0022P

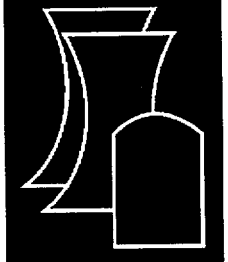

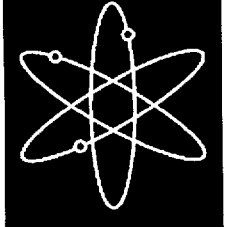

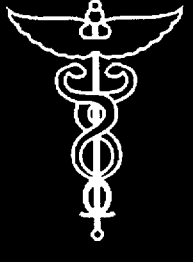

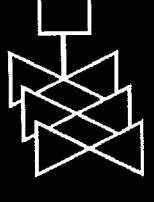

Seismic Analysis of a Reinforced Concrete Containment Vessel Model

Sandia National Laboratories

U.S. Nuclear Regulatory Commission
Office of Nuclear Regulatory Research
Washington, DC 20555-0001

AVAILABILITY OF REFERENCE MATERIALS IN NRC PUBLICATIONS

NRC Reference Material

As of November 1999, you may electronically access NUREG-series publications and other NRC records at NRC's Public Electronic Reading Room at www.nrc.gov/NRC/ADAMS/index.html.
Publicly released records include, to name a few, NUREG-series publications; *Federal Register* notices; applicant, licensee, and vendor documents and correspondence; NRC correspondence and internal memoranda; bulletins and information notices; inspection and investigative reports; licensee event reports; and Commission papers and their attachments.

NRC publications in the NUREG series, NRC regulations, and *Title 10, Energy*, in the Code of *Federal Regulations* may also be purchased from one of these two sources.

1. The Superintendent of Documents
   U.S. Government Printing Office
   Mail Stop SSOP
   Washington, DC 20402–0001
   Internet: bookstore.gpo.gov
   Telephone: 202-512-1800
   Fax: 202-512-2250
2. The National Technical Information Service
   Springfield, VA 22161–0002
   www.ntis.gov
   1–800–553–6847 or, locally, 703–605–6000

A single copy of each NRC draft report for comment is available free, to the extent of supply, upon written request as follows:

Address: Office of the Chief Information Officer,
Reproduction and Distribution
Services Section
U.S. Nuclear Regulatory Commission
Washington, DC 20555-0001
E-mail: DISTRIBUTION@nrc.gov
Facsimile: 301–415–2289

Some publications in the NUREG series that are posted at NRC's Web site address www.nrc.gov/NRC/NUREGS/indexnum.html are updated periodically and may differ from the last printed version. Although references to material found on a Web site bear the date the material was accessed, the material available on the date cited may subsequently be removed from the site.

Non-NRC Reference Material

Documents available from public and special technical libraries include all open literature items, such as books, journal articles, and transactions, *Federal Register* notices, Federal and State legislation, and congressional reports. Such documents as theses, dissertations, foreign reports and translations, and non-NRC conference proceedings may be purchased from their sponsoring organization.

Copies of industry codes and standards used in a substantive manner in the NRC regulatory process are maintained at—

The NRC Technical Library
Two White Flint North
11545 Rockville Pike
Rockville, MD 20852–2738

These standards are available in the library for reference use by the public. Codes and standards are usually copyrighted and may be purchased from the originating organization or, if they are American National Standards, from—

American National Standards Institute
11 West 42nd Street
New York, NY 10036–8002
www.ansi.org
212–642–4900

Legally binding regulatory requirements are stated only in laws; NRC regulations; licenses, including technical specifications; or orders, not in NUREG-series publications. The views expressed in contractor-prepared publications in this series are not necessarily those of the NRC.

The NUREG series comprises (1) technical and administrative reports and books prepared by the staff (NUREG–XXXX) or agency contractors (NUREG/CR–XXXX), (2) proceedings of conferences (NUREG/CP–XXXX), (3) reports resulting from international agreements (NUREG/IA–XXXX), (4) brochures (NUREG/BR–XXXX), and (5) compilations of legal decisions and orders of the Commission and Atomic and Safety Licensing Boards and of Directors' decisions under Section 2.206 of NRC's regulations (NUREG–0750).

NUREG/CR-6707
SAND2001/0022P

Seismic Analysis of a Reinforced Concrete Containment Vessel Model

Manuscript Completed: October 2000
Date Published: March 2001

Prepared by
J. L. Cherry/Sandia National Laboratories
R. J. James, L. Zhang, Y. R. Rashid/ANATECH Corporation

Sandia National Laboratories, Principal Contractor
P.O. Box 5800
Albuquerque, NM 87185-0744

ANATECH Corporation, Subcontractor
5435 Oberlin Drive
San Diego, CA 92121

A. J. Murphy, NRC Project Manager

Prepared for
Division of Engineering Technology
Office of Nuclear Regulatory Research
U.S. Nuclear Regulatory Commission
Washington, DC 20555-0001
NRC Job Code W6251

For sale by the Superintendent of Documents, U.S. Government Printing Office
Internet: bookstore.gpo.gov Phone: (202) 512-1800 Fax: (202) 512-2250
Mail: Stop SSOP, Washington, DC 20402-0001

ISBN 0-16-050775-8

Abstract

In a collaborative program between the United States Nuclear Regulatory Commission (NRC) and the Nuclear Power Engineering Corporation (NUPEC) of Japan, the seismic behavior of a scaled model Reinforced Concrete Containment Vessel (RCCV) has been investigated. Experimental and analytical work was performed at NUPEC under the sponsorship of the Ministry of International Trade and Industry; independent analytical work, sponsored by the NRC, was performed in the United States.

A 1:8 scale RCCV model was constructed by NUPEC and subjected to seismic simulation tests using the high-performance shaking table at the Tadotsu Engineering Laboratory. A series of tests representing design-level seismic ground motions was initially conducted. These were followed by a series of tests in which progressively larger base motions were applied until structural failure was induced.

As part of the collaborative program, Sandia National Laboratories and ANATECH Corp. conducted research in the seismic behavior of the scaled model RCCV structure. Three-dimensional finite element dynamic analyses were performed, first as pretest blind-predictions to evaluate the general capabilities of concrete-structures analytical methods, and second as posttest validation of the methods and interpretation of the test results. Because of the nonlinear behavior of the RCCV structures, even for design-level input motions, the analysis sequence must correspond to the test series. However, the large number of tests performed made such an endeavor very expensive to carry out, and it was necessary to be selective in the number and type of analyses to be performed. Moreover, the pretest analyses had, by necessity, to rely on proposed input motions, which differed significantly from their target form because of the interaction between the shake table and the structure that occurred during the actual tests. Consequently, the pretest analyses predict only general trends of the damage and failure regimes of the structure.

The RCCV analysis benefited considerably from the lessons learned in the course of the PCCV analysis (James et al., 1999a); however, the RCCV structural characteristics and test conditions introduced new behavior regimes that required additional concrete material-model improvements. These include the dependence of shear stiffness, compressive stiffness, and viscous damping on the number of crack-open-close cycles. These modeling improvements had their greatest effect on the failure-level predictions and showed the analysis results to be in reasonably good agreement with test data.

Contents

Figures

Figure **Page**

Tables

Table **Page**

Executive Summary

In a collaborative program between the United States Nuclear Regulatory Commission (NRC) and the Nuclear Power Engineering Corporation (NUPEC) of Japan, the seismic behavior of a Prestressed Concrete Containment Vessel (PCCV) model and a Reinforced Concrete Containment Vessel (RCCV) model is being investigated. The work performed at NUPEC is under the sponsorship of the Ministry of International Trade and Industry (MITI), while the work performed in the U.S. is sponsored by the NRC.

The NRC performance goals are to pursue risk-informed and performance-based approaches to reduce unnecessary regulatory burden and to enhance public confidence in the NRC's ability to protect public health and safety in a thorough, disciplined, and timely manner.

The NRC-sponsored program has been separated into three parts. The first part has been completed and is documented in James et al. (1999a), *Seismic Analysis of a Prestressed Concrete Containment Vessel Model.* It deals with the analysis of the scaled PCCV model and comparison of predictions to NUPEC's test results. The second part deals with the pre- and posttest analyses of the scaled RCCV model and comparisons to test data, which is presented in this report. The final part will be to evaluate a typical U.S. containment, based on what has been learned from the tests and analyses of the scaled models. Sample fragility curves will be developed for the typical U.S. containment.

NUPEC was responsible for the design (including scaling), fabrication, construction, seismic analysis, and dynamic testing of the RCCV model. The NRC collaboration with NUPEC provided independent pre- and posttest three-dimensional (3-D) finite element analysis of the RCCV model and evaluation of the test results.

The NRC's objective for this effort is to evaluate the maturity of analysis methods for predicting the time-dependent behavior of concrete containments subjected to design-level and failure-level earthquakes, and to identify needed improvements. Data was obtained for earthquake motions in the linear-response range and progressively stronger motions where significant structural damage began to accumulate up to major structural impairment and final failure. Test data were obtained for horizontal-only acceleration input, vertical-only acceleration input, simultaneous horizontal and vertical acceleration input, and simultaneous horizontal and vertical acceleration input with internal pressure.

As in the case of the PCCV, ANATECH Corp. was contracted by Sandia National Laboratories (SNL) to perform the seismic analyses of the RCCV. Both pretest and posttest 3D finite element dynamic analyses were performed. The pretest analyses relied on target seismic accelerations, while the posttest analyses used the measured accelerations at the basemat. The pretest predictions were documented in a report and released in draft form to NUPEC and the NRC before the tests were performed. The pretest results contained in the present report have been edited from the pretest draft report, but the technical content has not been changed.

In the design level tests that were analyzed, the measured input motions were similar to the target motions. However, for larger input motions, particularly horizontal-only motions where the vertical motion of the basemat was not controlled, the measured input motions were significantly different from the target motions. The pretest analyses assumed that vertical accelerations were zero at the basemat control points, while in the actual tests the model rocked and some of the vertical accelerations at these points were almost as large as the horizontal accelerations. Therefore, it was necessary to perform the posttest analyses with horizontal and vertical input accelerations, as measured by the accelerometers mounted on the basemat.

Seismic simulation testing of the RCCV scaled model was performed in 1998 and 1999 using the high-performance shaking table at the Tadotsu Engineering Laboratory. The posttest evaluations by NUPEC consist of evaluating the measured data for accelerations, displacements, and liner and rebar strains, as well as performing destructive examinations to evaluate concrete cracking, liner attachment integrity, and other forms of damage.

Frequency measurements performed after the first design-level horizontal-only seismic test showed a large drop in the fundamental frequency, which is indicative of significant stiffness degradation due to cracking. This behavior was not observed in the pretest analysis which used target input motion. However, it is easily explained by the fact

that the actual motion applied to the model was about 1.3 times higher than the target input. Moreover, the applied motion included vertical and rocking components that were of nearly equal magnitude to the horizontal. The actual time-history records of this test were not available for analytical simulation, but the damage was simulated through a pre-conditioning analysis which used recorded motion from a later dynamic test amplified by a factor similar to that recorded in the first test. The fundamental frequency is the structural response variable used in the preconditioning analysis to arrive at the appropriate level of damage.

The frequency degradation continued with each test performed, but at a decreasing rate, and appeared to reach a state of saturation after the 1.1S2(H+V) dynamic test. "Saturation" means that even increasing amplitude levels in subsequent dynamic tests did not significantly reduce the frequencies further. This is attributed to the extent of damage induced by the design level tests. This in turn reduces the structural amplification due to the frequency shift in subsequent tests under the same frequency content in the input. However, the functional integrity of the RCCV model was not impaired, as was verified by pressurizing the vessel to the design pressure and measuring the leak rate. One seismic test was conducted while the model was pressurized. Each of these tests confirmed that the liner maintained its leak-tightness during and after design-level earthquakes. The last pressure leak test was performed before the final seismic test that resulted in failure of the model. NUPEC's posttest evaluations indicate that, prior to the final (failure) test, the liner remained leak-tight, despite the appearance of a few distress locations showing localized buckling and striations induced by plastic flow. Liner rupture did not occur until the structural shear failure occurred during the final test in the series.

Time, schedule, and cost restricted the analyses to only a subset of the test series, which could not simulate the damage accumulation that occurred with each test performed. It was, therefore, necessary to insert pre-conditioning analyses before each design-level analysis in the sequence in order to simulate the prior damage that occurred. As mentioned earlier, comparison of the measured and calculated frequencies was used to measure the adequacy of prior damage simulation for the pre-conditioning analyses.

The lessons learned in the PCCV analysis effort, James et al. (1999a), were transferred to the RCCV analysis experience. These included the adoption of an improved shear-stiffness model for cracked concrete, the development of cracking-consistent damping, and the development of a shear failure criterion for the structure. The RCCV analysis effort produced new material modeling effects which, although observed in the RCCV to have strong effects for reinforced concrete, can be of generic nature to concrete structures in general. This structural behavior indicates that the compressive modulus normal to a crack surface, the local damping ratio, and the shear modulus tangential to the crack surface depend on the amplitude and number of crack open-close cycles. As discussed in the report, cycle-dependent degradation factors were developed for the aforementioned properties, which were applied in the constitutive model locally at the integration points. The input to these models is a single variable, which is the number of crack status reversals experienced by the material locally at the integration point. In addition, a criterion was developed that defines the amplitude of the crack open-close cycle before it can be counted as a loading cycle.

Intuitively, the cyclic dependence effect discussed above would be stronger in reinforced concrete than in prestressed concrete because of the larger crack width in reinforced concrete. It should be mentioned, however, that the relative magnitude of this effect should depend on the number and severity of the dynamic events. Consequently, it would impact the PCCV response later in the test sequence, as compared to RCCV where the effect is observed very early on. It should be of keen interest to examine this effect for the PCCV; however, schedule and budget constraints do not allow this evaluation to be performed and reported herein.

Another casualty of budget and schedule constraints is the use of the same fine-grid model of the RCCV throughout the analysis sequence. The pretest analysis series and the posttest design-level analyses were performed using a fine grid model discussed in Section 2, which consisted of two layers of elements through the thickness, 12 sectors around the circumference for the half symmetry model, and a highly refined grid around the major penetration. It was soon realized that the computation time needed to complete the entire posttest analysis sequence, including pre-conditioning analyses, would be prohibitively long. It was decided to abandon the fine-grid model, and a new model was developed that preserved the computational integrity of the structure and yet provided acceptable computation times. This coarse mesh model is described in Section 4. The newly developed analysis model was computationally optimized to preserve the dynamic characteristics, namely the mode shapes and frequencies, of the original model. It

is believed that the technical objectives of the analysis effort were not compromised by the switch to a coarser finite element model.

A very important observation is that direct extrapolation of the test results to assess the performance of any specific full scale U.S. containment cannot be attempted. There are many situations where the behavior of a full-scale structure will perform differently from the scaled test model, as discussed in Section 5.2. In addition, because of the sensitivity to frequency shift due to stiffness degradation exhibited by the test data, the performance of an RCCV is dependent on the past seismic history as well as the frequency content and magnitude of the specific seismic event. This is illustrated by the behavior the RCCV test model that survived a 5S2(H) test, but the accumulation of damage and associated fundamental frequency shift during the previous tests may have prevented a different outcome. It cannot be concluded that the model would survive a 5S2(H) as the first test, or that it could survive the 5S2(H) later with a slightly lower frequency content in the seismic input.

The RCCV testing program provided an opportunity to validate the previously developed structural shear-failure criterion for concrete structures subjected to severe motions, which was presented in James et al. (1999a). This criterion states that impending shear failure of the structure would occur at a shear strain value of 0.5%, with an uncertainty band of $\pm$ 0.05%, averaged over the entire cross-section of the structure. Shear failure occurred in the PCCV test when the average shear strain was about 0.45%, and one would expect that the corresponding value for the RCCV would be higher because of its larger reinforcement ratio. It should be noted that this criterion is a structural measure rather than a material property measure and, therefore, it can only be applied through the post-processing of the analysis results. The results for the RCCV posttest analysis indicate that the RCCV can withstand higher shear strains over a larger extent of the cross-section. This is attributed to the increased dowel action from the larger reinforcement ratio in an RCCV and to the reduced compressive loads relative to the PCCV. At failure level loads, the higher compressive loads will contribute to the initiation of concrete spalling and sudden brittle failure. However, this shear strain criterion indicates that, for all practical purposes, the RCCV was structurally compromised as a result of the 5S2 test, although the test results show that total failure occurred during the 9S2 test.

In general, the analysis results indicate reasonably good agreement between the calculated time histories and the measured data. Naturally, complete agreement is impossible, and the records show instances of poor agreement for some of the gauges and excellent agreement for others. Much better agreement was obtained for global measures of response rather than response measures that are directly affected by local concrete conditions. Considering the degree of details involved in the modeling and analysis of such complex tests, the level of agreement between the test data and the predictions indicates that existing analysis capabilities can be relied upon to predict the dynamic behavior of concrete containment structures. The tests and analytical predictions have provided better understanding of failure mechanisms of reactor containment structures under seismic loads, and moreover, improved the general state-of-the-art of concrete structural modeling.

It is believed that this analytical capability can be used to predict the seismic response of U.S. containment structures, and when used in conjunction with probabilistic methods, design uncertainties could be realistically accounted for by varying material properties, damping factors, ground accelerations, and other input parameters. This could provide important risk insights into the functional and structural integrity of U.S. containment vessels.

Acknowledgments

The test data in this report are provided by the Nuclear Power Engineering Corporation (NUPEC) and are based on reports to the Ministry of International Trade and Industry (MITI) of Japan. The Reinforced Concrete Containment Vessel tests were performed by NUPEC at Tadotsu Engineering Laboratory, located in Tadotsu, Japan. No modifications or changes were made to the recorded test results.

Information about the tests was provided by NUPEC, under an agreement between the U.S. Nuclear Regulatory Commission (NRC) and MITI. The terms and conditions of the technical exchange and general cooperation agreement between the NRC and the Agency of National Resources and Energy of MITI in the field of nuclear regulatory matters and nuclear safety research are given in the agreement "Collaboration on Concrete Containment Vessels (CCV) Seismic Proving Test Program and Information Exchange between USNRC and NUPEC."

The analyses described in this report were funded by the NRC. The authors gratefully acknowledge the efforts of Dr. Nilesh Chokshi, the NRC program manager, for the development and stewardship of the project and the valuable technical guidance he provided throughout its stages.

Sandia National Laboratories is operated for the United States Department of Energy under Contract DE-AC04-94AL85000. The results and conclusions described herein are based on analytical predictions performed at ANATECH Corp. and do not necessarily reflect the opinions of the NRC or NUPEC.

Acronyms and Initialisms

3-D	three-dimensional
CCV	Concrete Containment Vessels
LOCA	Loss of Coolant Accident
MITI	Ministry of International Trade and Industry
NRC	United States Nuclear Regulatory Commission
NUPEC	Nuclear Power Engineering Corporation
OBE	Operating Basis Earthquake
PCCV	Prestressed Concrete Containment Vessel
RCCV	Reinforced Concrete Containment Vessel
SNL	Sandia National Laboratories
SSE	Safe Shutdown Earthquake

1. INTRODUCTION

1.1 Summary

In a collaborative program between the U.S. Nuclear Regulatory Commission (NRC) and the Nuclear Power Engineering Corporation (NUPEC) of Japan under sponsorship of the Ministry of International Trade and Industry (MITI), the seismic behavior of a Reinforced Concrete Containment Vessel (RCCV) model was investigated. The scaled model was constructed by NUPEC and subjected to seismic simulation tests using the high-performance shake table at the Tadotsu Engineering Laboratory (Sasaki et al., 1998).

The primary objective of the testing program was to demonstrate the capability of the RCCV to withstand the design-basis earthquake with a significant safety margin against major damage or failure and to verify the functional integrity and leak-tightness of the vessel.

The scaled model was designed to be representative of an actual structure while meeting the limitations of the test equipment and the requirements needed for fabrication. Acceleration time histories of the base motion were developed for typical design-level earthquakes at locations of containment structures in Japan. These motions were scaled so that the fundamental frequency and the shear stresses in the wall near the basemat of the scaled model would be similar to that in an actual containment structure.

The scaled test model was first subjected to a series of low amplitude motions to determine fundamental frequencies and the characteristics of the test model and shake table. The response of the model to a design-basis earthquake was then evaluated by first conducting tests using the individual horizontal and vertical components followed by tests using combined horizontal and vertical components.

A Loss of Coolant Accident (LOCA), in combination with an operating basis event, was simulated by pressurizing the test model during a seismic simulation. Several sequential tests of the maximum level and extreme level design earthquakes, designated as S1 and S2 respectively, were also conducted. The margin of safety for the scaled test model was then determined by subjecting the model to larger and larger amplitude seismic accelerations until structural failure occurred. The test program also measured the fundamental frequencies of the test model after each test as a measure of the damage sustained by the model.

The S1 level event is equivalent to the maximum design earthquake used in Japan, and level S2 corresponds to the extreme design earthquake. The relative magnitudes of S1 and S2 earthquakes, as compared to the Operating Basis Earthquake (OBE) and the Safe Shutdown Earthquake (SSE) used in the United States, are shown in Figure 1.1.

1.2 Objectives and Scope

As part of the collaborative program with NUPEC, the NRC, through Sandia National Laboratories (SNL) and ANATECH Corp., conducted research in the analytical modeling of the seismic behavior of RCCV structures. The objective of this research was to evaluate the predictive capabilities of current analytical methods, with the eventual goal of improving these capabilities for containment performance evaluation under seismic events.

The scope of this work consisted of pretest predictions and posttest verification analyses of the NUPEC RCCV tests. These included a series of calculations under simulated design-level input motions followed by calculations under amplified motions that eventually led to the failure of the test model.

At the conclusion of the test program, the records of test data, which included shake table input and response data, were used to perform posttest analyses of the test model. The posttest calculations quantify the behavior of the structure under the actual test conditions. The analyses were conducted sequentially to simulate the sequence of the tests and allow cumulative damage to develop. However, all tests were not analyzed, and only a subset of the actual tests was selected for the analytical evaluations. For pretest calculations, this subset of the tests was chosen a priori as that most likely to cause or extend the damage. The tests selected for the posttest calculations were judged to be the most significant.

1.3 Scaling Issues

The scale of the model was selected by NUPEC, with careful attention given to construction and fabrication issues, as well as limitations of the shake table. If the size of the model is too small, it becomes very difficult to construct. However, the size cannot be too large, or the shake table will not have enough capacity to input the desired motions. Based on these limitations, the overall configuration was scaled at 1:8, the concrete

wall thickness was at 1:10 scale, and the steel liner and anchorage system was scaled at 1:4. The concrete wall thickness scale was selected to allow all the reinforcing bars to fit and to fail, while the scale of the liner was selected based on weldability issues. The top portion of an actual RCCV structure was replaced with a thick, flat concrete cap. Weights were attached to the top portion of the model to match the fundamental frequency and shear stresses in the wall near the basemat to that of a prototype structure.

In performing a seismic test on a scaled model, mass does not scale proportionately with geometry. To have similar magnitudes of displacement, stresses, and strains in the scaled model as would exist in a full-scale containment, either of the two similarity laws shown in Table 1.1 could be used. For the RCCV model, NUPEC used scaling rules that are similar to the Froude law shown in the table. NUPEC's calculations show that the RCCV model scaling parameters, shown in Table 1.1, result in stresses and strains in the cylinder wall near the basemat that are similar to the stresses and strains that would exist in a full-scale vessel.

In a full-scale vessel, the largest shear stresses would be expected in the wall near the basemat, with the shear stresses at higher elevations decreasing in proportion to the total mass above a plane passing through the elevation point. Because of differences in the mass distribution between the scaled model and a full-scale vessel, the shear stresses above the wall-basemat juncture would be different in the model than in a full-scale vessel.

The results of a scaled model test, especially a dynamic test for which mass does not scale, must be very carefully reviewed to determine expected similarities and differences between the structural response of the scaled model and a full-scale containment. No attempt is made in this report to predict the functional integrity, structural integrity, or seismic margin of a full-scale U.S. containment based on the scaled-model tests. However, some useful insights and general conclusions are made at the end of the report.

1.4 RCCV Test Model

In an actual nuclear plant, the reactor vessel and concrete containment structure is a continuous part of the reactor building. Intermediate floors that support auxiliary equipment needed to operate the plant are constructed as an integral part of the RCCV walls.

Figure 1.2 shows a schematic of the RCCV test model. In the model, a section of the reactor building containing the RCCV containment and intermediate floors was isolated from the rest of the building. The isolated structure was scaled to fit within the capacity of the shake table while retaining enough size for fabrication. Figure 1.2, taken from reference 2, shows a schematic of the RCCV test model. The model is a 200 mm thick by 2.410 m tall reinforced concrete cylinder with an inside diameter of 3.625 m that is built-in on a 1 m thick concrete basemat. The basemat is 9m square and is anchored to the shake table with a pattern of bolt groups, 4 bolts per group. The access tunnel is modeled with 538 mm diameter penetrations through the RCCV wall along a diametric line that is 90° from the axis of the horizontal shaking direction. Two intermediate floors, each 130 mm thick, frame into the cylindrical wall creating roughly three equal segments along the height of the wall. The access tunnel penetrations occur at the top of the first intermediate floor in the middle section of the wall. The floors are modeled horizontally for a distance of 1 m away from the wall so that the outer diameter of the floors is 6.025 m. The top of the RCCV test model consists of a 550-mm thick by 6.025-m diameter section with an 800 mm diameter penetration at the centerline. A 400-mm thick by 1.250-m high circular wall is built-in to the top of this section to support added weights. The weights are added to achieve a fundamental frequency of vibration consistent with the scaling to the actual structure. The basemat weighs 213 metric tons, the cylindrical section with intermediate floors and top section weighs 76 metric tons, and the attached mass weighs 276 metric tons. A steel liner, 1.6 mm thick, is anchored to the inside of the RCCV cylinder with longitudinal T stiffeners embedded in the concrete. The overall geometry of the test model is 1:8 scale, while the concrete wall thickness is scaled at 1:10 and the liner thickness is scaled at 1:4. The design operating pressure for a full-scale RCCV is 3.16 kg/cm^2 (45 psi), and is 2.34 kg/cm^2 (33 psi) for the scaled model.

Many seismic tests were performed on the scaled model, as shown in Table 1.2. Numerous low-level vibration tests were performed to determine resonant frequencies and other basic characteristics; these low-level tests are not shown in Table 1.2. In addition, NUPEC performed leak checks after many of the major tests by pressurizing the vessel to its design-level and measuring for leaks; these leak tests are not shown in Table 1.2, either. Because of the number of tests performed, analyses were only performed on a limited subset of the tests, as shown in Table 1.2.

The model was instrumented with 49 acceleration gauges, 23 displacement gauges, a pressure gauge, and 228 strain gauges (on the liner and reinforcing bars). Some of the strain gauges were in one direction only, some were placed in pairs with relative orientation of 90° and some gauge rosettes were oriented at 0, 45, and 90°. Other gauges were also recorded that were used by the control system, such as pressure gauges in the hydraulic actuators or acceleration control gauges. During each seismic simulation test, data were collected at 0.0025-second intervals for all of the tests.

Table 1.1. Similarity law parameters

Parameter	Full-Scale Vessel	Froude Similarity Law	Cauchy Similarity Law	RCCV Model (Similar to Froude)
Length	1	1:n	1:n	Mixed Scale (1:8 Geometry; 1:10 Concrete Wall Thickness; 1:4 Liner Plate Thickness)
Mass density	1	n	1	Lead Weights Added - 276 tonnes (Roughly Equivalent to Increasing Density by a Factor of 8)
Acceleration	1	1	n	1
Stress, Strain, Modulus	1	1	1	1 in Wall Section near Basemat; About 2 near Top of Wall Section
Time	1	$1/(n)^{0.5}$	1/n	$1/(8)^{0.5} = 1/2.83$
Frequency	1	$(n)^{0.5}$	n	$(8)^{0.5} = 2.83$

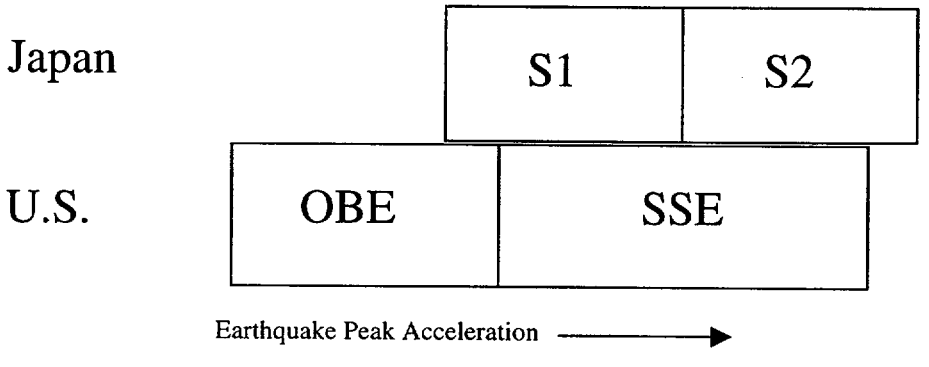

S1/S2: Maximum/Extreme Design Earthquakes (Japan)
OBE/SSE: Operating Basis/Safe-Shutdown Earthquakes (U.S.)

Figure 1.1. Comparison of design earthquakes between U.S. and Japan

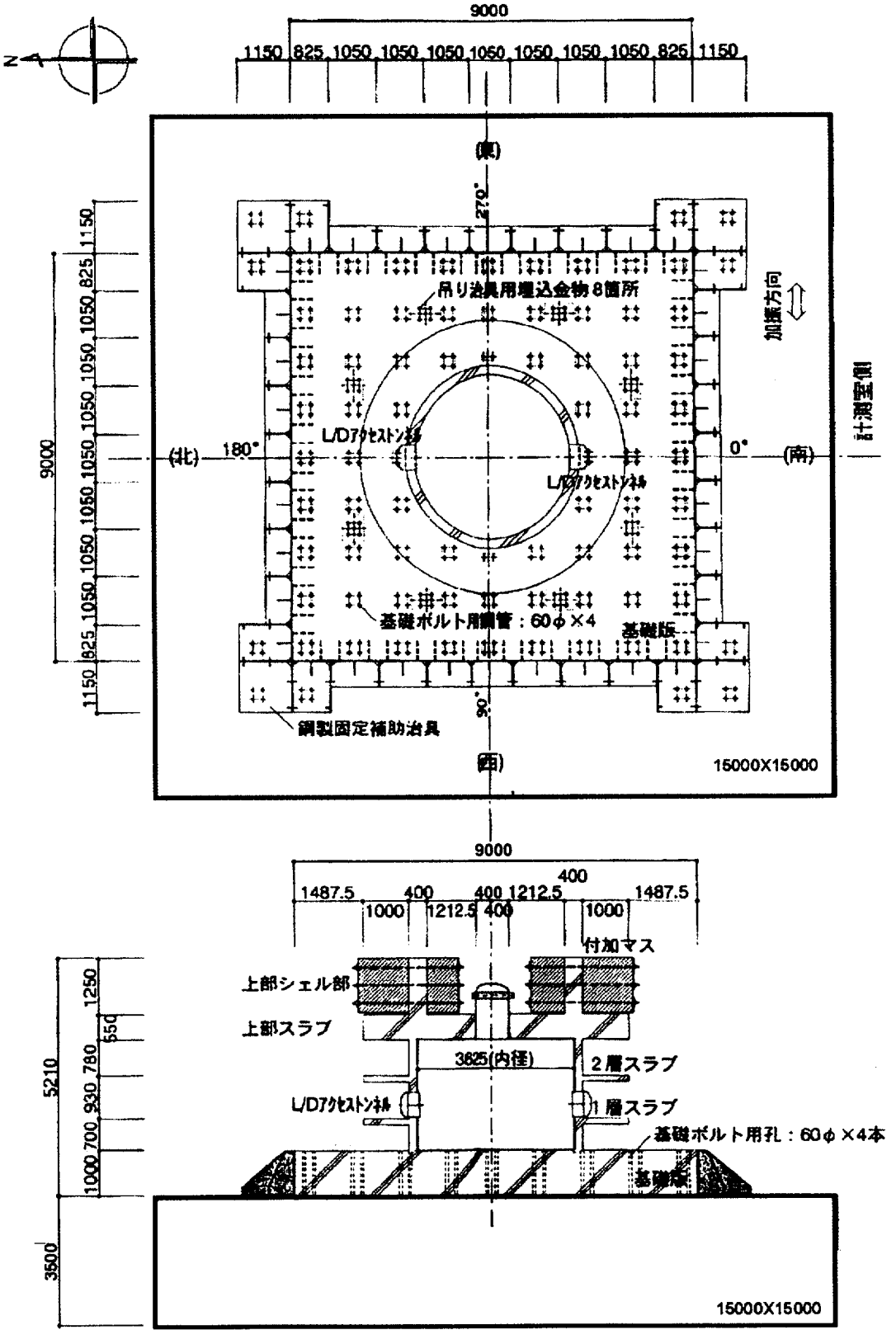

Figure 1.2 Schematic for RCCV test model

Table 1.2. NUPEC test and U.S. analysis sequence

Test Sequence	Pretest Analysis	Posttest Analysis
Pressure Test		*
1.3S1(H)		
1.1S1(H)		
1.1S1(V)		
1.15S1(H+V)		
1.1S1(H+V)	*	*
1.1S2(H)		
1.1S2(V)		
1.1S2(H+V)	*	*
1.2S1(H+V) + LOCA		
2S2(H)	*	*
3S2(H)		*
4S2(H)	*	*
5S2(H)		*
9S2(H)		

2. NUMERICAL MODELING

2.1 Background

The calculations were performed using the ANATECH concrete material model[ab] coupled to the ABAQUS[c] general purpose finite element program (Hibbit et al., 1997). To predict damage that may accumulate in the series of seismic tests planned for the CCV test model, the material model must account for the history dependence of cracking and for the strength and stiffness degradation under cyclic loading. This requires the time-marching, nonlinear dynamic analyses to be performed in series to simulate the sequence of tests to be conducted. Because of the large storage and run times required, care was taken to ensure that the number of degrees of freedom in the finite element model was small enough for efficient calculations while adequately capturing the critical response of the test specimen. Figures 2.1 through 2.9 illustrate the baseline finite element model used in the pretest calculations. As discussed in Section 4, a reduced model was used for the posttest analyses to reduce the analysis time. The following section discusses modeling assumptions relative to this model, and a subsequent section describes the method used to establish the mesh density.

2.2 Modeling Assumptions

2.2.1 Basemat

Both pretest and posttest calculations are based on the assumption that the basemat responds as a rigid unit. The pretest analyses assume that the actual acceleration experienced by the basemat will be the target input acceleration history. The posttest analyses used the accelerations actually measured during the test by acceleration gauges. Only a ring section of the basemat around the wall junction is modeled, as shown in Figures 2.1 and 2.2, with boundary conditions imposed on the bottom and the vertical cuts of the basemat. The posttest reduced model applied boundary conditions at the same locations.

For the dynamic calculations, identical acceleration histories are prescribed for all the nodes of these boundaries. The basemat ring is modeled to approximate the area from the wall junction to the first set of bolts that secure the basemat to the shake table. The width of the ring is about 2.5 times the thickness of the wall on either side of the wall. The justification for this assumption is that the basemat is securely bolted to the shake table and that the control points for the target input acceleration are on top of the basemat.

2.2.2 Symmetry

The next assumption is that the geometry of the test specimen is symmetric about a vertical plane that bisects the structure. The pretest analysis model retained the half of the vessel containing the equipment hatch penetration. This is a large penetration that is supported with a thickened section of the RCCV wall and has a thicker liner and additional reinforcement. A 180°, 3-D model of this half of the RCCV is used. This choice of analysis model implies that another equipment hatch penetration exists at a diametrically opposite location. The posttest analysis model did not include the equipment hatch. Experience with the PCCV testing and analysis (James et al., 1999a) indicates that ignoring the dissymmetry has a small effect on the calculated response. This is also confirmed by the test data, which shows largely symmetric deformations.

The analytical consequence of this symmetry assumption is that the symmetry plane will prevent any global twisting deformation that could develop in the test specimen since the actual geometry is not symmetric. Also, any rocking that may develop perpendicular to the direction of shaking is prevented by the symmetry plane. The thickened wall and added reinforcement at the equipment hatch penetration will cause a hard spot in the RCCV wall that is likely to induce local hoop bending in the wall. This local bending can contribute to a failure in the test specimen, and this response is included in the pretest model, but not in the posttest model.

---

[a] James, R. J. and R. S. Dunham, ANACAP-U, ANATECH Concrete Analysis Package, Version 2.5, User's Manual, Revision 4, *ANATECH* Corp. San Diego, 1997.

[b] James, R. J., R. S. Dunham, R. A. Dameron, and D. R. Parker, ANACAP-U, ANATECH Concrete Analysis Package, Version 2.5, Verification and Validation Manual Revision 1, *ANATECH* Report ANA-QA-144, 1998a.

[c] ABAQUS is a trademark of Hibbitt, Karlsson & Sorensen, Inc., of Pawtucket, RI.

2.2.3 Liner

The RCCV liner (Figure 2.3) is modeled as fully bonded to the concrete with no local effects of anchorage discontinuities. The liner elements are thus strain compatible with the concrete and will reflect local effects of concrete damage. Liner plasticity is included in the analysis. To reduce the time required to complete a seismic analysis, the bending component of the liner is ignored and the liner is modeled with plane stress membrane-type elements. The only liner differences between the pretest analysis model and the posttest analysis model is that the elements are bigger in the posttest version.

2.2.4 Reinforcing Bars

Reinforcing bars are explicitly modeled with truss-type subelements embedded in the concrete continuum elements at the appropriate locations in space. Figures 2.4 and 2.5 show the pretest modeling for the axial and hoop reinforcement in the RCCV wall. Figures 2.6 and 2.7 illustrate the reinforcement in the floors and top section. Figures 2.8 and 2.9 show stirrups and miscellaneous reinforcing bars, such as the extra reinforcing around the penetration. Figures 2.4 through 2.9 show the reinforcing bar placement in the pretest analysis model. Although not shown, the posttest analysis model included the same reinforcing bars, with the exception of details around the equipment hatch that were not included in the reduced model. The bar stiffness and force are superimposed on the concrete element, and thus the effect of the bars is smeared over the element through the continuum element shape functions.

The effects of rebar yield and plastic strain hardening are included in both models. The rebars are assumed to be fully bonded to the concrete. For these analyses, no bond slip or anchorage loss was included. These effects can be important at the point of failure and may govern the local failure mechanism. For example, when spalling occurs, the exposed rebars lose confinement and may buckle under compression or be ineffective in tension. At the point of total failure, the concrete spalls, rubblizes, and separates from the rebar, which is not predicted by the analysis models.

2.2.5 Other Structural Elements

Truss elements are used to model the bolts that attach the weights to the top section. These elements are pretensioned and add prestress to the top section. Both the baseline and the reduced models assume that the top section and all attached masses of the test specimen remain elastic. No effects from cracking or compressive yield of the concrete in this top section were included in the calculations. The intent of the modeling in this region was to adequately represent the stiffness and the distribution of mass. The attached masses are modeled with lead material encased in steel shells (as constructed) to capture the distribution of inertial loads and the rocking that develops.

2.3 Finite Element Mesh

The baseline finite element model was developed to minimize the computational effort while adequately capturing the critical response of interest. The method used for this mesh optimization was first to build a refined model and establish mode shapes, frequencies, and the static pushover capacity. The mesh was then optimized by comparing the mode shapes, frequencies, and static pushover capacity of reduced degree-of-freedom models with those of the refined model. The number of degrees of freedom was optimized by eliminating much of the basemat, reducing the number of elements through the wall thickness, along the length and circumference in the RCCV, and eliminating bending degrees of freedom in the liner and plates. Based on past experience with similar calculations, the baseline model used in the pretest analyses is considered adequate to capture the shear capacity at the wall-basemat junction.

For the posttest analysis model, the baseline model was reduced even further, and this model is referred to as the reduced model throughout this report.

2.4 Material Models

The material model used for the concrete in the RCCV wall and basemat was the ANATECH concrete material model, which is a modern version of the classic smeared cracking model (Rashid, 1968). The behavior of this model is summarized in Appendix A of James et al. (1999a). The material properties used in the pretest and posttest models for this concrete are given in Tables 2.1a and 2.1b. These properties varied somewhat from the measured strength values shown in Table 2.1c.

Based on Raphael's formula (Raphael, 1984), $\sigma_t = 1.7 f_c^{2/3}$ (in units of psi), the material is assumed to have a tensile strength between 35 kg/cm^2 (510 psi) and 40 kg/cm^2 (580 psi) for the pretest

Table 2.1a. Concrete material properties used in pretest analyses

Location	Comp Strength, f_c' kg/cm^2 (psi)	Modulus kg/cm^2 (psi)	Fracture Strain ($\times 10^{-6}$)
Basemat	442 (6287)	2.90×10^5 (4.22×10^6)	191.4
1st Layer Shell	390 (5553)	2.73×10^5 (3.96×10^6)	187.5
1st Floor Slab	434 (6170)	2.88×10^5 (4.18×10^6)	190.8
2nd Layer Shell	366 (5203)	2.64×10^5 (3.83×10^6)	185.5
2nd Flood Slab	374 (5320)	2.67×10^5 (3.88×10^6)	186.1
3rd Layer Shell	368 (5236)	2.65×10^5 (3.85×10^6)	185.7
Upper Slab	388 (5520)	2.72×10^5 (3.95×10^6)	187.3
Upper Shell	388 (5520)	2.72×10^5 (3.95×10^6)	187.3

Table 2.1b. Concrete material properties used in posttest analyses

Location	Comp Strength, f_c' kg/cm^2 (psi)	Modulus kg/cm^2 (psi)	Static Fracture Strain ($\times 10^{-6}$)	Dynamic Fracture Strain ($\times 10^{-6}$)
Basemat	377 (5467)	$2.37\text{x}10^5$ (3.37×10^6)	80	122.4
1st Layer Shell	333 (4829)	$2.23\text{x}10^5$ (3.17×10^6)	80	122.4
1st Floor Slab	370 (5365)	$2.35\text{x}10^5$ (3.34×10^6)	80	122.4
2nd Layer Shell	312 (4524)	$2.16\text{x}10^5$ (3.07×10^6)	80	122.4
2nd Flood Slab	319 (4626)	$2.18\text{x}10^5$ (3.10×10^6)	80	122.4
3rd Layer Shell	314 (4553)	$2.17\text{x}10^5$ (3.09×10^6)	80	122.4
Upper Slab	331 (4800)	$2.22\text{x}10^5$ (3.16×10^6)	80	122.4
Upper Shell	331 (4800)	$2.22\text{x}10^5$ (3.16×10^6)	--	--

Table 2.1c. Actual concrete material properties at time of first test

Location	Comp Strength, f_c' kg/cm^2 (psi)
Basemat	440 (6250)
1st Layer Shell	361 (5133)
1st Floor Slab	395 (5612)
2nd Layer Shell	322 (4582)
2nd Flood Slab	351 (4988)
3rd Layer Shell	299 (4249)
Upper Slab	301 (4278)
Upper Shell	308 (4379)

Table 2.2. Material properties of rebar and liner used in analyses

Property	Rebar*	Liner*	Bolting*
Modulus kg/cm^2 (psi)	2.0E6 (2.9E7)	2.31E6 (3.35E7)	2.1E6 (3.0E7)
Poisson's Ratio	--	0.3	0.3
Weight Density kg/cm^3 (#/in^3)	--	7.86E-3 (0.284)	--

* See Figures 2.10 and 2.11

Table 2.3. Elastic material properties used in analyses

Property	Concrete	Weights
Modulus	--	1.41E5 kg/cm^2 (2.0E6 psi)
Poisson's Ratio	0.17	0.40
Weight Density	0.0024 kg/cm^3 (150 lb/ft^3)	

analyses and 32 kg/cm^2 (470 psi) and 36 kg/cm^2 (530 psi) for the posttest analyses. Under uniaxial compression, the model assumes that the material will reach its maximum compressive strength at 2300e-6 strain and begin softening under additional strain.

The concrete material characterization described in Appendix A of James et al. (1999a) has had extensive application and verification over the years on many types of reinforced and prestressed concrete structures. However, dynamic, cyclic calculations for shear dominated loads is a relatively uncharted area.

The pretest calculations were based on the shear model used in the PCCV analyses (James et al., 1999a). However, for the RCCV posttest analyses, the shear model was modified as discussed in Section 4.

The steel material models for the reinforcing bars, tendons, and liner are based on classical von Mises plasticity. The respective stress-strain relationships determined from NUPEC test data and used in the analyses are shown in Figures 2.10 and 2.11. The steel elastic properties used in the analyses are shown in Table 2.2.

For the top section, an elastic concrete material is used, and the attached masses are modeled with lead material encased in steel shells, both linear elastic. Since the exact volume of the attached weights is not modeled, the weight density of this material is adjusted to give the correct mass. These properties, which are used for both pretest and posttest analyses, are summarized in Table 2.3.

2.5 Loading and Analysis Procedure

The RCCV test model was subjected to various levels of acceleration input in the horizontal and vertical directions. The target input acceleration histories used for all pretest analyses for level S1 are reproduced in Figure 2.12, and those for level S2 are reproduced in Figure 2.13. NUPEC scaled these S1 and S2 earthquakes from seismic design criteria for full-scale vessels. The scaling rules used are shown in Table 1.1.

For the margin, the magnitude of the S2 acceleration was multiplied by a constant, such as 2 in an 2S2 test, or 3 in an 3S2 test.

The S1 input is larger than an operating basis earthquake and is similar to a safe shutdown earthquake, which is used in the United States. The target S1 input is digitized every 0.003536 seconds for a duration of 19.22 seconds and has a peak acceleration of 0.29 g (286 cm/sec^2) horizontally and 0.146g (143 cm/sec^2).

The S2 level target input acceleration history is digitized every 0.007071 seconds for a duration of 42.42 seconds. The peak accelerations for the S2 target input is 0.42g (407 cm/sec^2) horizontally and 0.21g (204 cm/sec^2) vertically.

All pretest analyses were performed using a constant step size of 0.007071 seconds. This step size was selected based on experience with the PCCV analysis, where it was shown that the difference between the 0.008 second step and a 0.004 second step in the energy content of the input record is 5.9% and 4% for the horizontal and the vertical components, respectively. Thus, using input records digitized with half as many points loses about 5% of the input energy but reduces execution time in half. The solution is marched in time using the Hilber-Hughes integration operator with equilibrium iteration as needed for each time step.

The posttest analyses did not use the S1 or S2 target accelerations to define the input motion, but rather used measured accelerations at the basemat. There were some significant differences between planned target input accelerations and the acceleration values that actually occurred at the basemat of the model. Therefore, the posttest analyses used the actual values. Test data were recorded at 0.0025-second intervals. The posttest analyses used a 0.005-second time step for all the analyses. The crack-consistent damping model was used in the pretest and posttest analyses. This model uses a variable damping ratio that is set internally by the model as function of the crack status. The range of variability was defined through input to be between 1% and 4%. In this way, the amount of damping that gets applied varies with time, from point to point in the structure, and can be different in different directions.

For evaluation of the analytical simulations, the calculated accelerations at points on the top mass are plotted for comparison with similar points measured in the tests. Calculated rebar and liner strain histories are also plotted at various locations in the analysis model for comparison to test data at similar locations on the test model. Figure 2.14 shows the locations used on the analysis model for comparison with measured test data.

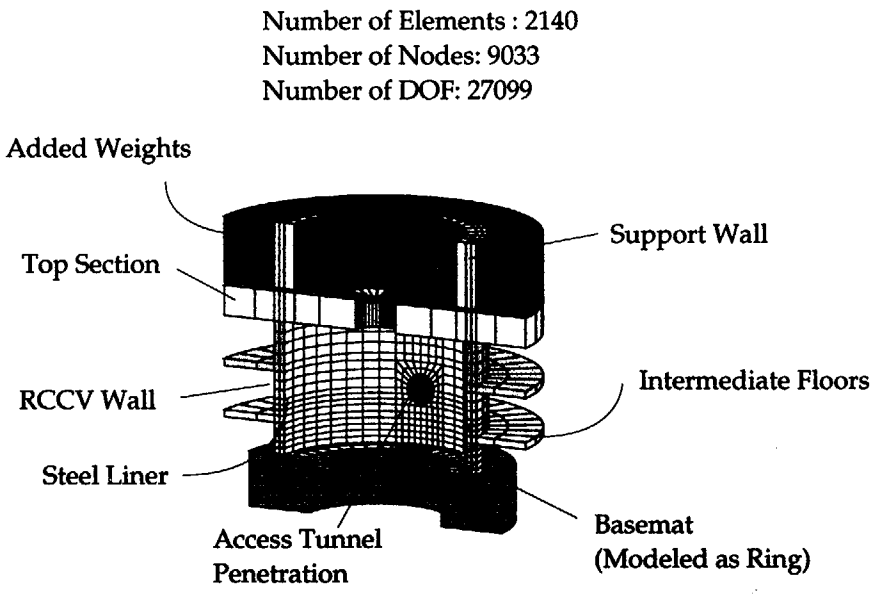

Figure 2.1 Finite element model of RCCV

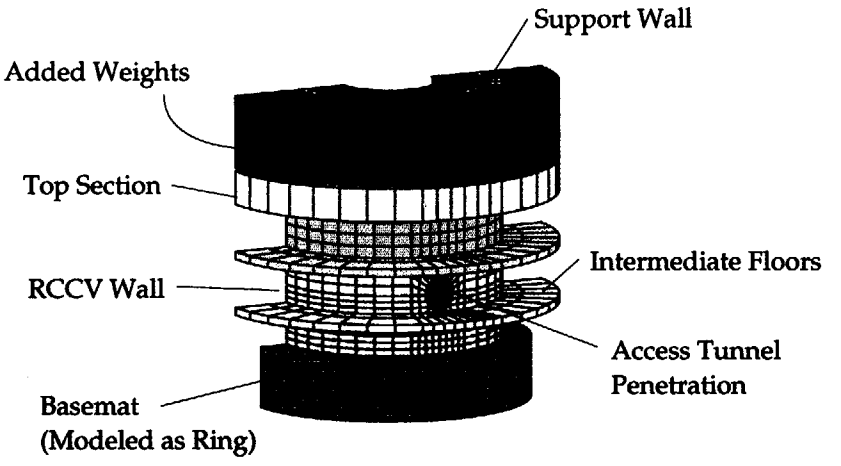

Figure 2.2 Finite element model of RCCV, outside view

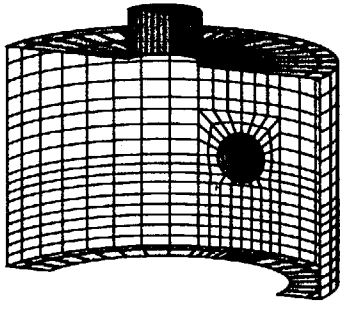

Figure 2.3 Plate elements for liner and access cover modeling

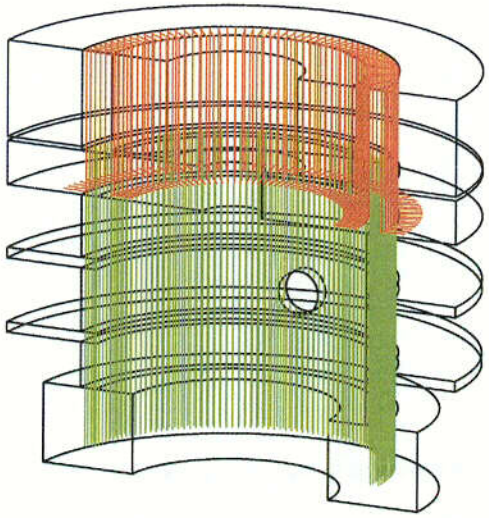

Figure 2.4 Axial rebars in RCCV model

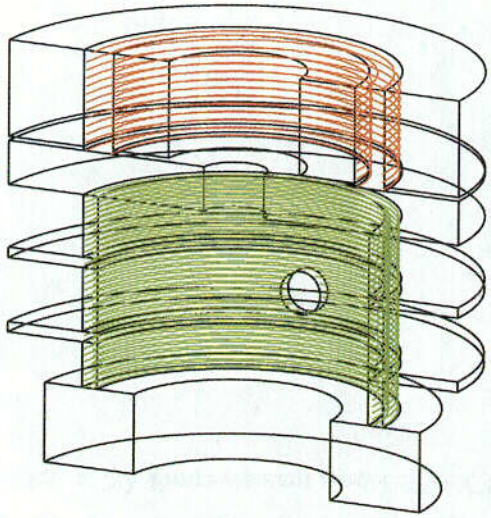

Figure 2.5 Hoop rebars in RCCV model

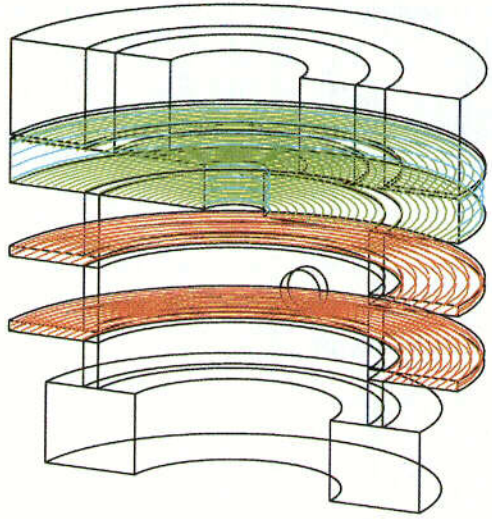

Figure 2.6 Hoop rebars in foor slabs and top section

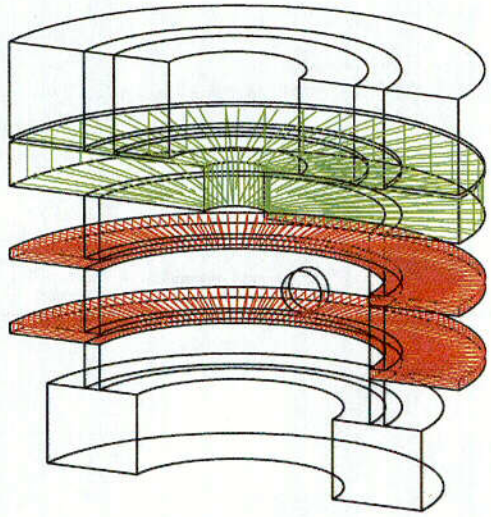

Figure 2.7 Radial rebars in floor slabs and top section

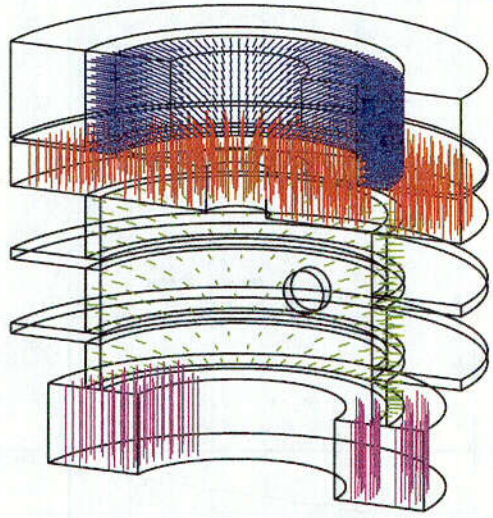

Figure 2.8 Stirrup bars in RCCV model

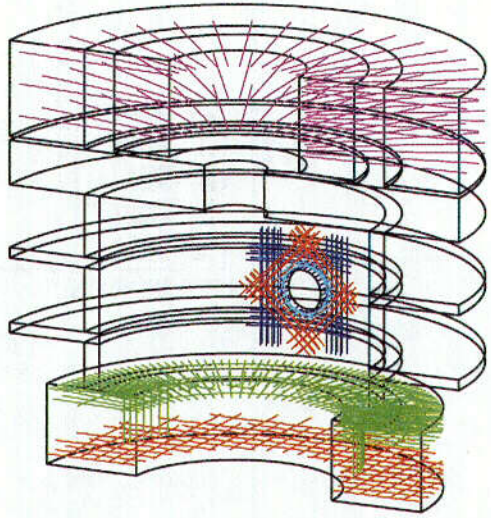

Figure 2.9 Miscellaneous rebars and PC steel bars in RCCV model

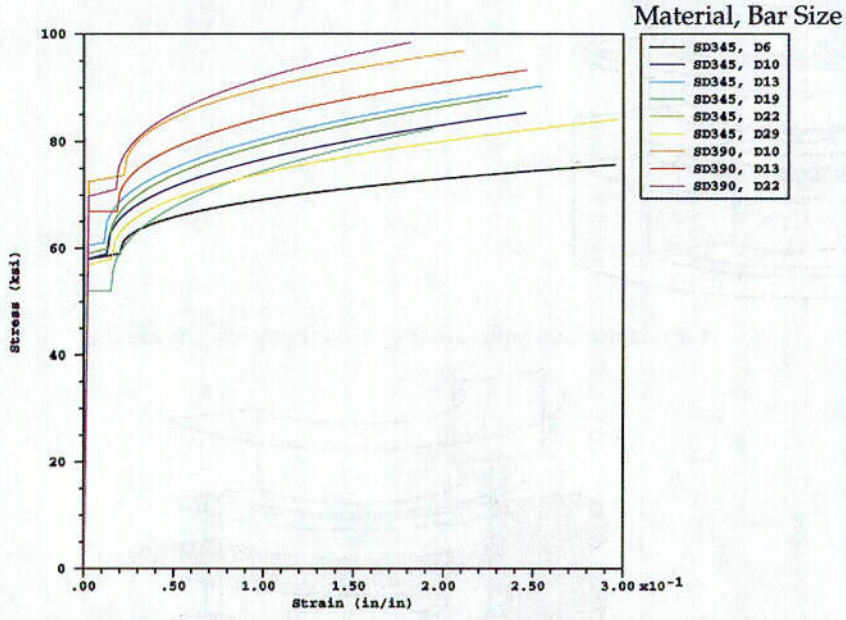

Figure 2.10 Stress-strain relations for rebar material

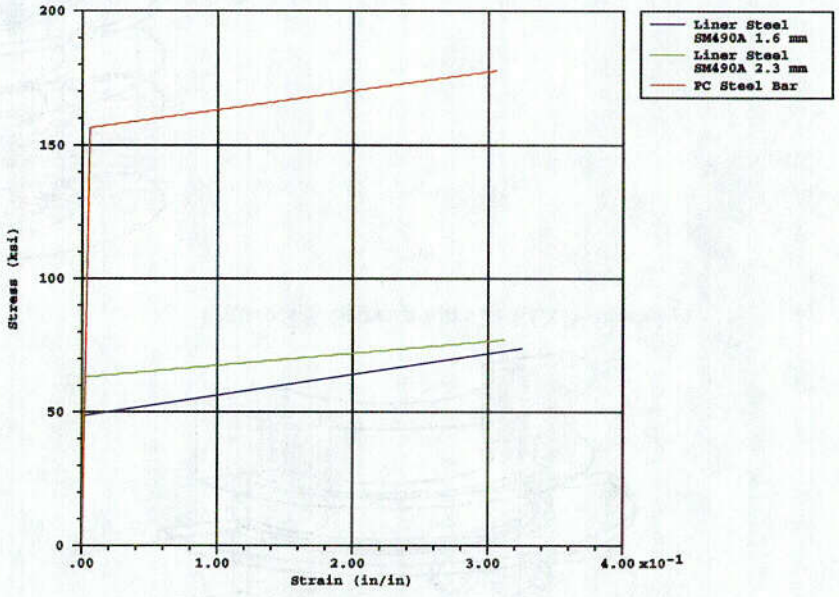

Figure 2.11 Liner and bolting material stress-strain relations

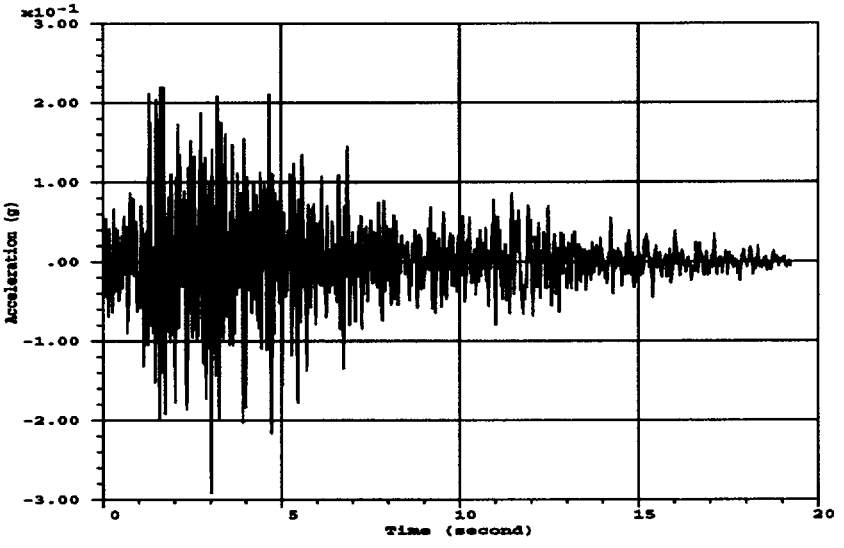

Horizontal Acceleration Record

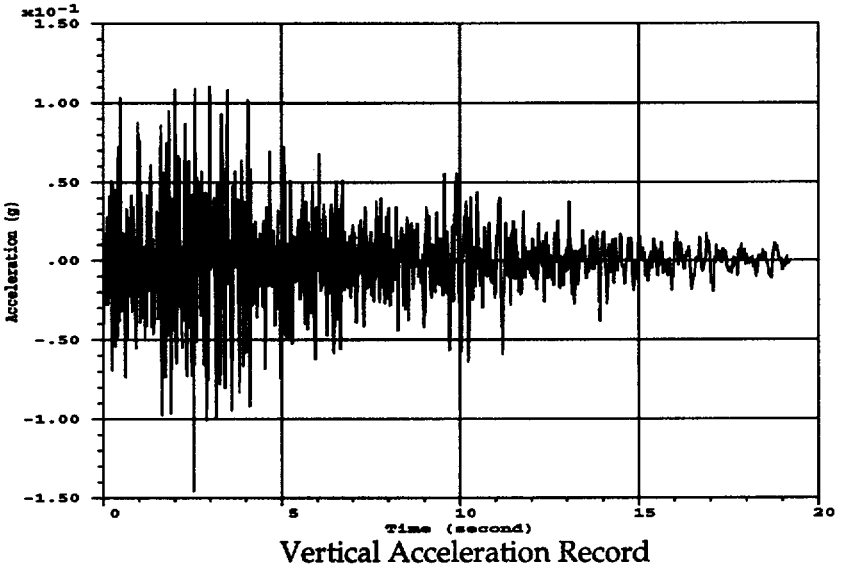

Vertical Acceleration Record

Figure 2.12 Level S1 target input acceleration records

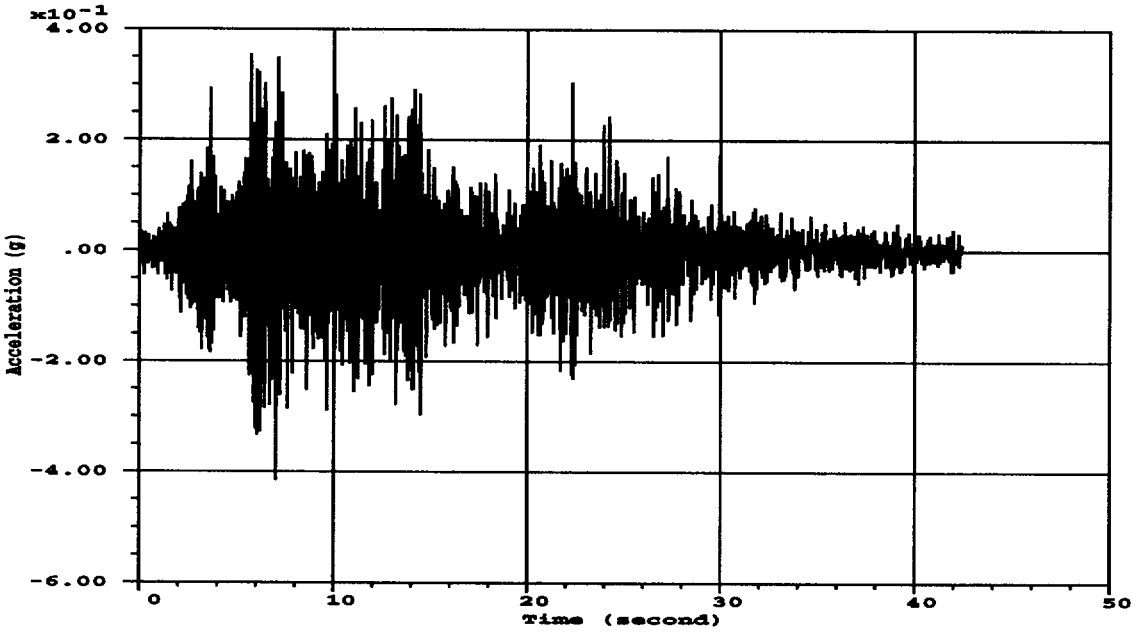

Horizontal Acceleration Record

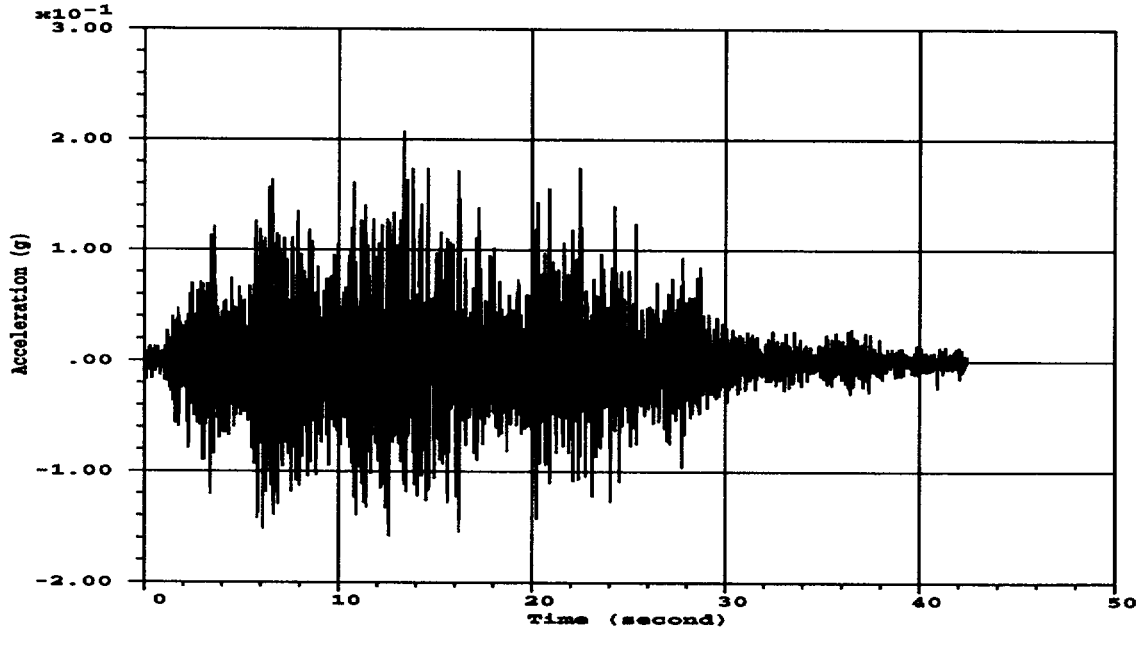

Vertical Acceleration Record

Figure 2.13 Level S2 target input acceleration records

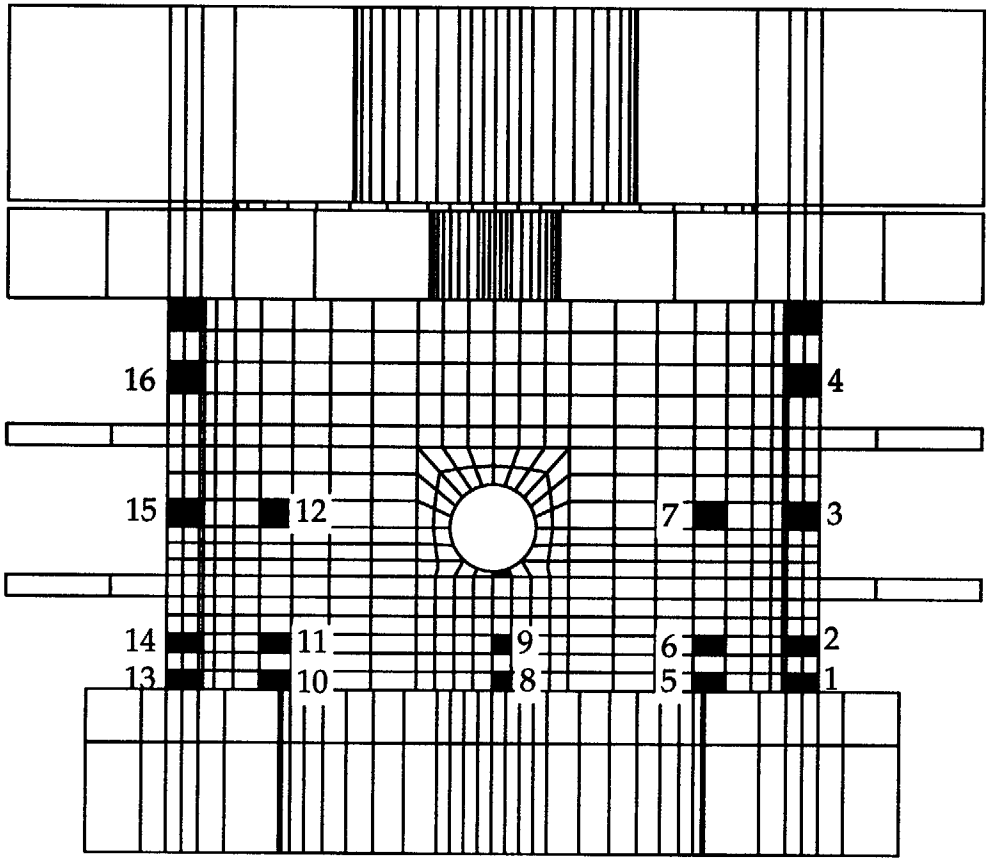

Figure 2.14 Selected locations for strain history data

3. PRETEST CALCULATIONS

3.1 Preliminary Calculations

As an aid in developing the RCCV model and analysis parameters, preliminary calculations were conducted prior to simulation of the seismic response. As discussed in the previous section, the goal was to optimize the finite element mesh by minimizing the number of degrees of freedom. Comparison of mode shapes, frequencies, and static capacities under lateral pushover between various levels of mesh refinement formed the basis of this mesh optimization. However, these preliminary calculations also added insight into the behavior of the RCCV model and how the model might perform under the given seismic loading. All of the analyses discussed in this chapter used the baseline analysis model discussed in Section 2.

3.1.1 Mode Shapes and Frequencies

The mode shapes and frequencies are extracted to evaluate the fundamental dynamic characteristics of the model to aid in establishing time step sizes. Figure 3.1 shows the first fundamental mode shape corresponding to a frequency of 15.1 Hz. This mode is dominated by sliding shear deformation, although there does appear to be evidence of rocking of the top mass, which causes some bending deformations in the walls. The response period for this mode is 0.0662 seconds so that a time increment of 0.007071 (every other data point in the S1 level event and every point in the S2 event) corresponds to 9.4 integration points per period. Figure 3.2 shows the second mode shape at a frequency of 41.6 Hz. This mode is clearly an axial mode, which induces near uniform axial tension and compression in the RCCV wall and cantilever bending in the intermediate floors. The third mode, shown in Figure 3.3, is dominated by rocking of the top mass and bending in the upstream-downstream sections of the wall. This mode is excited at a frequency of 42.6 Hz.

3.1.2 Input Response Spectra

Although the RCCV analysis is a nonlinear time-history analysis, it is instructive to evaluate the relative participation of the fundamental modes in the S1 and S2 loading by examining their response spectra. Figures 3.4 and 3.5 provide the spectral accelerations for the horizontal and vertical components of the S1 and S2 level events, respectively. The response spectrum for S1 indicates that the first fundamental mode at 15.1 Hz dominates the response, with an expected amplification of 3.0 to 0.9g for 3% damping. However, the response due to the first axial mode at 41.6 Hz can be amplified only to 0.25 g, and hardly any amplification exists for the rocking mode at 42.6 Hz. Similarly for the S2 level event, the response due to the first fundamental mode can be amplified by a factor of 3, while the vertical and rocking modes are outside the frequency range of significant amplification. Based on these results, a time step size of 0.007071 seconds is selected as the best compromise between computer resource requirements and solution accuracy.

3.1.3 Static Pushover Capacity

A static pushover analysis is conducted to verify the integrity of the finite element model and as a bounding estimate for the capacity of the test model. This analysis is conducted by fixing the displacements on the cut boundaries of the basemat and incrementally applying a horizontal body force load on the top section. This horizontal g force is incrementally increased until the computational model predicts the structure's ultimate capacity, which is defined in the sense that an additional increment in load causes a large increase in displacement. For this calculation, the horizontal force is applied monotonically in one direction. The horizontal reaction load, which is equal to the product of top mass and g-load, is plotted against the horizontal displacement of the top section relative to the basemat. Figure 3.6 shows the static pushover capacity. This figure also shows the estimated dynamic capacity of the RCCV test model, which is obtained by applying a knockdown factor to the statically calculated force-displacement response.

For the pretest predictions, it was assumed that the dynamic knockdown factor for the RCCV would be similar to the factor determined for the PCCV in James et al. (1999a). The knockdown factor is a function of loading history, damage accumulation, and so forth. This assumption was made only for estimating the RCCV response. The knockdown factor is the ratio between the static capacity curve and the peak dynamic horizontal forces in the test sequence. The average shear strain, calculated as the horizontal displacement of the top section divided by the distance above the basemat, is used as a common basis for the PCCV test and the RCCV estimate. Based on this assumption, the capacity of the RCCV is estimated at 1000 tons with a horizontal displacement of approximately 15 mm. This estimated dy-

namic capacity is compared to the results of dynamic analyses of the RCCV. It is also compared to the actual measured results of the test series.

3.2 Design Level Analysis

3.2.1 General Approach

The target input acceleration histories for the horizontal and vertical components of the S1 and S2 level events are shown in Figures 2.12 and 2.13, respectively. Time scaling provides data points at increments of 0.003536 seconds and 0.007071 seconds, respectively, for S1 and S2 events. The scaled total time is 19.22 seconds for S1 and 42.42 seconds for S2. The peak accelerations for the S1 level event are 0.29g horizontal and 0.15g vertical. The peak accelerations for the S2 level event are 0.42g horizontally and 0.21g vertical.

As shown in Table 1.2, the test plan called for an initial pressure test followed by S1(H), S1(V), and S1(H+V) tests. The letters H and V stand for the horizontal and vertical component, respectively, of the input accelerations as identified in Section 2. A leak test followed the S1 design level tests to verify liner integrity. Similarly, for S2, the test sequence was S2(H), then S2(V), then S2(H+V), followed by a static leak test. A loss of coolant accident in conjunction with the S1 level event, S1(H+V)+LOCA, followed by a leak tightness test, were the next tests in the sequence. Following these tests, there was a series of S2(H+V) tests for public demonstrations. Finally, the RCCV model was subjected to a series of tests with increased level of shaking, designated as 2S2(H), 3S2(H), etc., until failure of the model occurred. Only the horizontal component of acceleration was input during the failure level tests. Leak tests were conducted after each seismic test.

Because of time and budget constraints, only a subset of the test sequence is selected for pretest analysis. The pretest analysis sequence consists of S1(H+V) and S2(H+V). The pressure tests are not analyzed in the pretest calculations based on the assumption that the pressure induced cracking would not significantly affect the failure of the model.

The analysis begins with the application of gravity loads. The first dynamic analysis is then conducted by applying the input accelerations at the cut boundaries on the basemat. The solution is marched in time using the Hilber-Hughes integration operator, with equilibrium iterations performed as needed for each time step to allow cracking and load redistribution to develop. A static step is applied at the end of the time history to remove the residual inertial loads and return the system to static equilibrium. Eigenvalue extraction is then carried out using the current stress and cracking state to evaluate the change in the fundamental frequencies caused by the degradation in stiffness. The accumulated damage in the structure and the residual stress/strain states form the initial conditions for the next dynamic analysis using another time history input. For the pretest calculations, stiffness proportional damping of 3% at the first fundamental frequency is uniformly applied to the concrete material. For the posttest calculations, the cracking consistent damping model is used and updated to be cyclic dependent.

Due to the size of the model, only nodal point variables and element information at selected locations, shown in Figure 2.14, are saved at each time step from which time history plots are constructed. Response variables for nodal points on the top section and basemat are saved for generating time history plots for accelerations and displacements.

3.2.2 S1 Analysis Results

The model's response to the S1(H+V) input target acceleration is presented here, with more detailed results given in Appendix A. Figures 3.7 and 3.8 show the horizontal and vertical displacements of the top section relative to the basemat. These plots show a peak horizontal relative displacement of 1.1 mm occurring at 1.8 seconds. The relative vertical displacement is about 0.11 mm due to dead load alone, with a peak average movement of 0.035 mm. At diametrically opposite points in the direction of horizontal shaking, peak relative vertical displacements of 0.35 mm are calculated, indicating rocking of the top mass. Figure 3.9 present plots of the horizontal and vertical accelerations of the top mass, which show a peak horizontal acceleration of 1g and a peak vertical acceleration of 0.23g, both occurring at about 1.8 seconds. Figure 3.10 shows the cracking patterns. For any material point where cracking has occurred, a circle indicates the crack plane, which is perpendicular to the principal direction in which the stress/strain states have reached the cracking capacity of the concrete. An open crack is plotted in red while a closed crack is plotted in green. This figure indicates that the cracks develop principally due to bending at the wall-basemat junction near the 90° and 270° locations and transition to shear cracks (crack surfaces approaching 45° angles) as they spread toward the

penetration. Figure 3.11 shows the maximum principal strain contours in the concrete at the end of the S1(H+V) test simulation and the peak tensile strains of 0.028%. The cracking is more extensive in the shear region around locations 305° and 55° at the wall-basemat junction. Figure 3.12 shows the vertical strain contours, also after the termination of the S1(H+V) motion. In the region of cracking, tensile strains of 0.015 % are predicted. An estimate of the crack width can be obtained by multiplying this value of strain by the spacing of the hoop rebar. Using this procedure, a crack width of about 0.01 mm is estimated. Such a crack size is hard to detect by visual inspection. Figures 3.13 and 3.14 present contour plots of maximum principal strain and vertical strain, respectively, for the liner at the end of the S1(H+V) simulation. These plots indicate that no damage is predicted in the liner. Figures 3.15, 3.16, and 3.17 show the calculated mode shapes and frequencies following the S1(H+V) simulation. Comparing these frequencies to the initially calculated frequencies indicates a very small change due to cracking.

Plots of liner and rebar strain histories are contained in Appendix A. These include Figures A-1 through A.3, which show the axial and hoop liner strain histories for points identified in Figure 2.14, namely, points 1, 2, 8, 9, 13, and 14, which indicate elastic liner behavior. The strains are highest near the upstream and downstream locations (90° and 270°) with vertical strains of about 145E-6 and hoop strains of about 29E-6. Strain histories for the axial and circumferencial rebars are plotted in Figures A-4 through A-11 and Figures A-12 through A-15, respectively. As shown, the reinforcing steel remains elastic for the S1(H+V) test simulation. The largest vertical rebar strain is about 710E-6 and occurs near the wall basemat junction at 90°. The hoop rebar strains are very small and the drift seen in some records is due to cracking.

3.2.3 S2 Analysis Results

The S2(H+V) analysis is restarted after the static equilibrium step following the S1(H+V) dynamic analysis, using the residual stress, strain and cracking distributions as initial conditions. The horizontal and vertical components of the S2 target input acceleration histories, shown in Figure 2.13, are applied as before on all the surface nodes along the bottom and cut sections of the basemat. The solution is marched in time with equilibrium iterations applied at each dynamic step to allow for the development of the material's nonlinear behavior. The S2 input is defined for 43 seconds, and the analysis is continued for 40 seconds using time steps of 0.007071 seconds. At the end of the time history, a static step is applied to remove any inertial forces remaining in the system and to bring the structure to rest. Eigenvalue extraction is then conducted to determine the change in frequencies that may have occurred due to stiffness degradation. Figures 3.18 through 3.29, with more details provided in Appendix A, document the predicted response histories of the model to the S2(H+V) target acceleration input.

Figures 3.18 and 3.19 show the horizontal and vertical displacements of the top section relative to the basemat. The plots show a peak relative horizontal displacement of 2.2 mm at about 7 seconds that corresponds to the time of the peak acceleration in the S2 input. The plots also indicate an upward drift in the relative vertical displacement of about 0.2 mm. This is attributed to imperfect crack closure due to crack surface asperities and mismatch.

The concrete material model includes provisions for modeling the asperities on a crack surface under the assumption that a crack never closes exactly. Thus, under cyclic loading, compressive stress can develop normal to the crack due to surface roughness even before the crack is fully closed. This effect is the reason why the model predicts this slight increase in the relative distance between the top section and basemat as cracking damage builds up in the concrete.

The peak vertical relative displacement about the mean value is predicted as 0.7 mm for the upstream and downstream locations, indicating rocking of the top section. Figure 3.20 shows the computed horizontal and vertical acceleration response of the top section. The peak horizontal acceleration is 1.3g occurring at about 7 seconds, and the peak vertical acceleration is 0.45g occurring at about 14 seconds.

Figure 3.21 shows cracking patterns predicted by the pretest model at the end of the S2(H+V) simulation. Cracking is evident in the bottom portion of the RCCV wall between the basemat and the first floor slab. In the region around the access tunnel penetration, the cracking is seen to be at 45° angles, indicating dominant shear response. As one moves toward the 90° and 270° locations, upstream and downstream to the shaking direction, the cracking transitions to more horizontal orientations due to bending loads. Shear cracking is also evident around the penetration, with diagonal cracks emanating from the hole at 45°.

The shear cracks are predicted to be non-symmetric in this area with more cracking to the side of the penetration toward the 270° side. This is attributed to the non-symmetric nature of the input acceleration history, which has larger acceleration peaks in the negative direction than the positive direction. Thus, cracking in the structure may depend on the nature of the actual input at the basemat in the test. Figure 3.22 shows points in the model where the effective stress has exceeded the uniaxial compressive yield strength. These plots use magnified deformations and indicate local damage regions with possible spallation at 90° and 270°.

Figure 3.23 shows the maximum principal strain contours, which indicate localized damage in several areas. The peak principal strain of 4% is indicative of spallation on the outside of the wall near the 90° and 270° locations. Figure 3.24 shows vertical strain contours in the concrete after the S2(H+V) simulation. Using a spacing of 81 mm for the hoop rebars, the crack widths are estimated at 0.2 mm for the bending type cracks. Assuming the principal strains are more representative of the shear cracks near the penetration, the width of these cracks is estimated at 0.4 mm.

Figures 3.25 and 3.26 show liner maximum principal and vertical strains, respectively, at the end of the S2(H+V) motion. These plots indicate that the peak principal strains are mainly due to axial elongation caused by imperfect crack closure, thereby inducing a residual state of stress in the liner, although the behavior of the liner is elastic.

Figures 3.27 through 3.29 show the mode shapes and frequencies for the model after the accumulation of damage from S2(H+V). A reduction in the stiffness of the model due to cracking is evident from these figures. The first mode is now reduced from 15.1 Hz to 12.1 Hz. The axial extension mode is reduced from 41.5 Hz to 36.8 Hz, and the rocking mode is reduced from 42.6 Hz to 28.9 Hz. The S2 response spectra (see Figure 3.5) has about the same amplitude of response for resonant frequencies between 8 and 20 Hz. Therefore, the fundamental sliding shear mode frequency shift will not significantly amplify or de-amplify the response unless the frequency decreases to less than 8 Hz. Below resonant frequencies of 8 Hz, the response spectra curve shows that a small decrease in resonant frequency will significantly reduce the response amplification.

Figures A-16 through A-18 in Appendix A provide vertical and hoop liner strain histories at selected points roughly corresponding to gauge locations in the test. These plots also show strain drift due to the cracking in the concrete. However, the magnitudes of the strains indicate linear behavior for the liner, with the highest strains occurring near the wall-basemat juncture toward the 90° and 270° locations. Figures A-19 through A-26 show the calculated strain histories for vertical reinforcement bars near the gauge locations in the test. Figures A-27 through A-30 show strain histories for hoop rebars. The plots indicate that some residual stress will exist in the bars after the test due to cracking damage. However, the reinforcing steel does not appear to reach yield, so no plastic strains occur.

3.3 Pretest Failure-Level Analyses

3.3.1 Analytical Predictions

For the pretest failure-level calculations, the analysis model is subjected to a series of ground motions of 2S2(H), 3S2(H), 4S2(H), 5S2(H), and 9S2(H) until failure is predicted. However, because of the large uncertainty in the input motion discussed earlier, it was decided to perform only scoping calculations to obtain some measure of structural behavior under high seismic motion. Thus, the analysis was conducted for 2S2(H) and 4S2(H) only. Selected results are shown here and in Appendix A. Appendix B contains posttest analysis results with test comparisons, and Appendix C provides the derivation of the cycle dependence of the RCCV.

For the 2S2(H) event, the horizontal and vertical accelerations of the top mass are shown in Figure 3.30. The relative horizontal and vertical displacements at two points in the top mass are shown in Figures 3.31 and 3.32. Figures 3.33 and 3.34 show extensive cracking in the cylindrical wall, extending into the basemat. Figure 3.35 shows relatively few points where the concrete has reached its compressive strength. The concrete strains are shown in Figures 3.36 and 3.37 for the inner and outer surfaces, respectively. Liner strains and stresses are plotted respectively in Figures 3.38 and 3.39. These plots indicate generally elastic behavior.

The results for the 4S2(H) event are presented here and in Appendix A. Figures 3.40, 3.41, and 3.42 present the accelerations and displacements respectively, which show significant opening up of the time record, indicating significant reduction in the frequency. Similarly, the number of points of compressive yielding has increased significantly, as shown in Figure 3.43. The concrete strains are presented in Figures 3.44 and 3.45, which indicate significant widening of the cracks. Liner strains and stresses are

depicted in Figures 3.46 and 3.47, which show the liner to be in the plastic regime. Strain time histories for the rebars and the liner are contained in Appendix A.

3.3.2 Failure Prediction and Comparison to Static Pushover

Because of significant differences between the target input accelerations, and the basemat accelerations that were measured during the test, it was not possible to compare the failure-level analyses with the actual test results. However, it is instructive to compare the 2S2(H) and the 4S2(H) predictions to the failure level results obtained from the static pushover analysis. Figure 3.48 shows the static pushover curve and the dynamic estimate curve, with the 2S2(H) and 4S2(H) predicted peak accelerations plotted on the curve. As noted earlier, the dynamic capacity estimate curve is obtained by applying a knockdown factor to the static pushover curve. Figure 3.48 indicates that the RCCV model is close to failure at the 4S2(H) level motion. It should be noted, however, that 4S2(H) input motion is obtained by simply multiplying the amplitude of the S2(H+V) target motion by 4. The actual input motion in the test was different than these assumed target motions, especially in the vertical direction. Nevertheless, the present analysis shows that if the input motion is of the type 4S2(H), then, by the failure criterion developed for the PCCV model (see James et al., 1999a) the structure would fail in shear. This failure criterion states that 'a concrete containment structure would be at a state of impending failure during an earthquake when the shear strain averaged over 80% area of any cross-section exceeds 0.5%.' This is illustrated in Figures 3.49 and 3.50, which respectively show the shear strain contours up to 5% and up to the maximum values attained at the time of predicted failure.

3.4 Comparison to Test Data

The test model was initially subjected to a pressure test followed by a S1(H) test, which were not included in the pretest analysis sequence. The decision to exclude these tests from the analysis was motivated by cost considerations and justified by the assumption that such tests would not significantly alter the response of the model when subjected to the S1(H+V) motion and higher amplitude tests. As a result, the test data revealed that the S1(H) test resulted in significant cracking damage in the model as a result of larger horizontal acceleration than targeted, and more significantly, a large vertical component that was not part of the target input motion.

The first analytical simulation used the S1(H+V) target motions for input, while the actual test motion differed significantly from the target values (about 1.3 times larger than the target values). Because of these differences in the applied loading between the analysis and the test, more cracking damage is observed after the S1(H+V) test than was predicted by the analyses. Moreover, the experimentally determined fundamental frequency was initially 13.5 Hz, while the analyses predicted a frequency of 15 Hz. Following the pressure and the S1(H) tests, the frequency had decreased to 9.5 Hz, and after the S1(H+V) test, the frequency was measured at 8 Hz. As noted previously, at resonant frequencies below 8 Hz, a small decrease in resonant frequency will significantly reduce the response amplification. While the pretest analysis (only the S1(H+V) was analyzed) showed negligible change in the frequency before and after the analysis, the lowest frequency decreased by 5.5 Hz during the actual tests {1.3S1(H), 1.1S1(H), 1.1S1(V), 1.15S1(H+V), and 1.1S1(H+V)}.

By the end of the S2(H+V) tests, the measured resonant frequencies had decreased to about 6.5 Hz. In the S2(H+V) analysis, the lowest resonant frequency decreased by about 20% to 12 Hz.

After the 2S2(H) test, the measured resonant frequency was about 6 Hz, which continued to decrease during subsequent tests. After the 4S2(H) test, the resonant frequency was about 5.5 Hz. During the analysis of the 2S2(H) and 4S2(H), the lowest lateral resonant frequency continued to decrease. At the end of the 4S2(H) analysis, the resonant frequency was about 7 Hz.

There are at least three reasons that the analytical resonant frequencies didn't degrade as much as the test results.

1. The input loads were different (i.e., larger) in the test than the input loads used in the analysis,

2. The test model was cycled many times more than the analytical model (i.e., only a few of the test cases were analyzed), and

3. As cracks opened in the analysis model, the concrete shear stiffness did not reduce as much as occurred in the test model.

Because of these differences between the analysis and the actual test, it is not meaningful to compare pretest analytical results with test measurements.

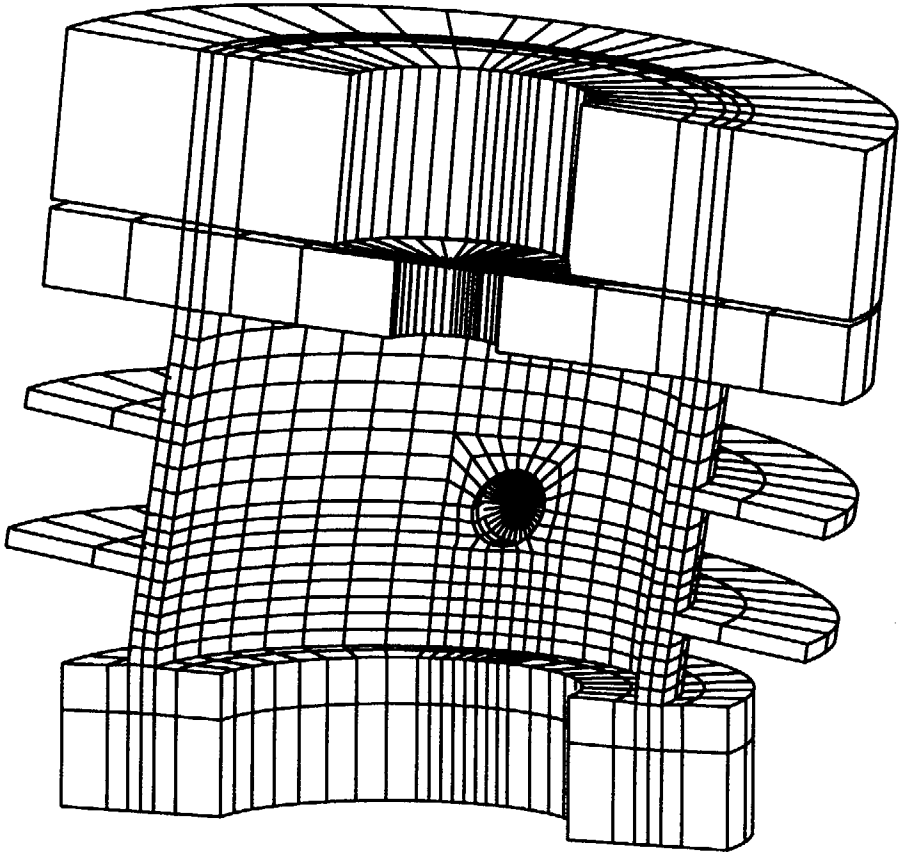

Frequency=15.092 Hz

Figure 3.1 Modal shape and frequency for mode 1, undamaged state

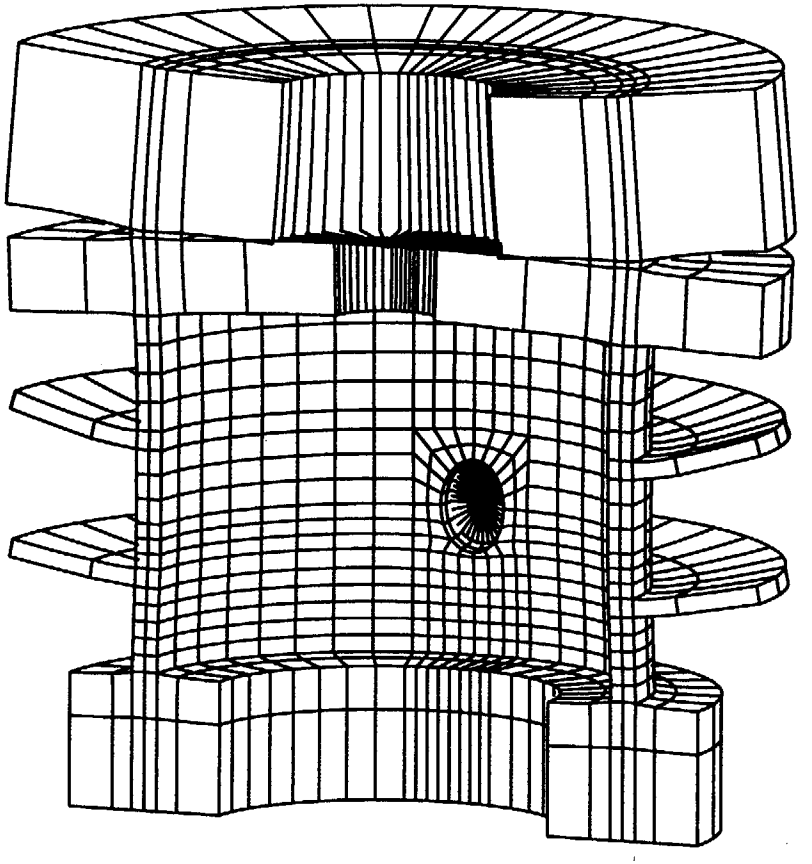

Frequency=41.556 Hz

Figure 3.2 Modal shape and frequency for mode 2, undamaged state

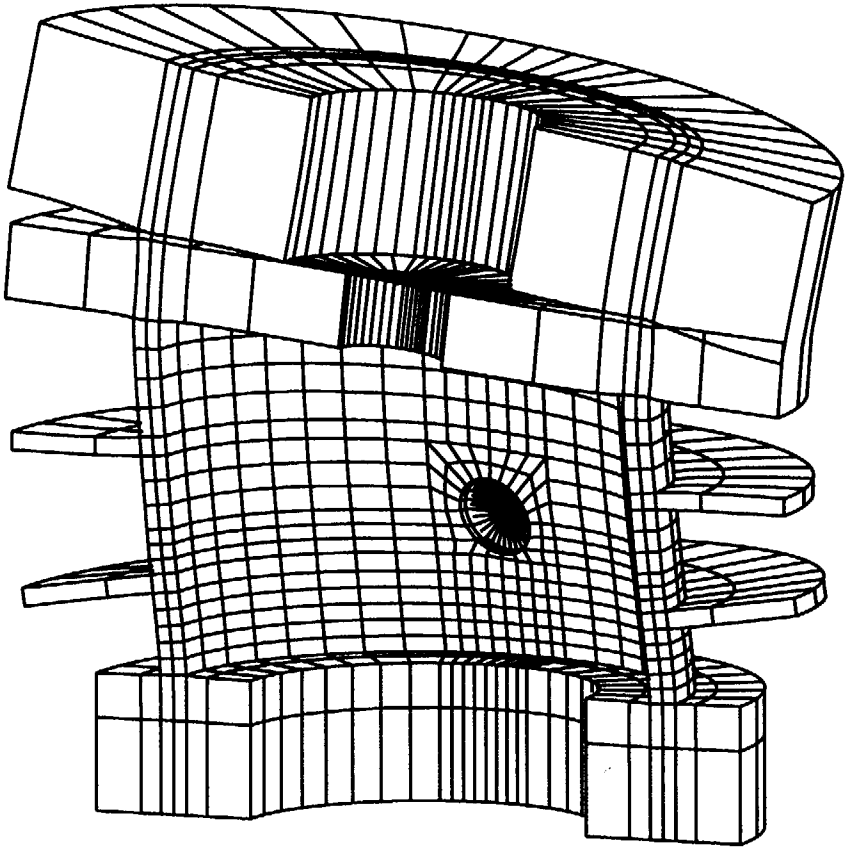

Frequency=42.592 Hz

Figure 3.3 Modal shape and frequency for mode 3, undamaged state

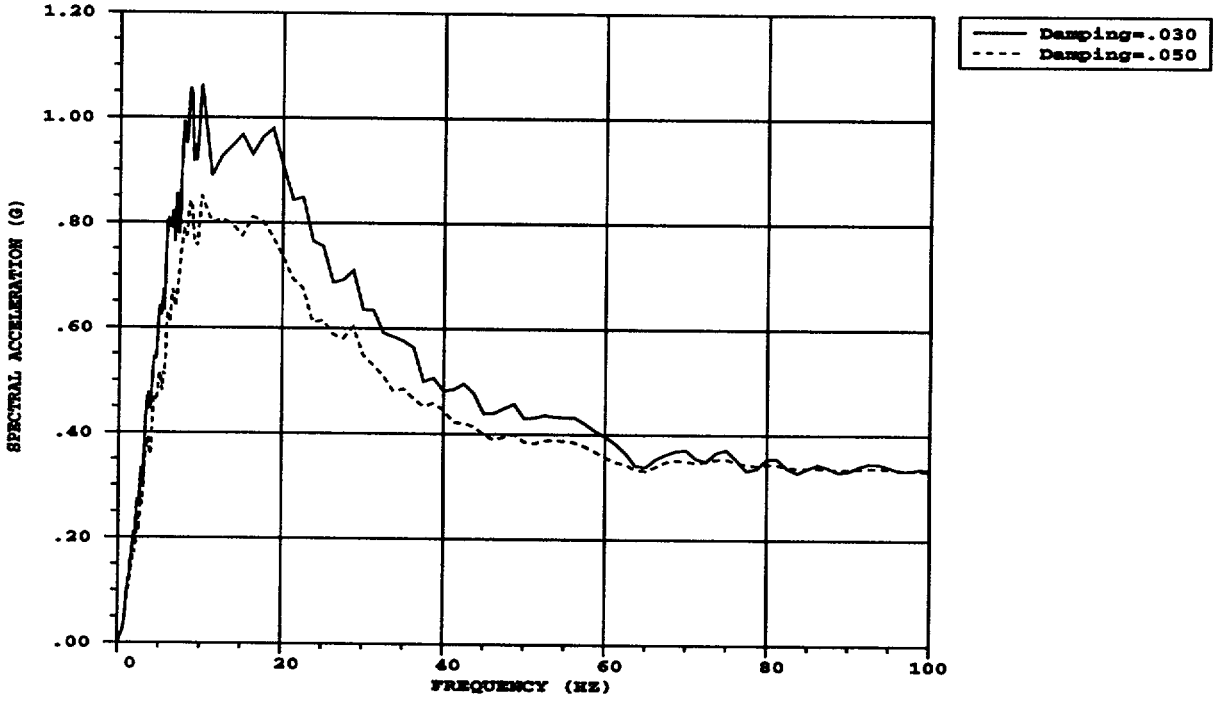

Spectral Acceleration of Horizontal Record

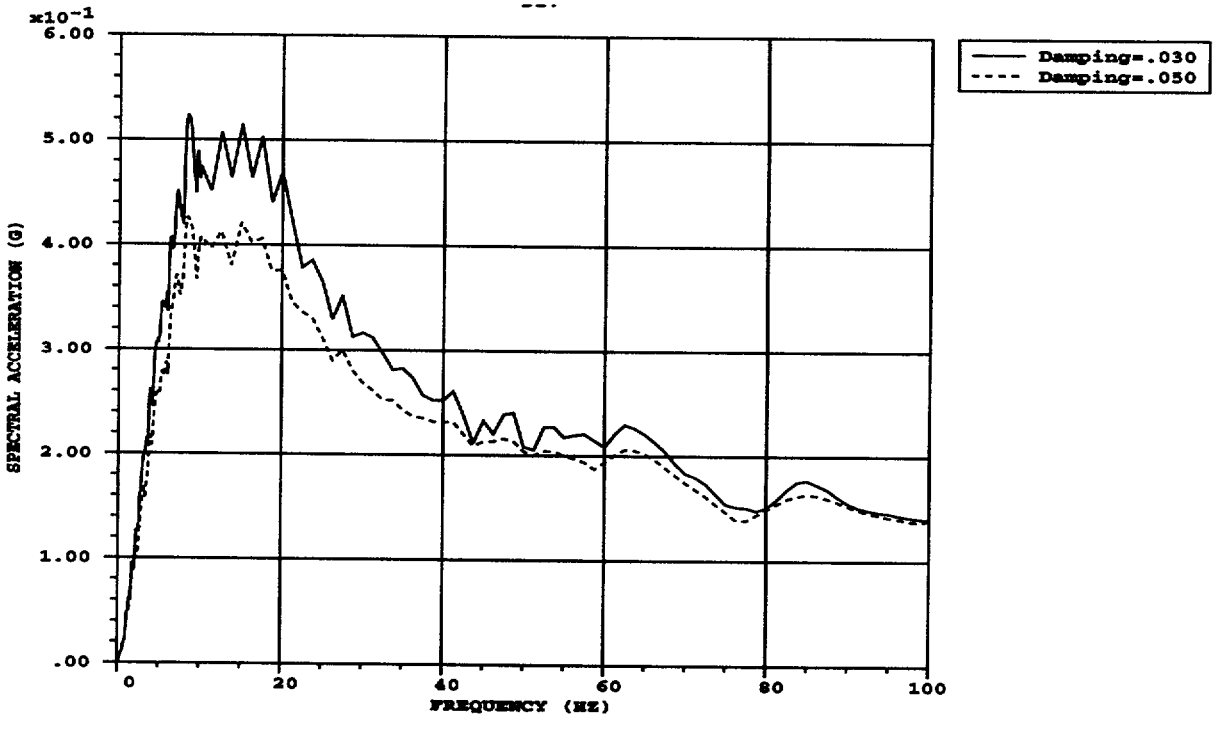

Spectral Acceleration of Vertical Record

Figure 3.4 Response spectra of Level S1 target input acceleration records

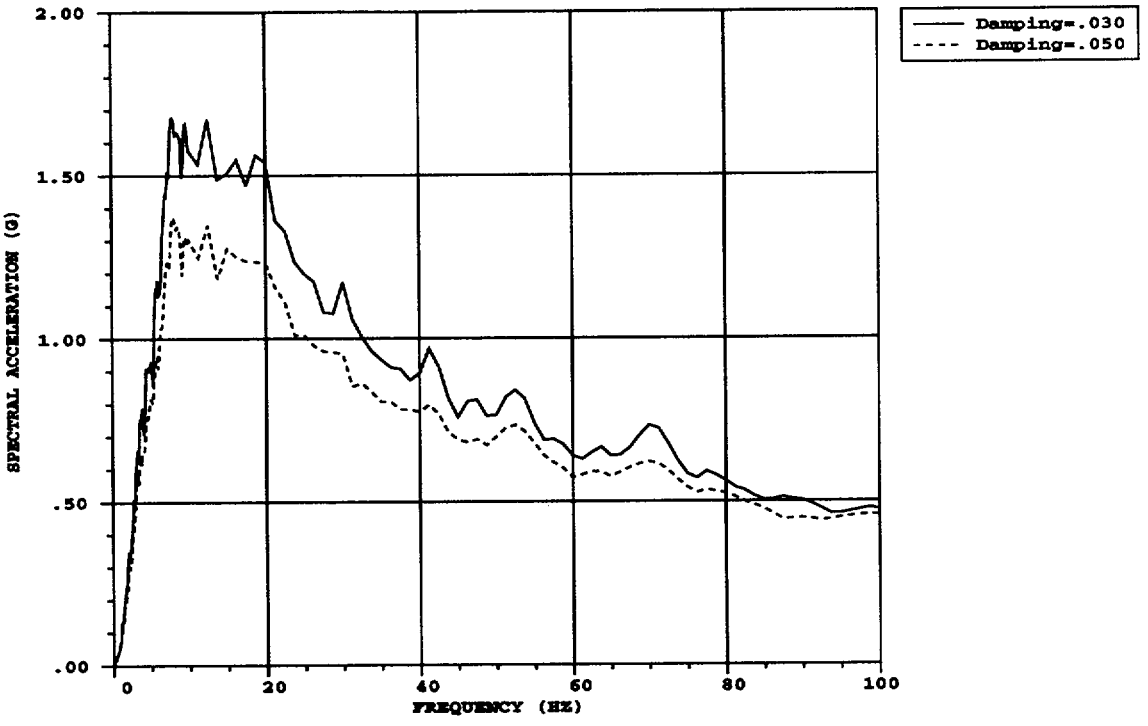

Spectral Acceleration of Horizontal Record

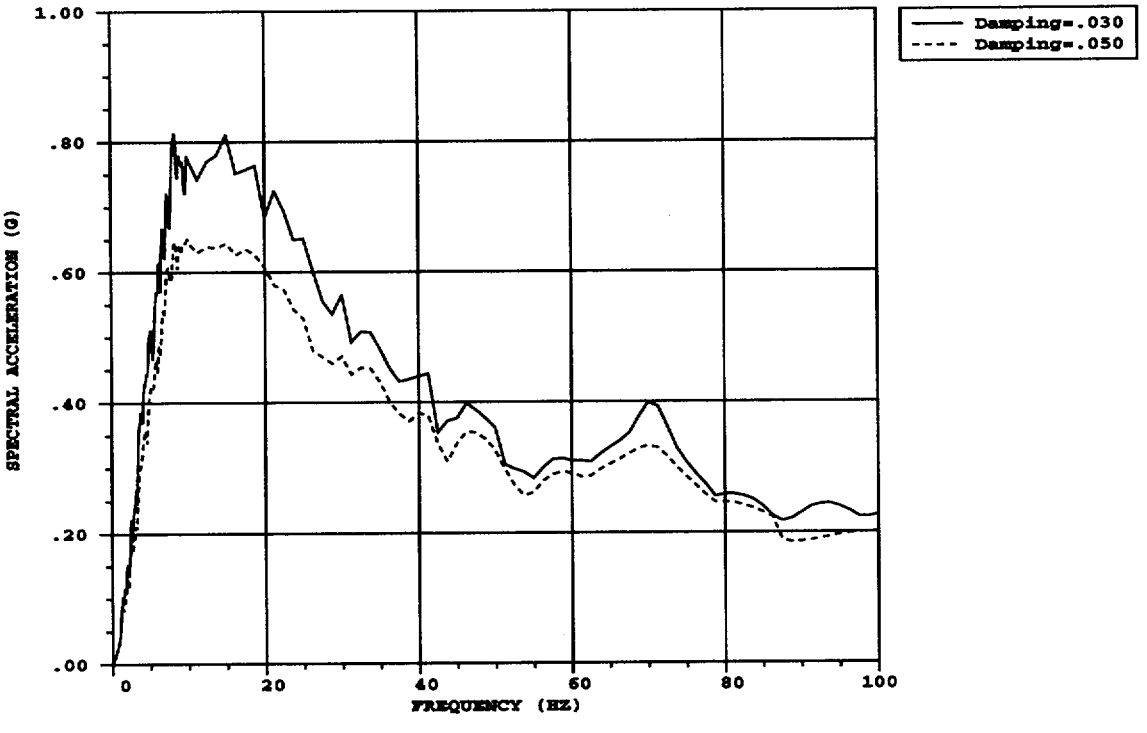

Spectral Acceleration of Vertical Record

Figure 3.5 Response spectra of Level S2 target input acceleration records

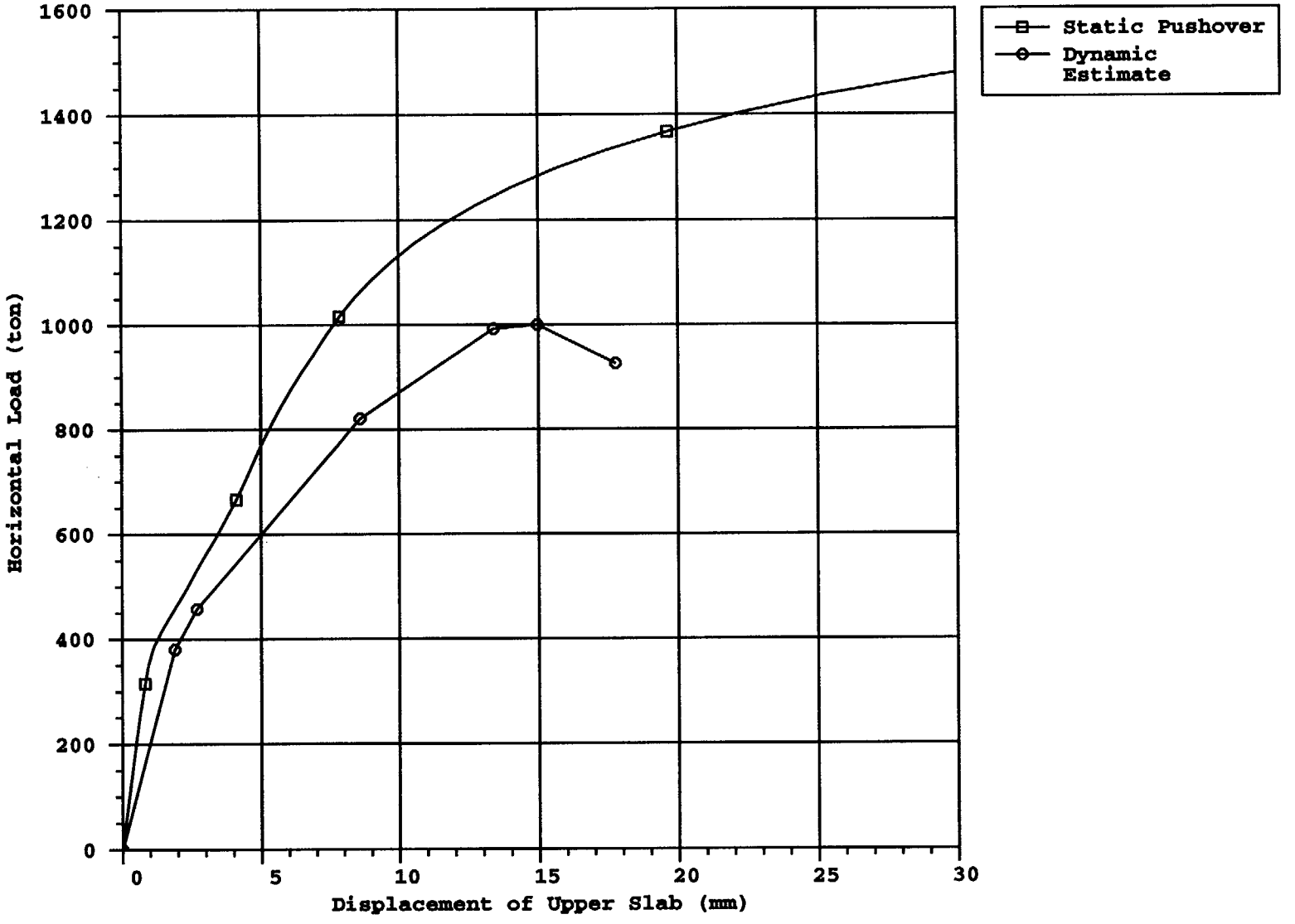

Figure 3.6 Dynamic capacity estimate based on static pushover

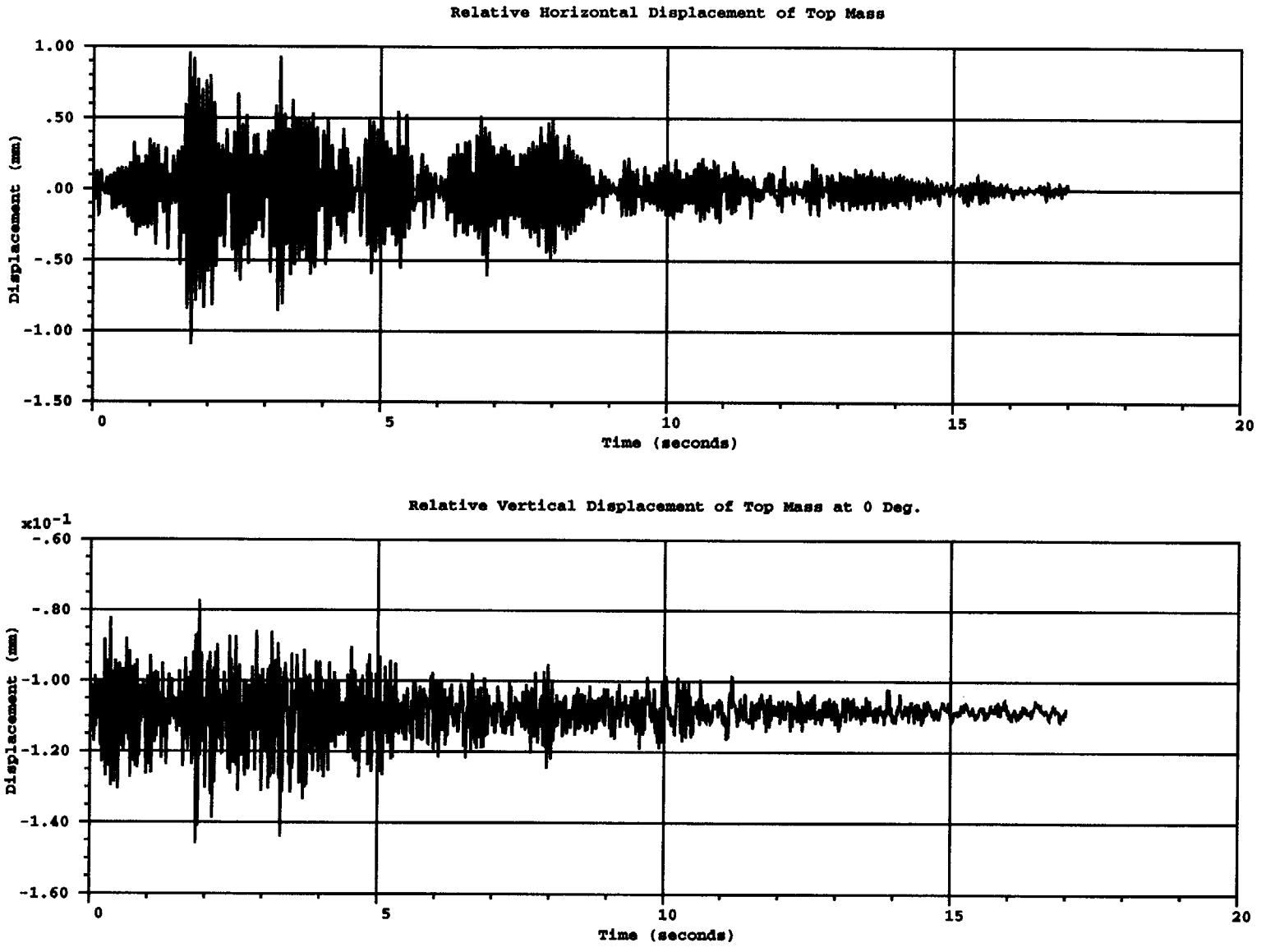

Figure 3.7 Relative displacements of RCCV under S1(H+V)

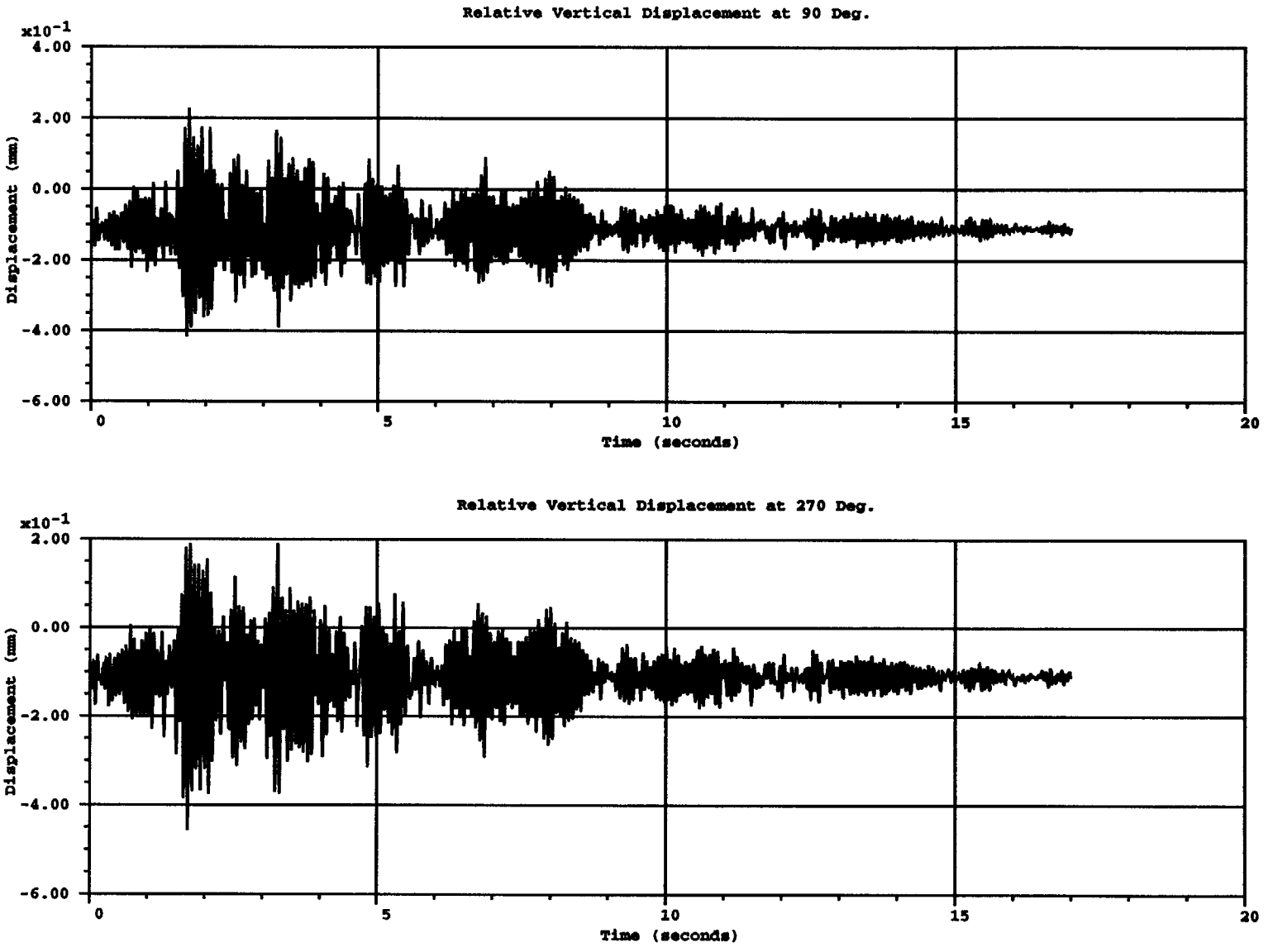

Figure 3.8 Relative displacements of RCCV under S1(H+V)

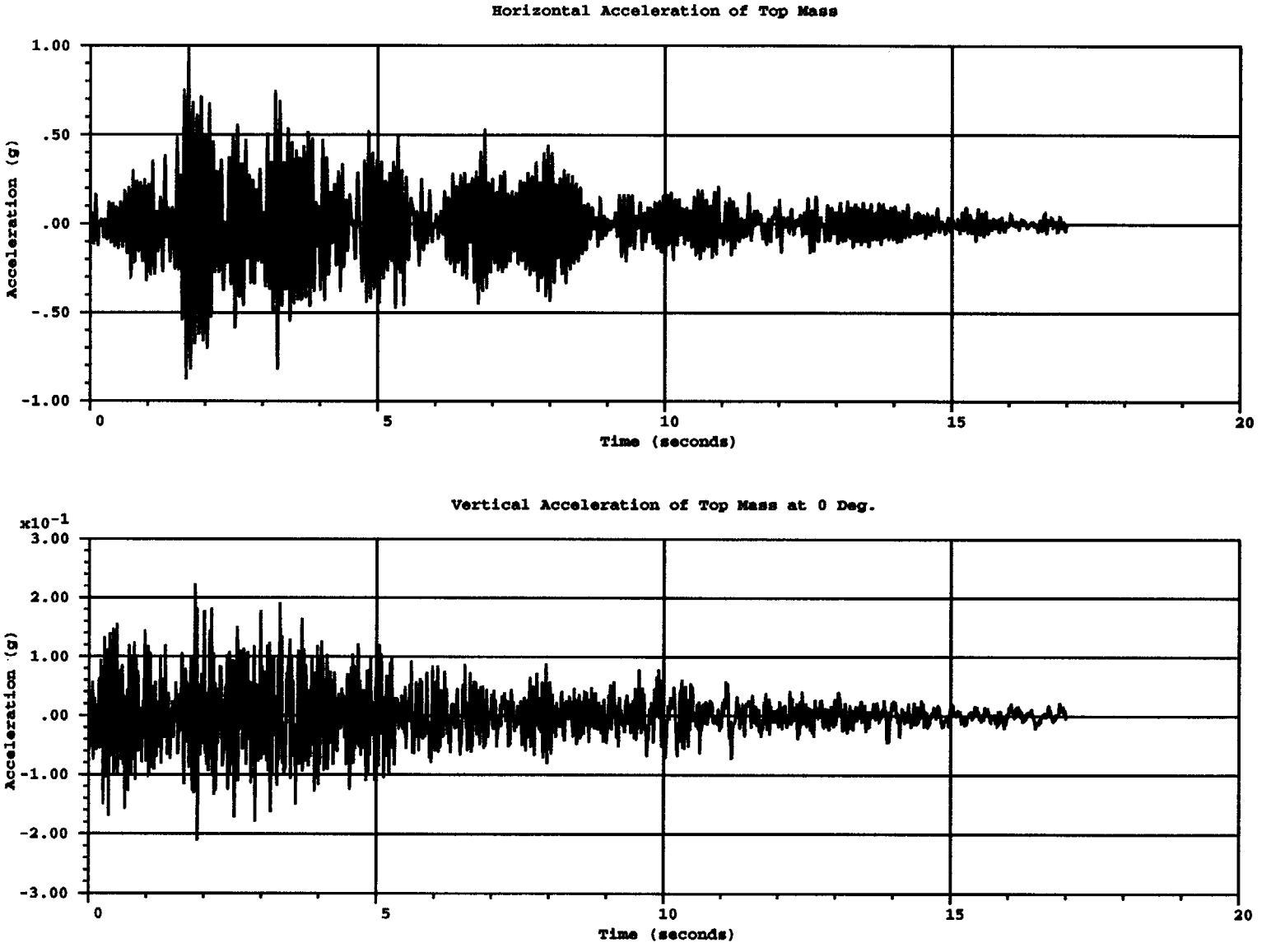

Figure 3.9 Total accelerations of RCCV under S1(H+V)

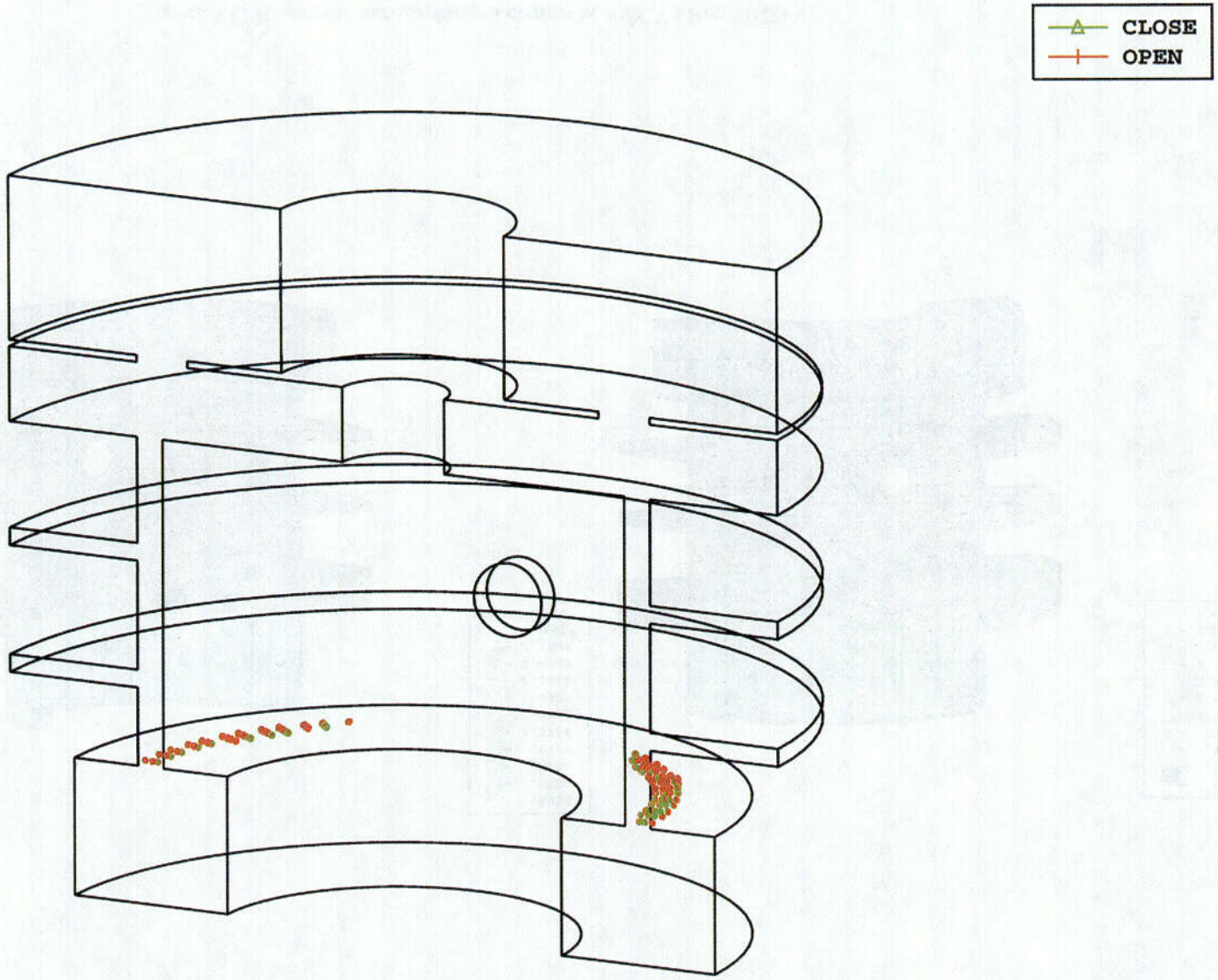

Figure 3.10 Cracking patterns for RCCV after S1(H+V)

C-4

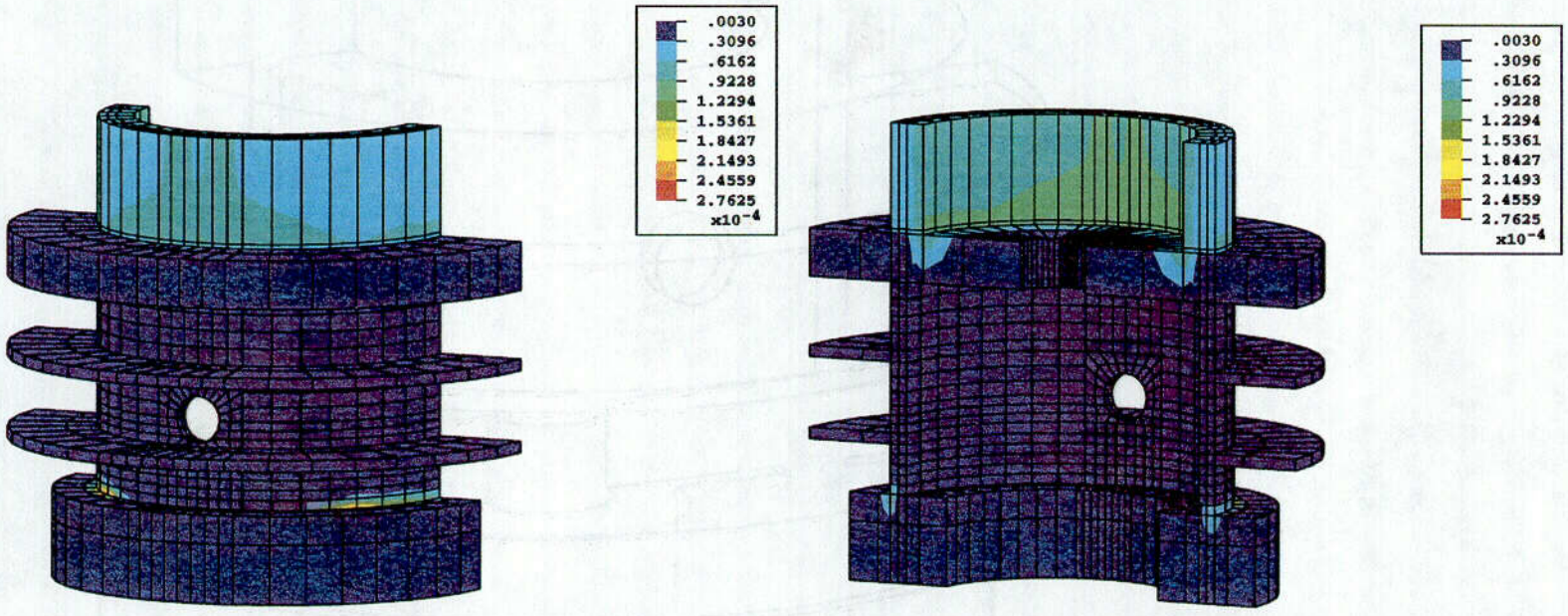

Figure 3.11 Concrete max. principal strains in RCCV after S1(H+V)

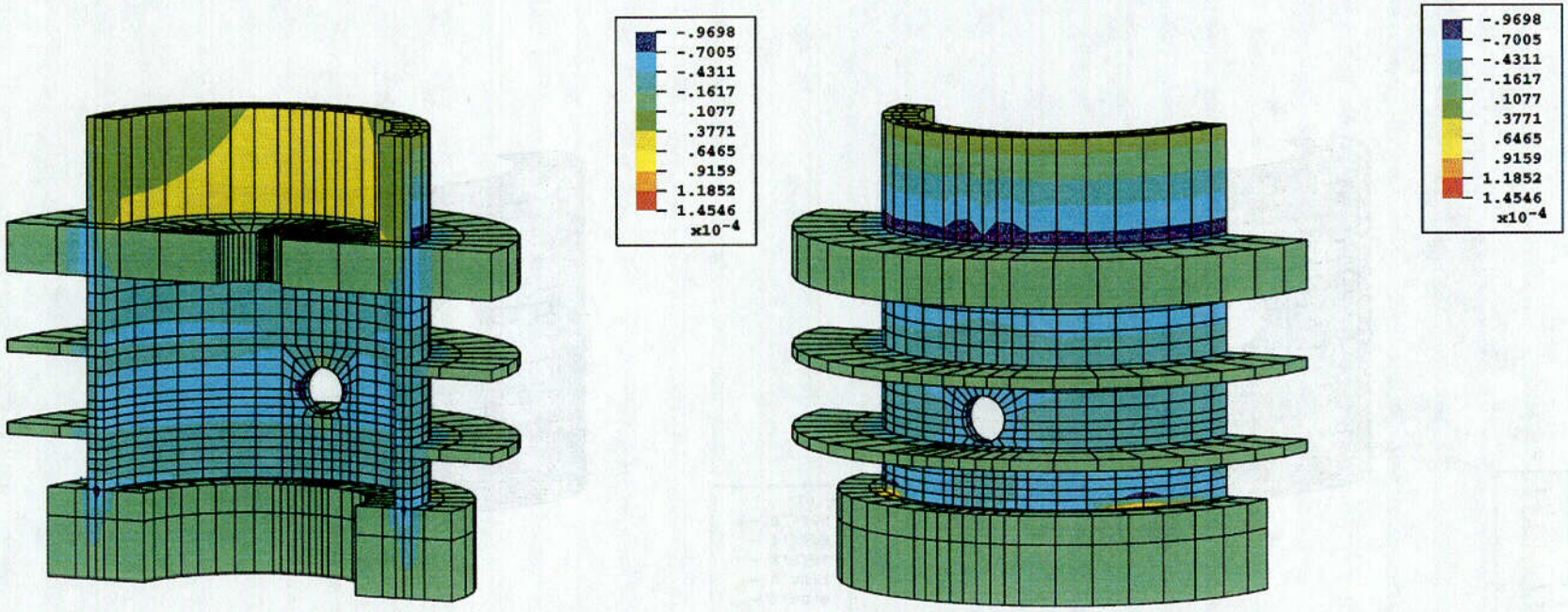

Figure 3.12 Concrete vertical strains in RCCV after S1(H+V)

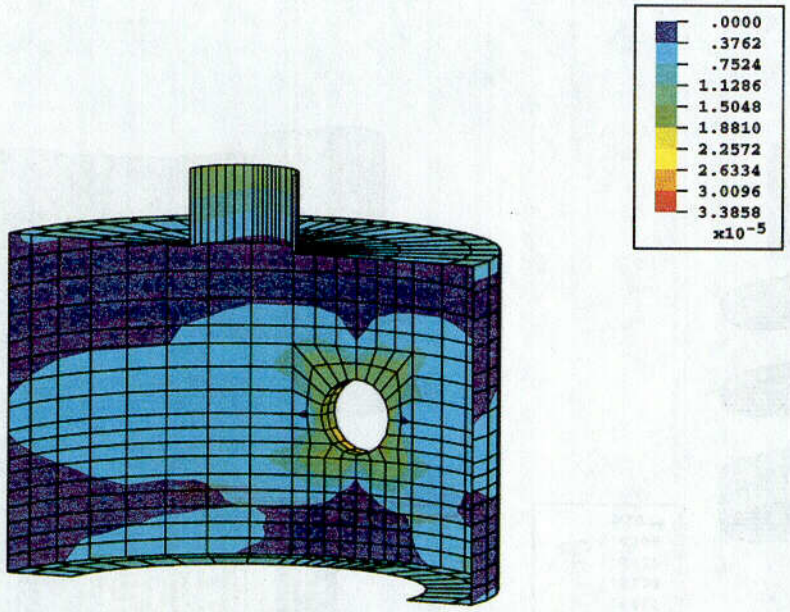

Figure 3.13 Liner max. principal strains in RCCV after S1(H+V)

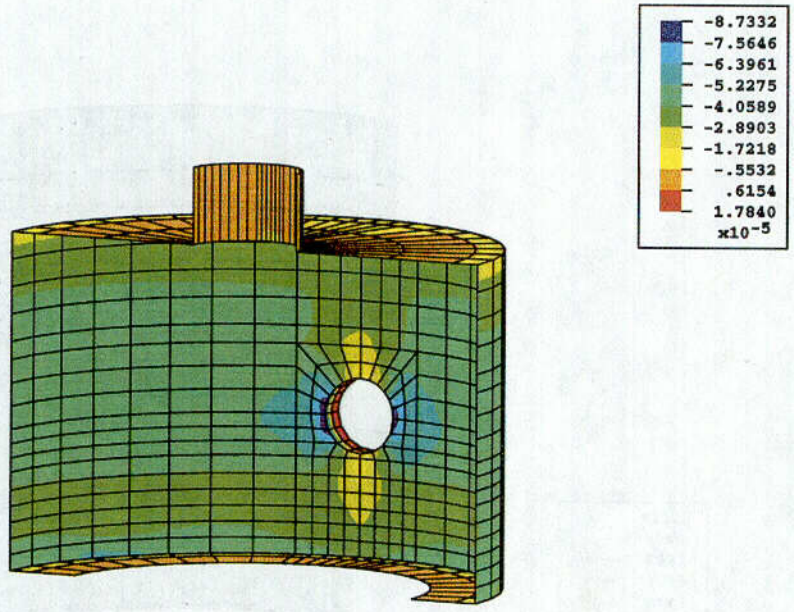

Figure 3.14 Liner vertical strains in RCCV after S1(H+V)

C-1

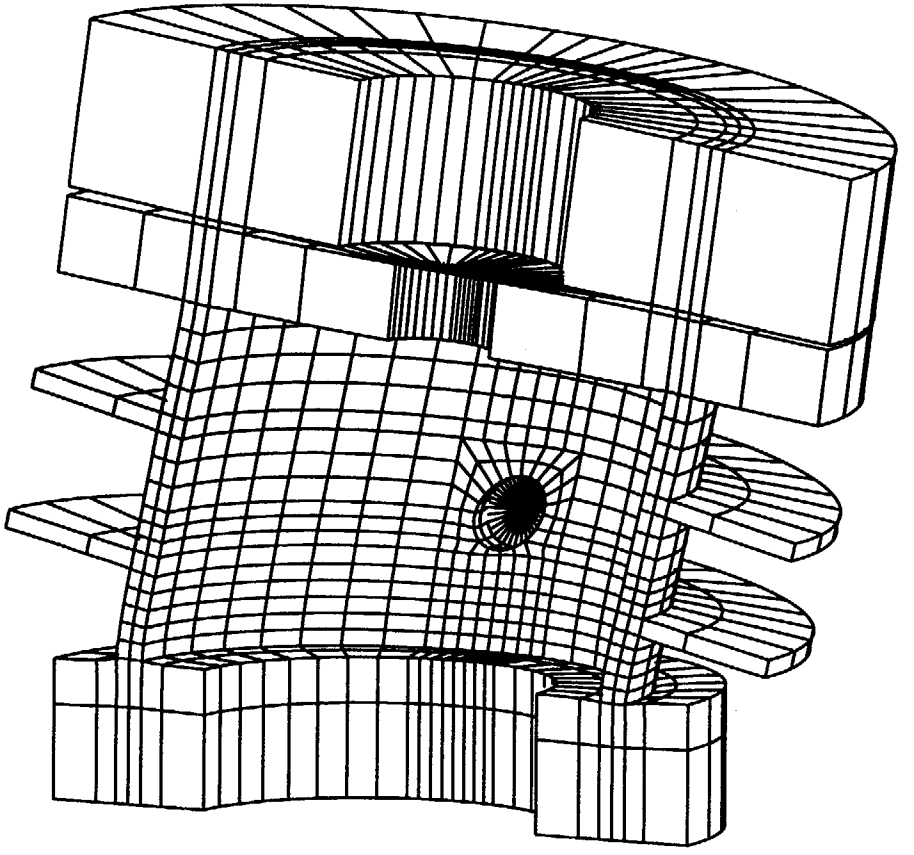

Frequency=15.077 Hz

Figure 3.15 Modal shape and frequency for mode 1 after S1(H+V)

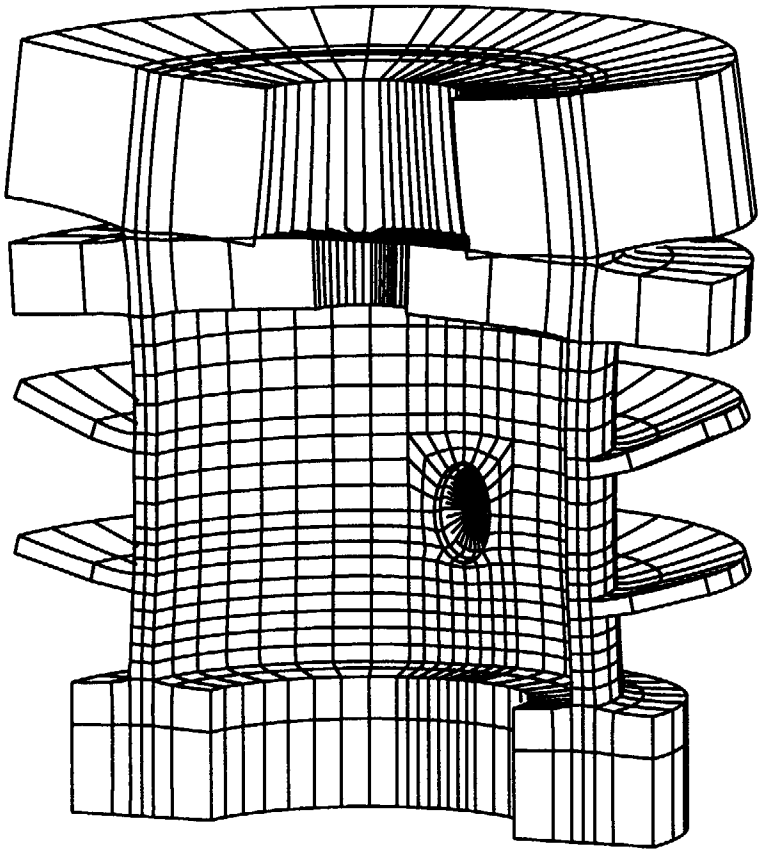

Frequency=41.524 Hz

Figure 3.16 Modal shape and frequency for mode 2 after S1(H+V)

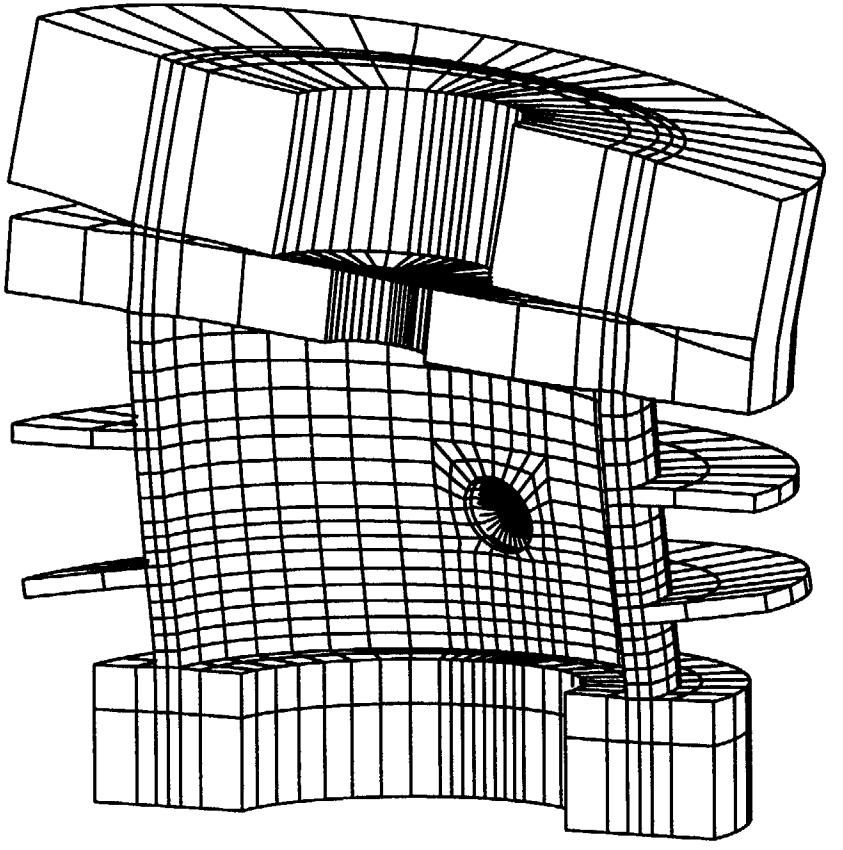

Frequency=42.565 Hz

Figure 3.17 Modal shape and frequency for mode 3 after S1(H+V)

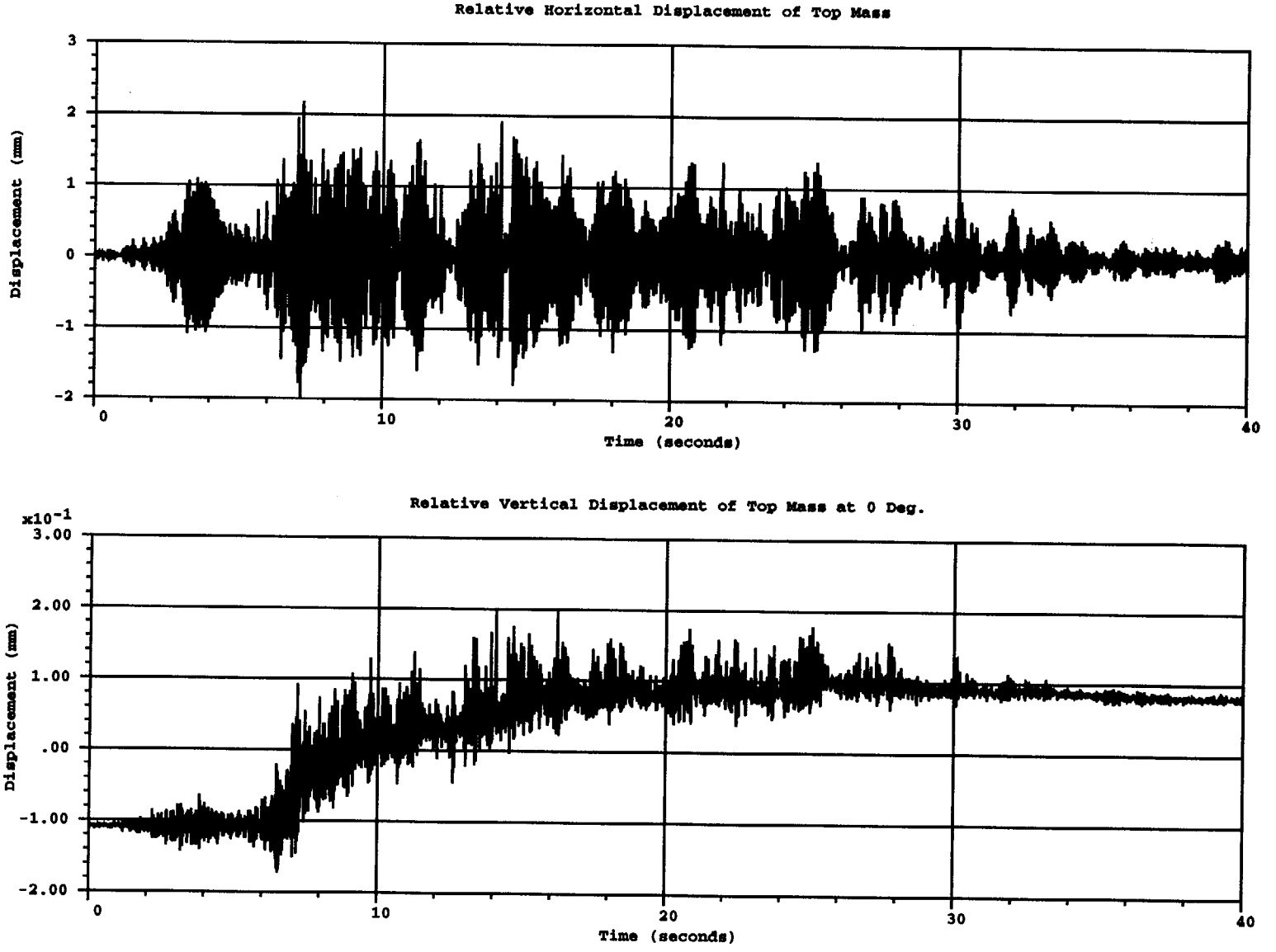

Figure 3.18 Relative displacements of RCCV under S2(H+V)

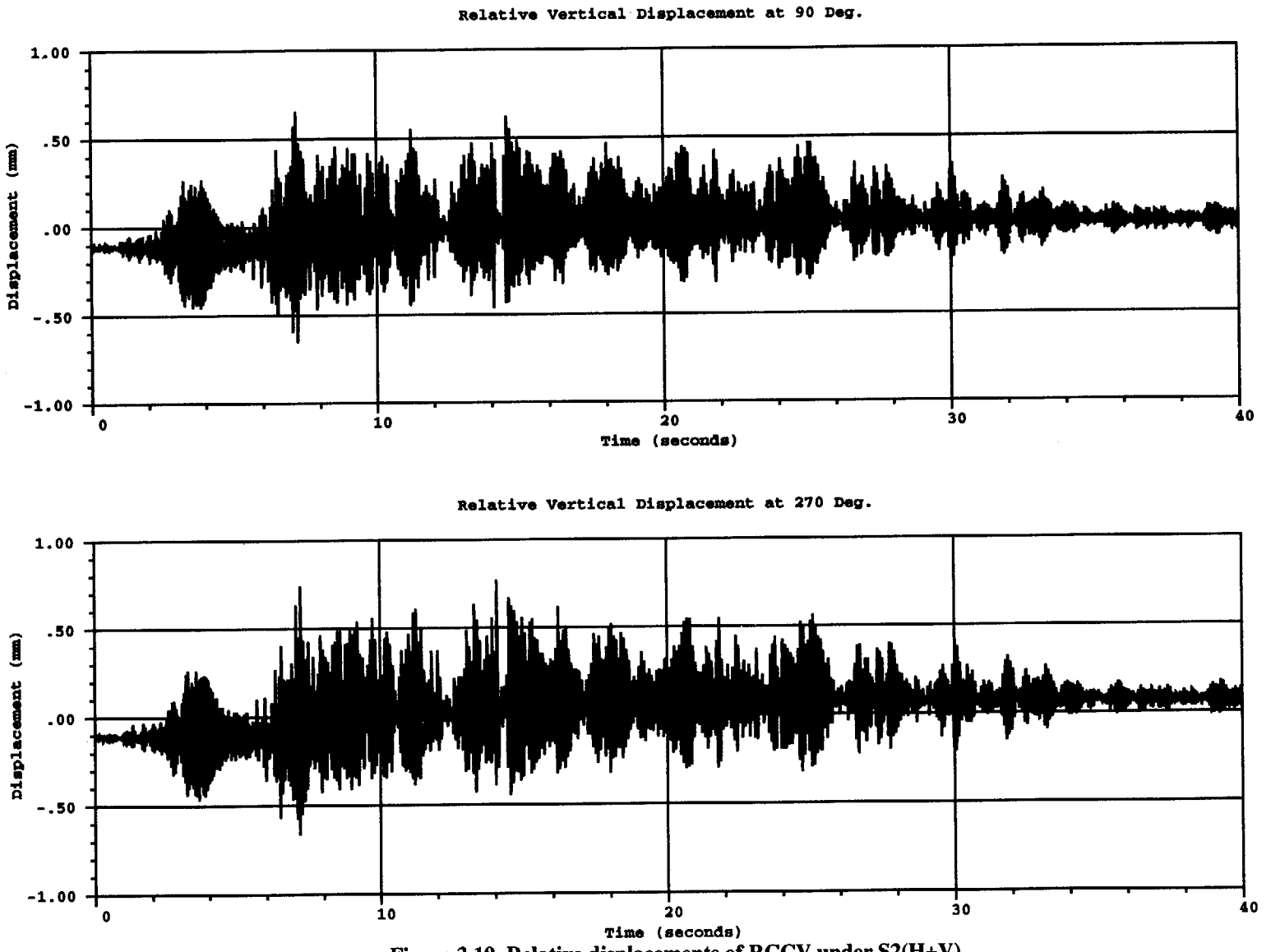

Figure 3.19 Relative displacements of RCCV under S2(H+V)

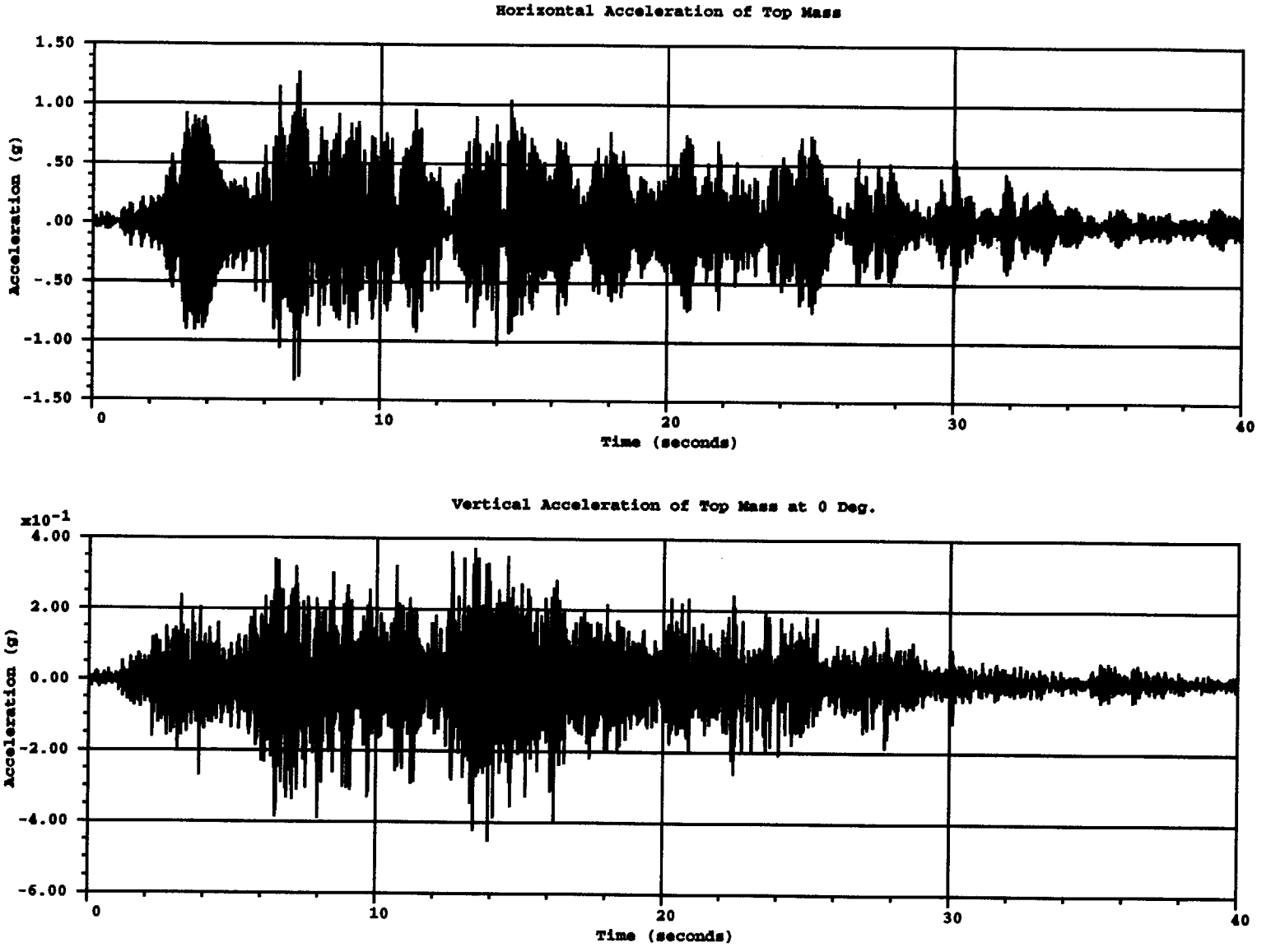

Figure 3.20 Total accelerations of RCCV under S2(H+V)

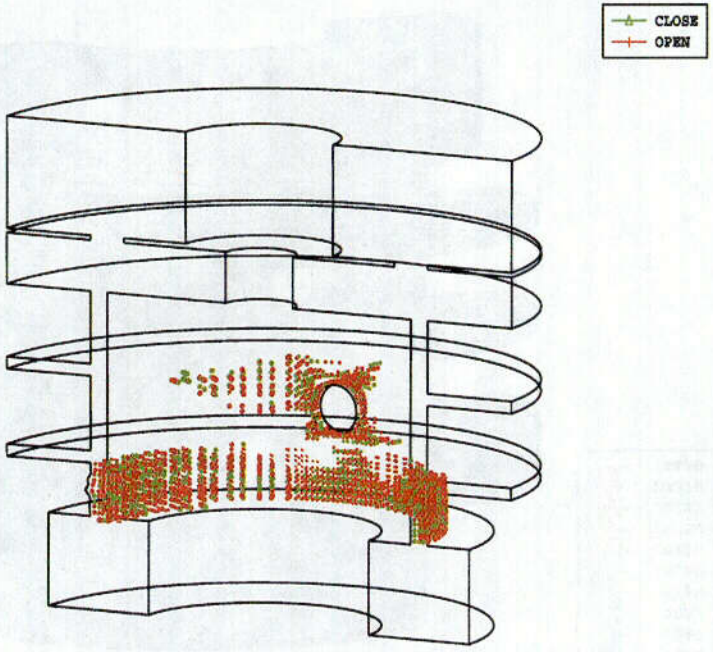

Figure 3.21 Cracking patterns for RCCV after S2(H+V)

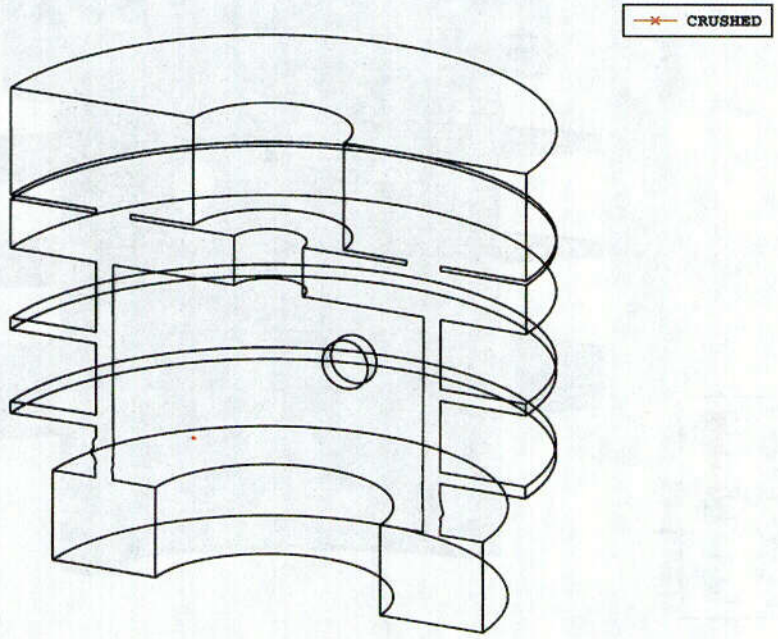

Figure 3.22 Points in compressive yield for RCCV after S2(H+V)

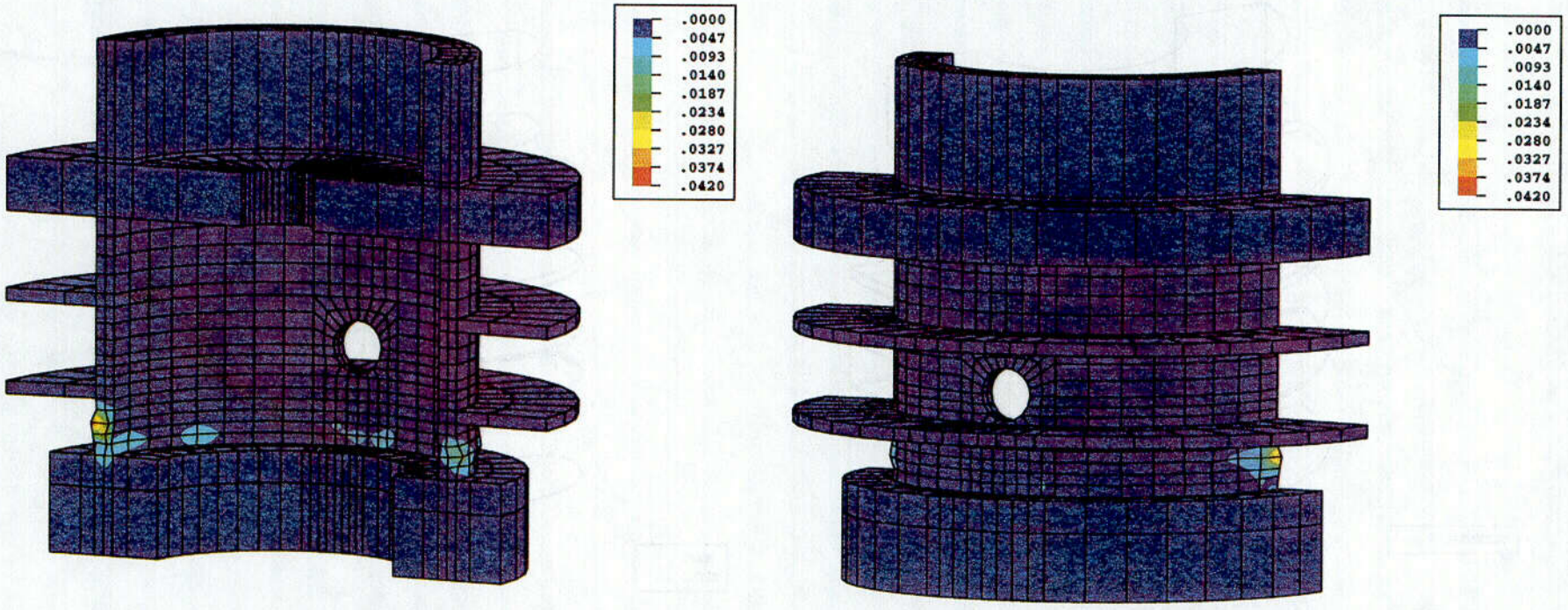

Figure 3.23 Concrete max. principal strains in RCCV after S2(H+V)

C-9

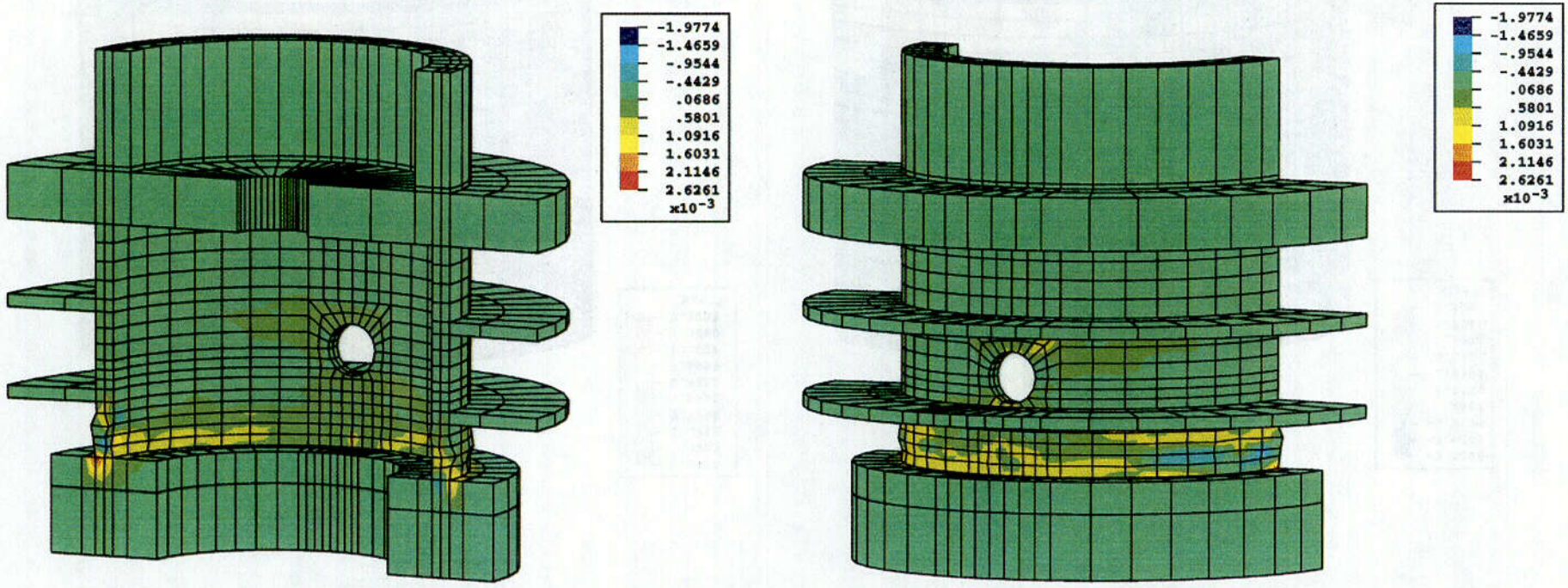

Figure 3.24 Concrete vertical strains in RCCV after S2(H+V)

C-10

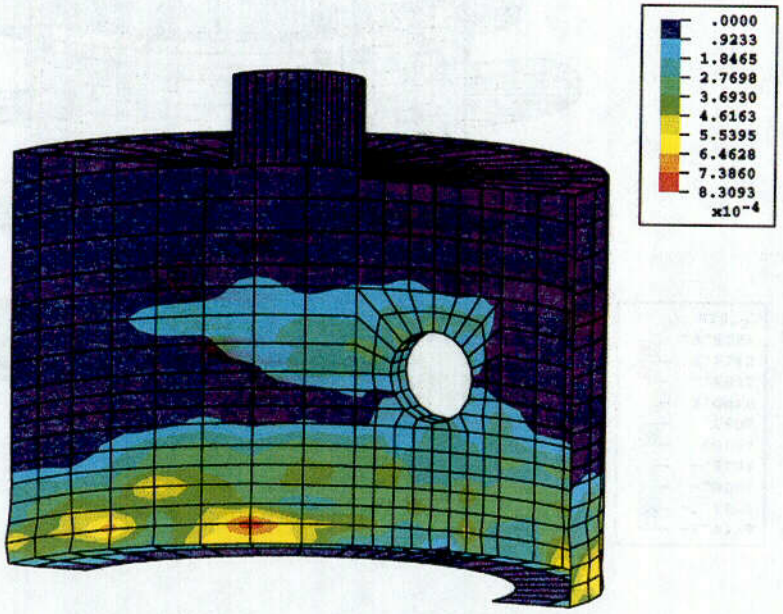

Figure 3.25 Liner max. principal strains in RCCV after S2(H+V)

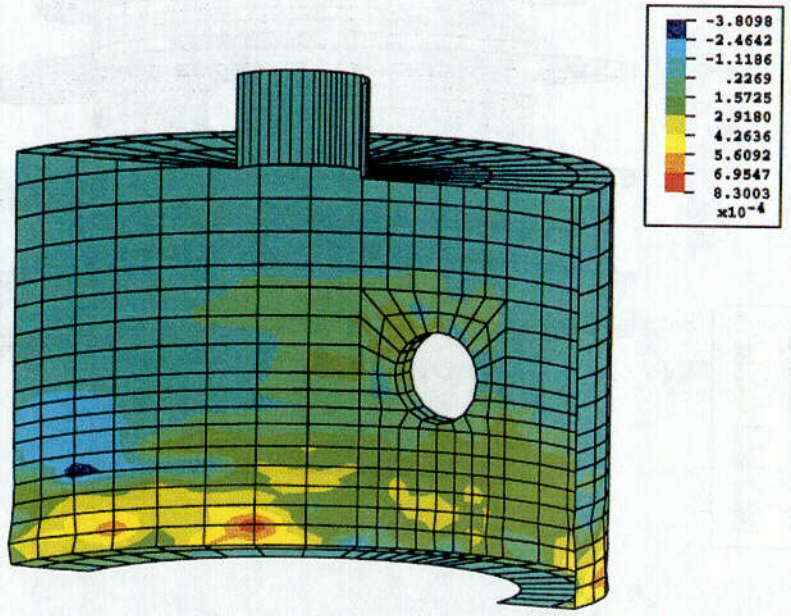

Figure 3.26 Liner vertical strains in RCCV after S2(H+V)

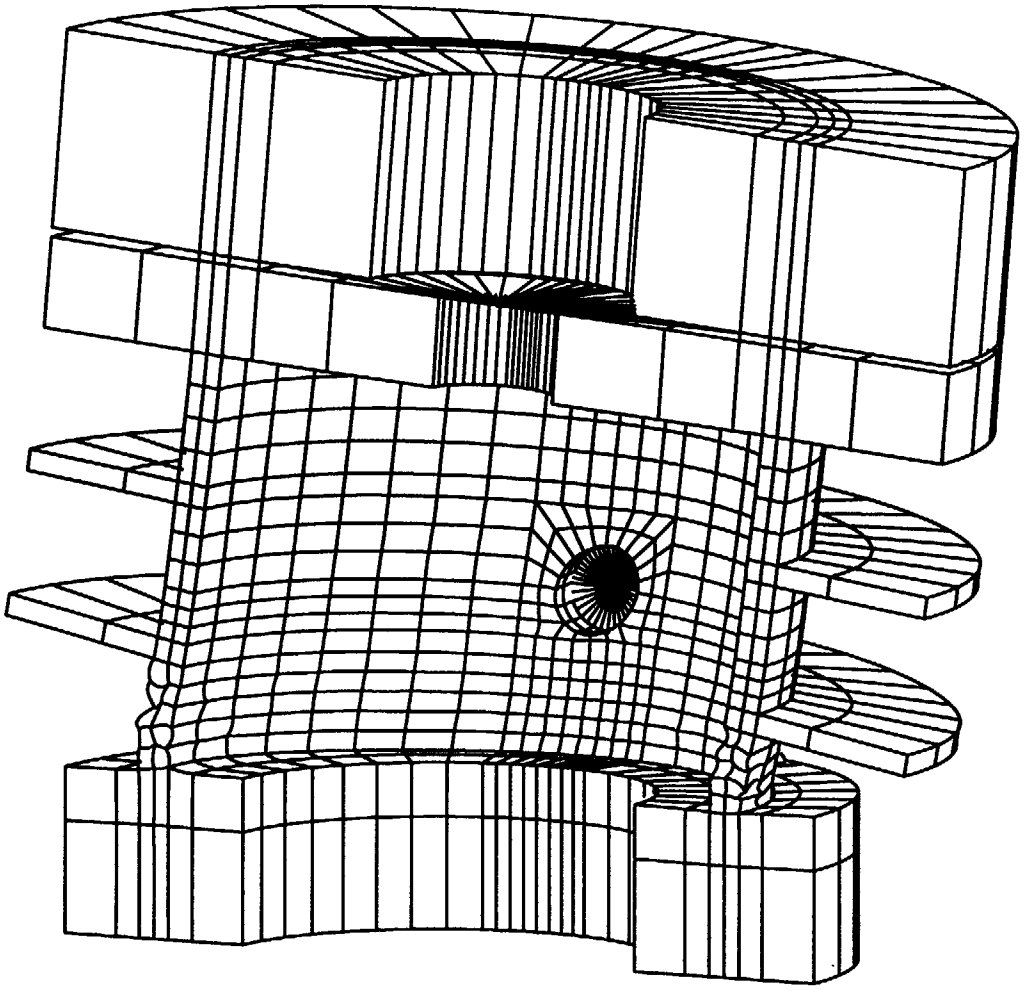

Figure 3.27 Modal shape and frequency for mode 1 after S2(H+V)

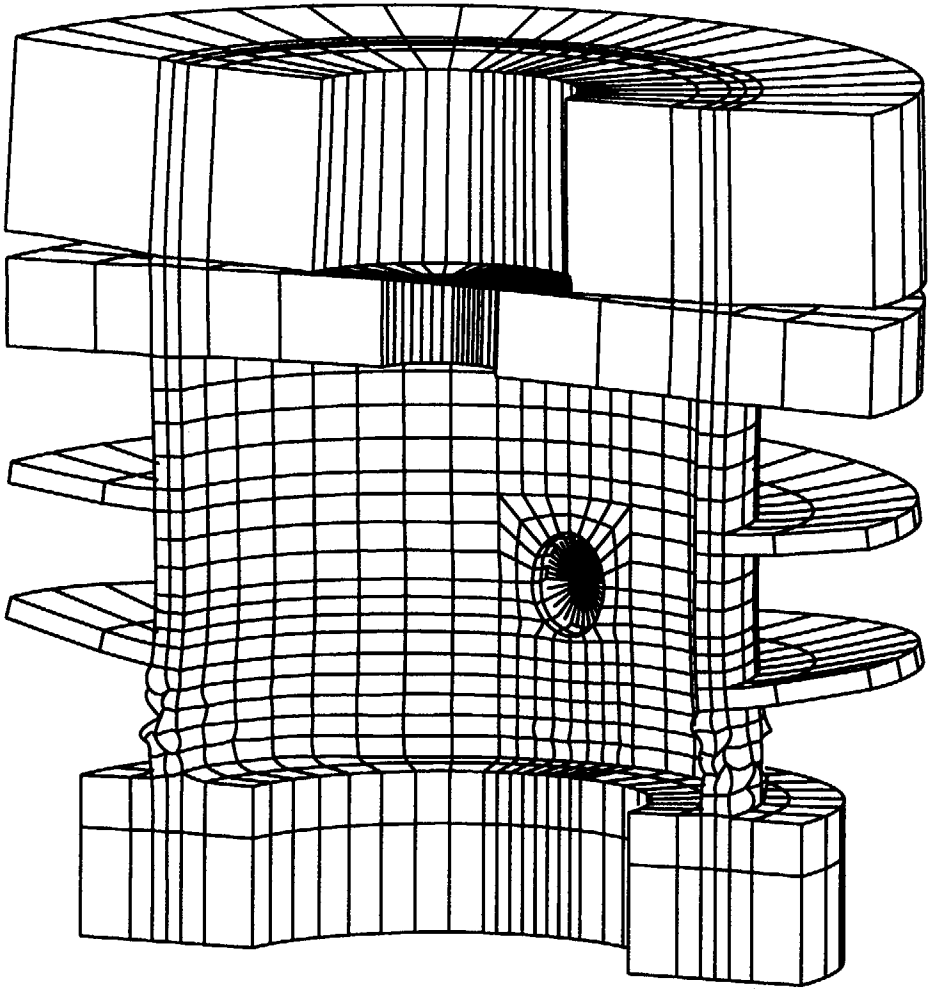

Frequency=36.816 Hz

Figure 3.28 Modal shape and frequency for mode 2 after S2(H+V)

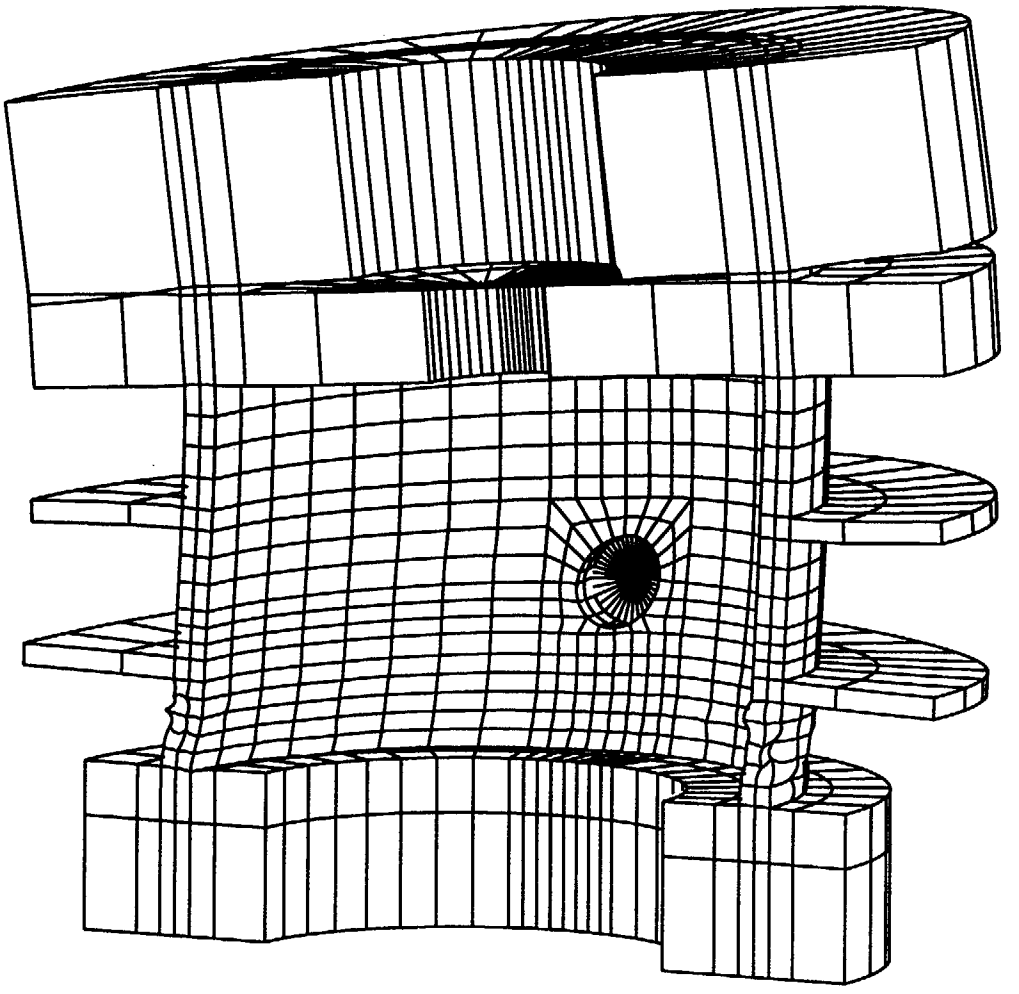

Frequency=38.880 Hz

Figure 3.29 Modal shape and frequency for mode 3 after S2(H+V)

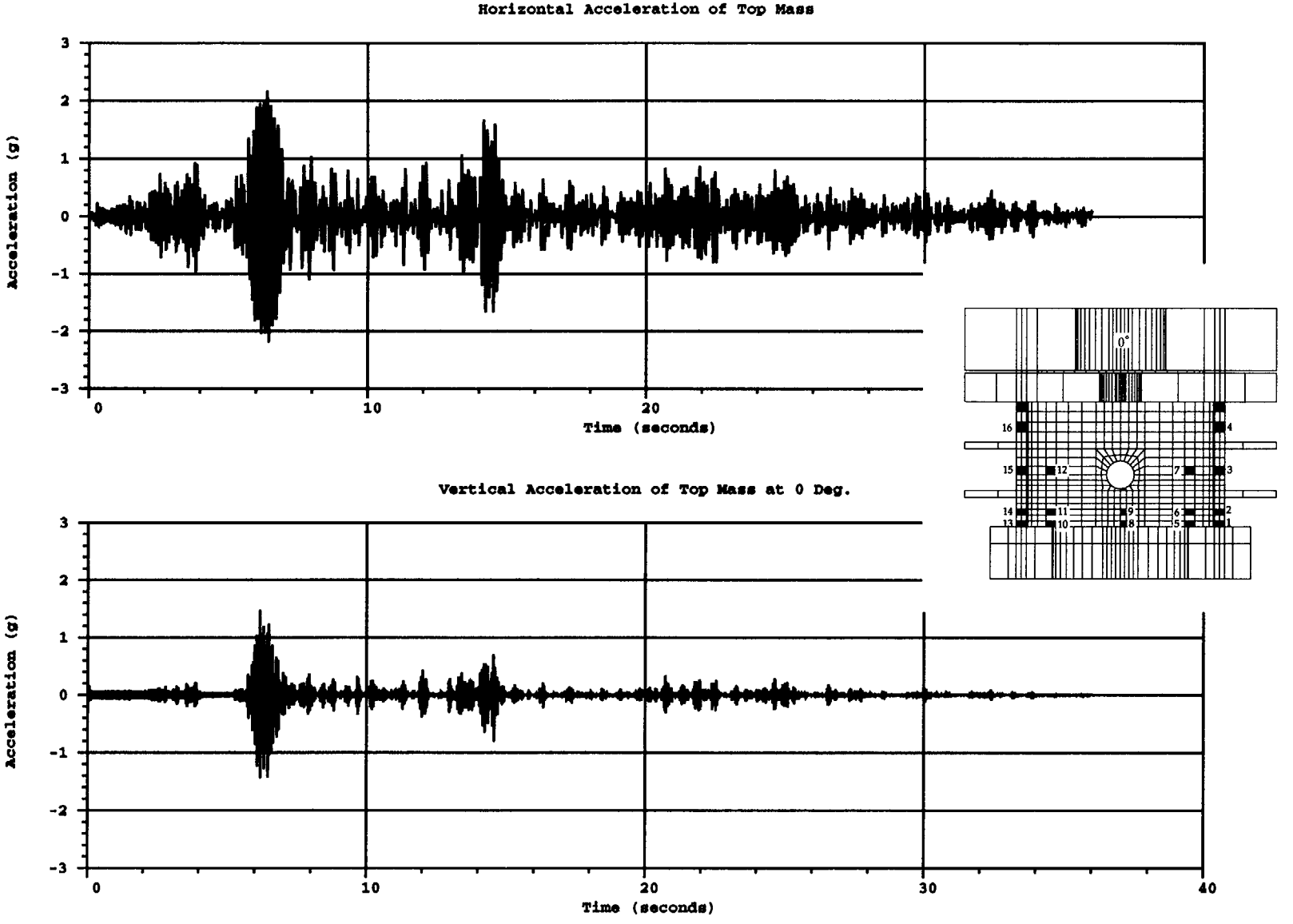

Figure 3.30 Total accelerations of RCCV under 2S2(H)

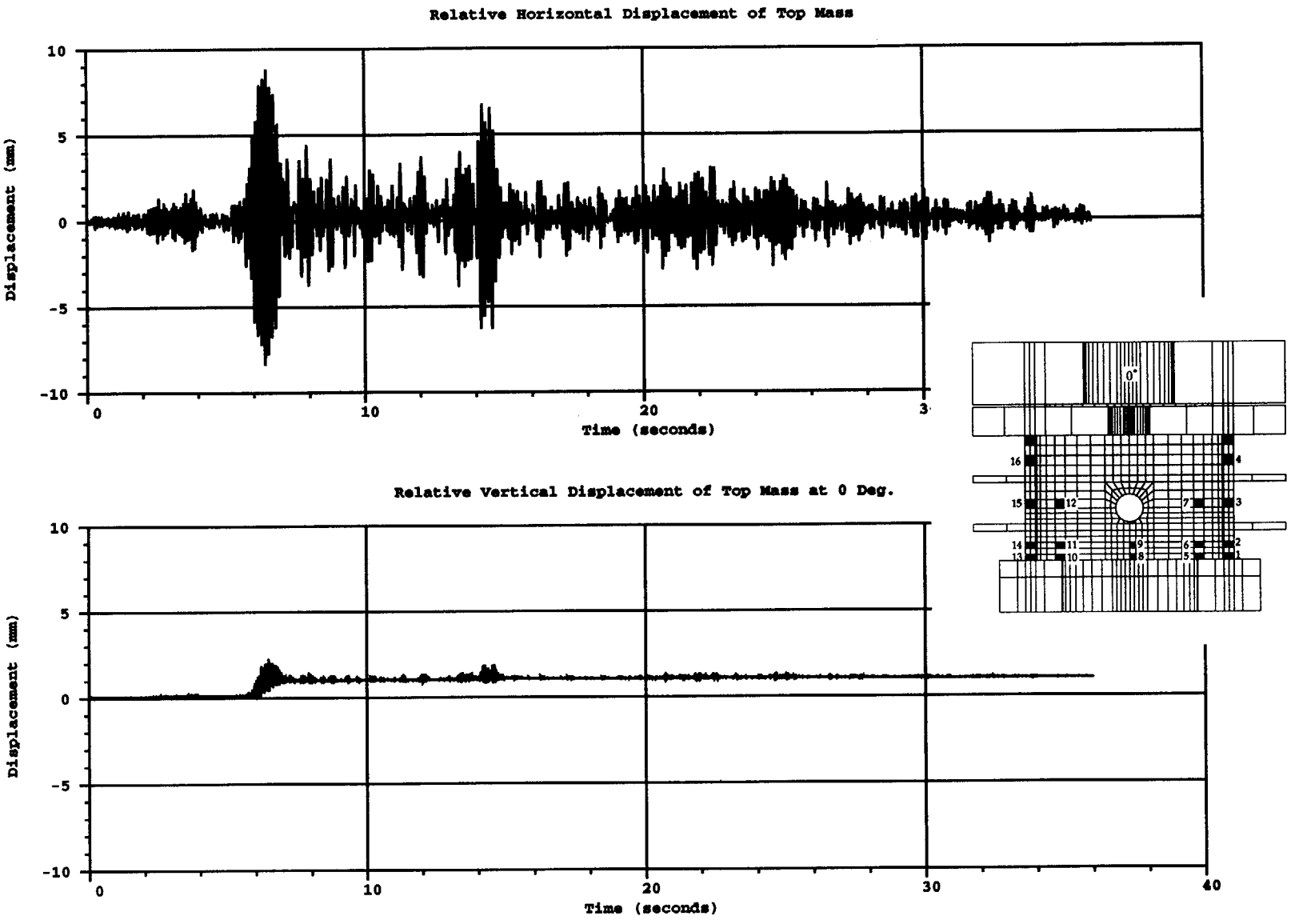

Figure 3.31 Relative displacements of RCCV under 2S2(H)

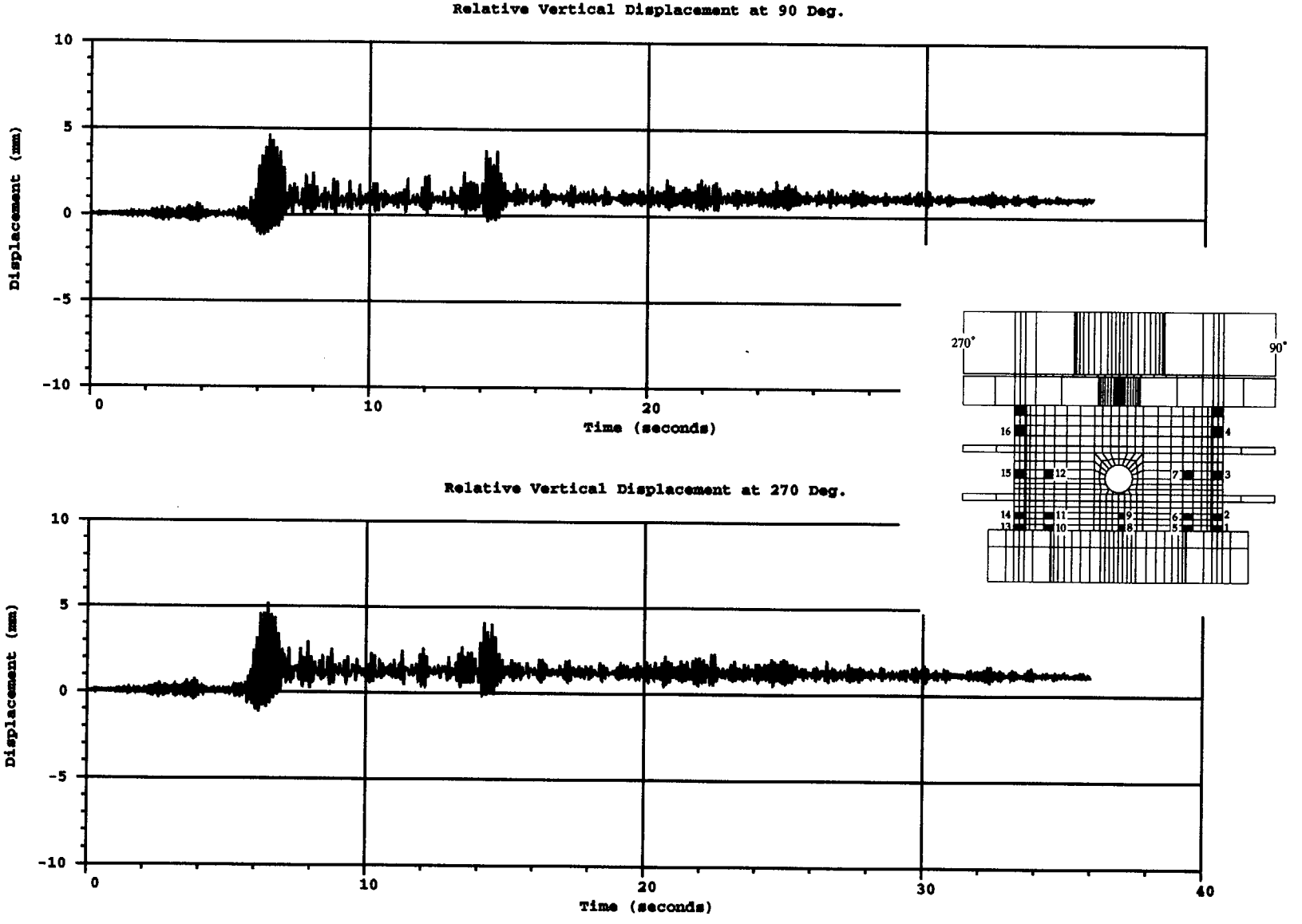

Figure 3.32 Relative vertical displacements of RCCV under 2S2(H)

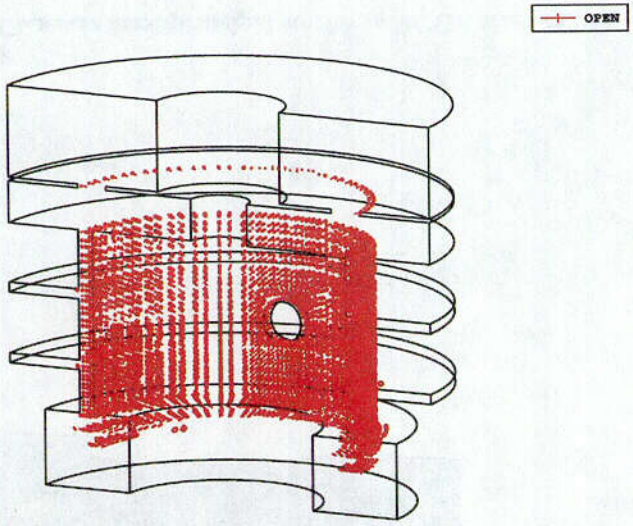

Figure 3.33 Open crack surfaces in RCCV after 2S2(H)

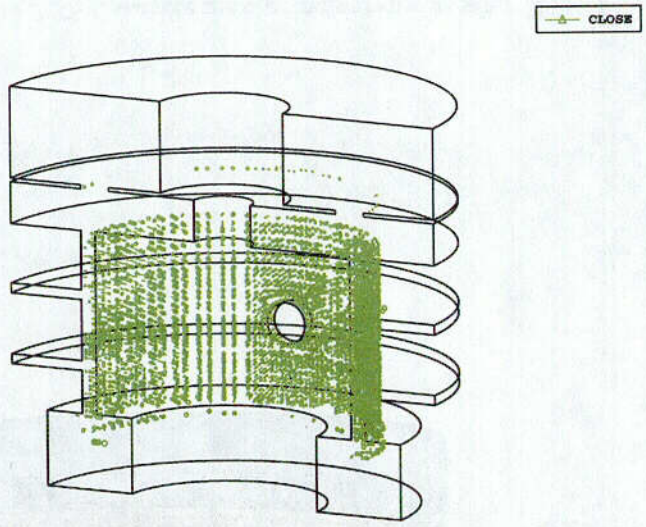

Figure 3.34 Close crack surfaces in RCCV after 2S2(H)

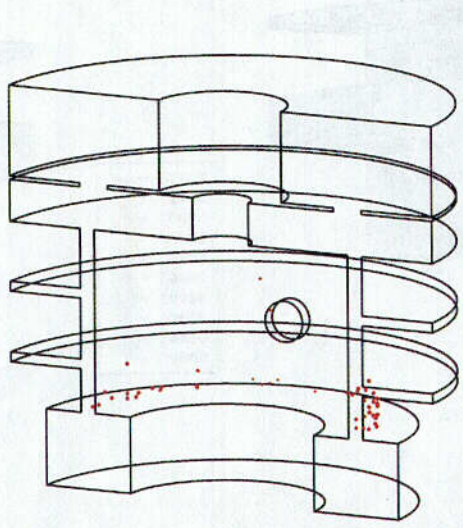

Figure 3.35 Points in compressive yield in RCCV after 2S2(H)

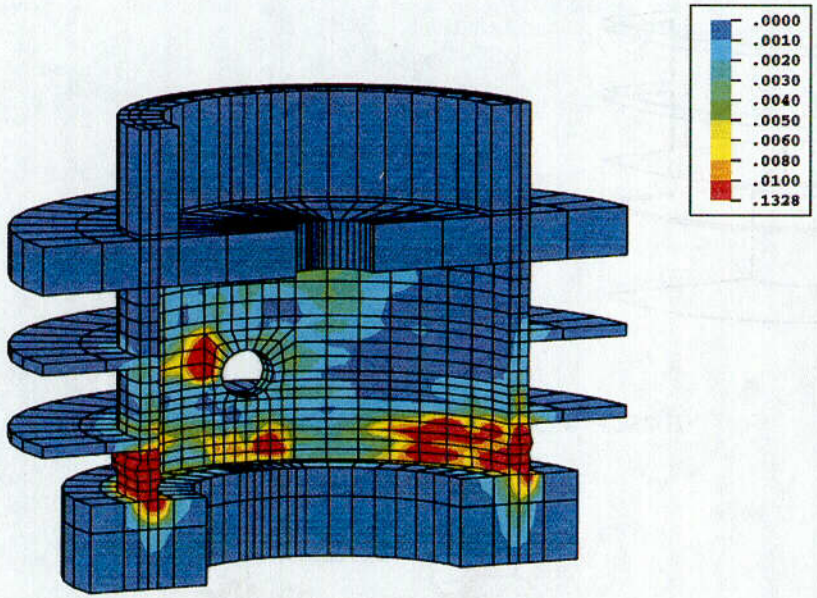

Figure 3.36 Concrete max. principal strains in RCCV after 2S2(H)

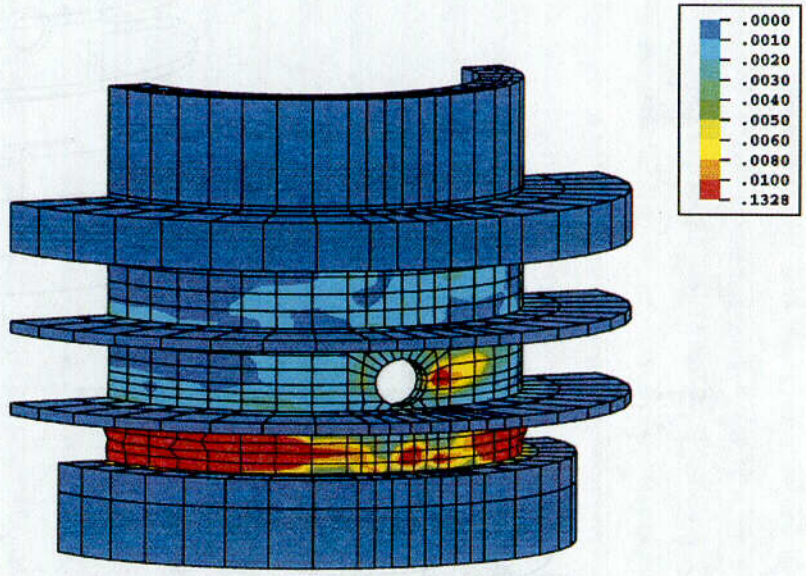

Figure 3.37 Concrete max. principal strains after 2S2(H)

C-13

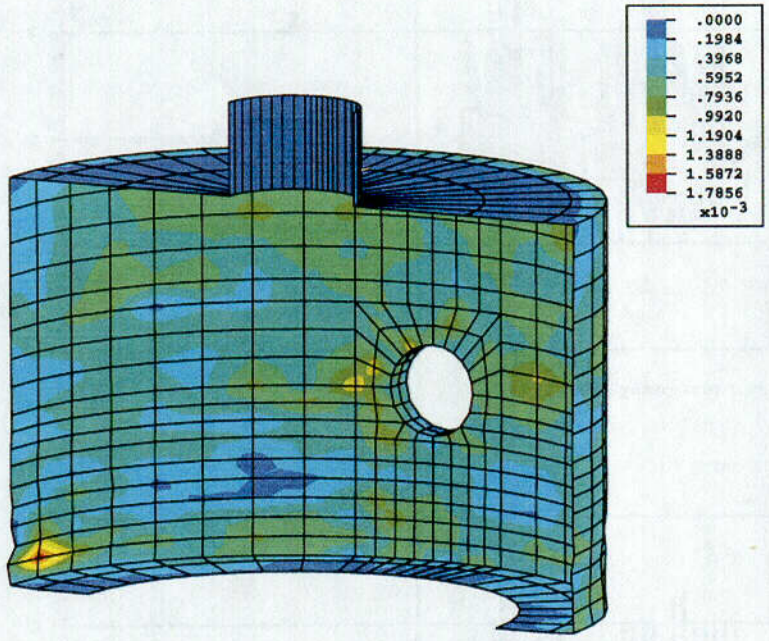

Figure 3.38 Liner max. principal strains in RCCV after 2S2(H)

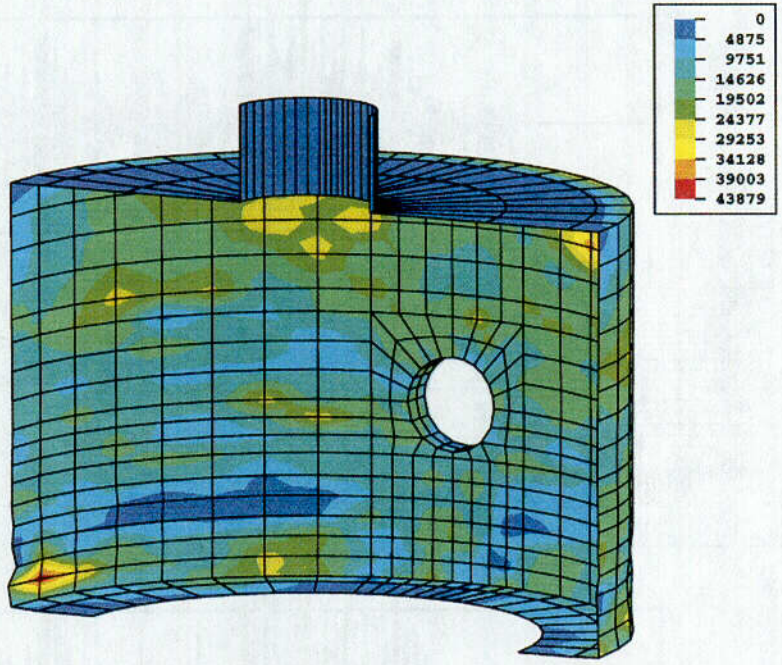

Figure 3.39 Liner max. principal stresses in RCCV after 2S2(H)

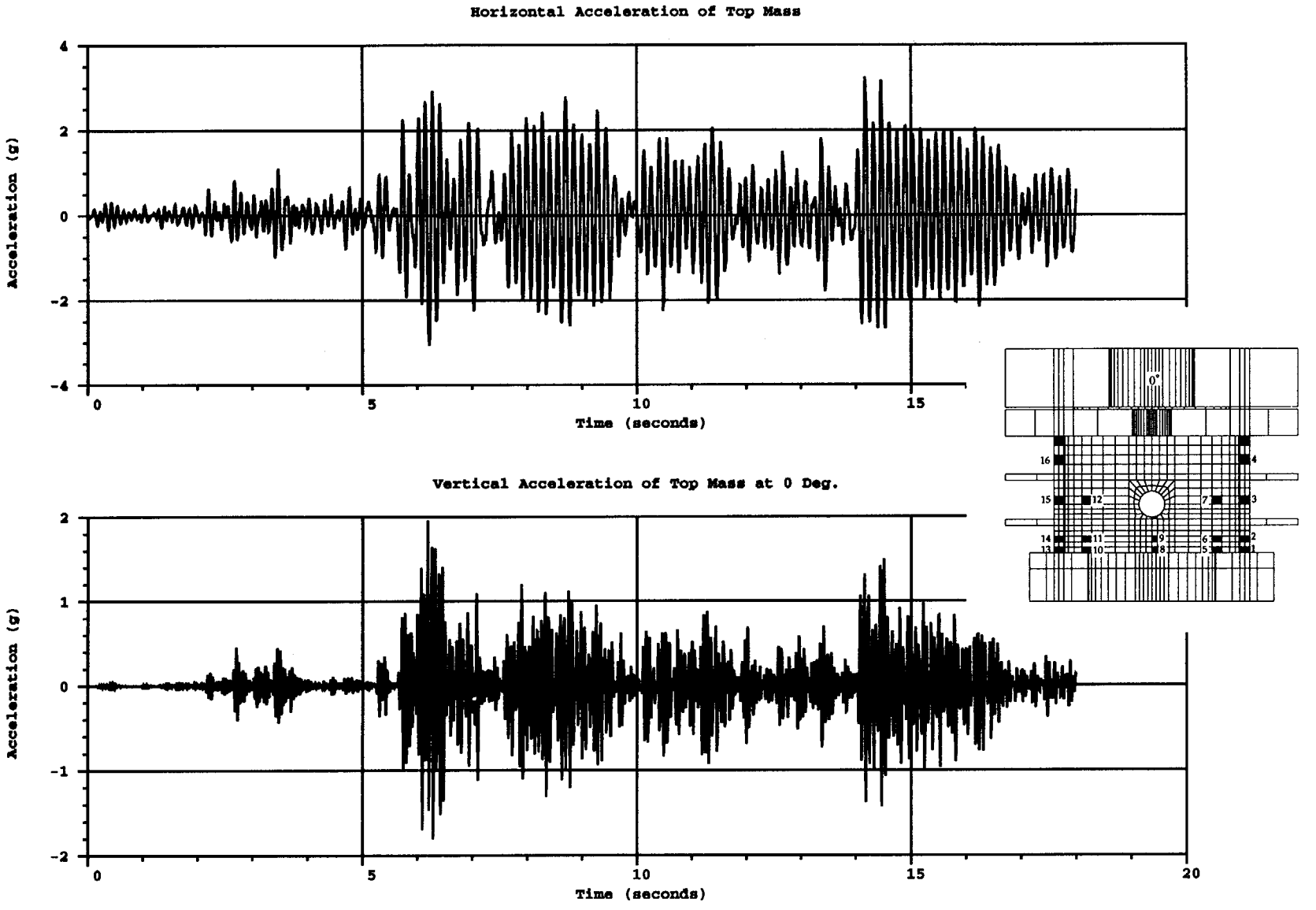

Figure 3.40 Total accelerations of RCCV under 4S2(H)

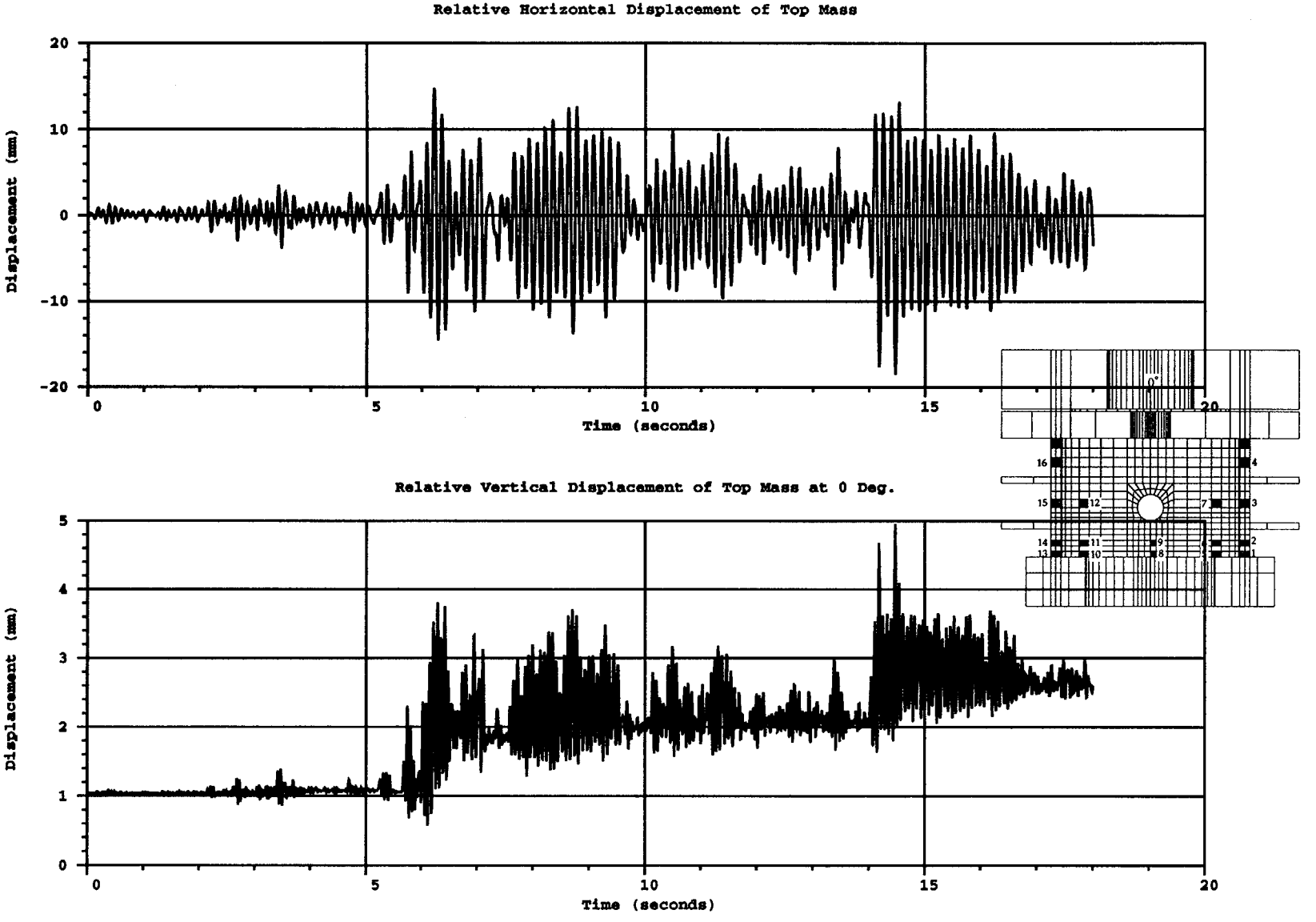

Figure 3.41 Relative displacements of RCCV under 4S2(H)

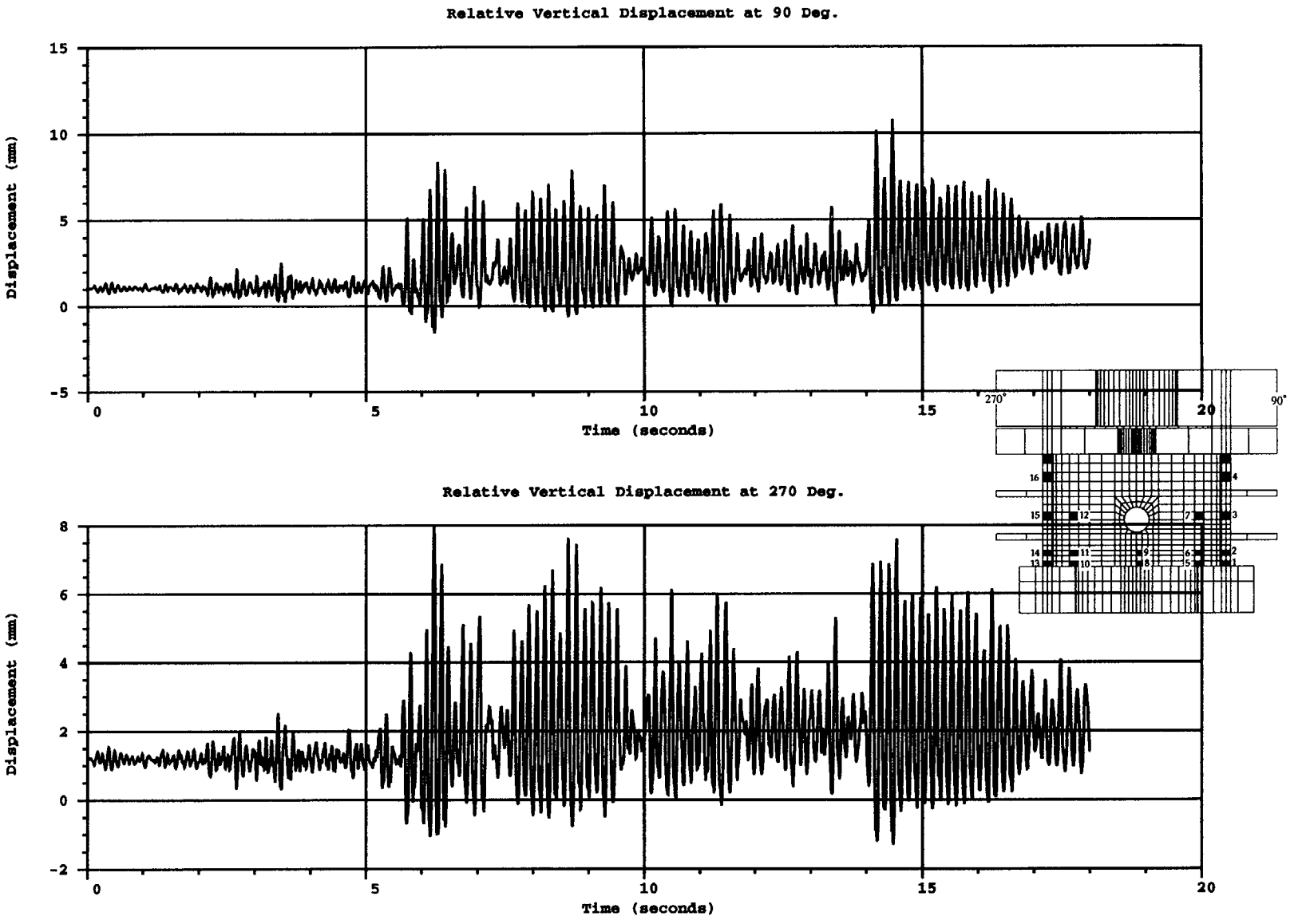

Figure 3.42 Relative vertical displacements of RCCV under 4S2(H)

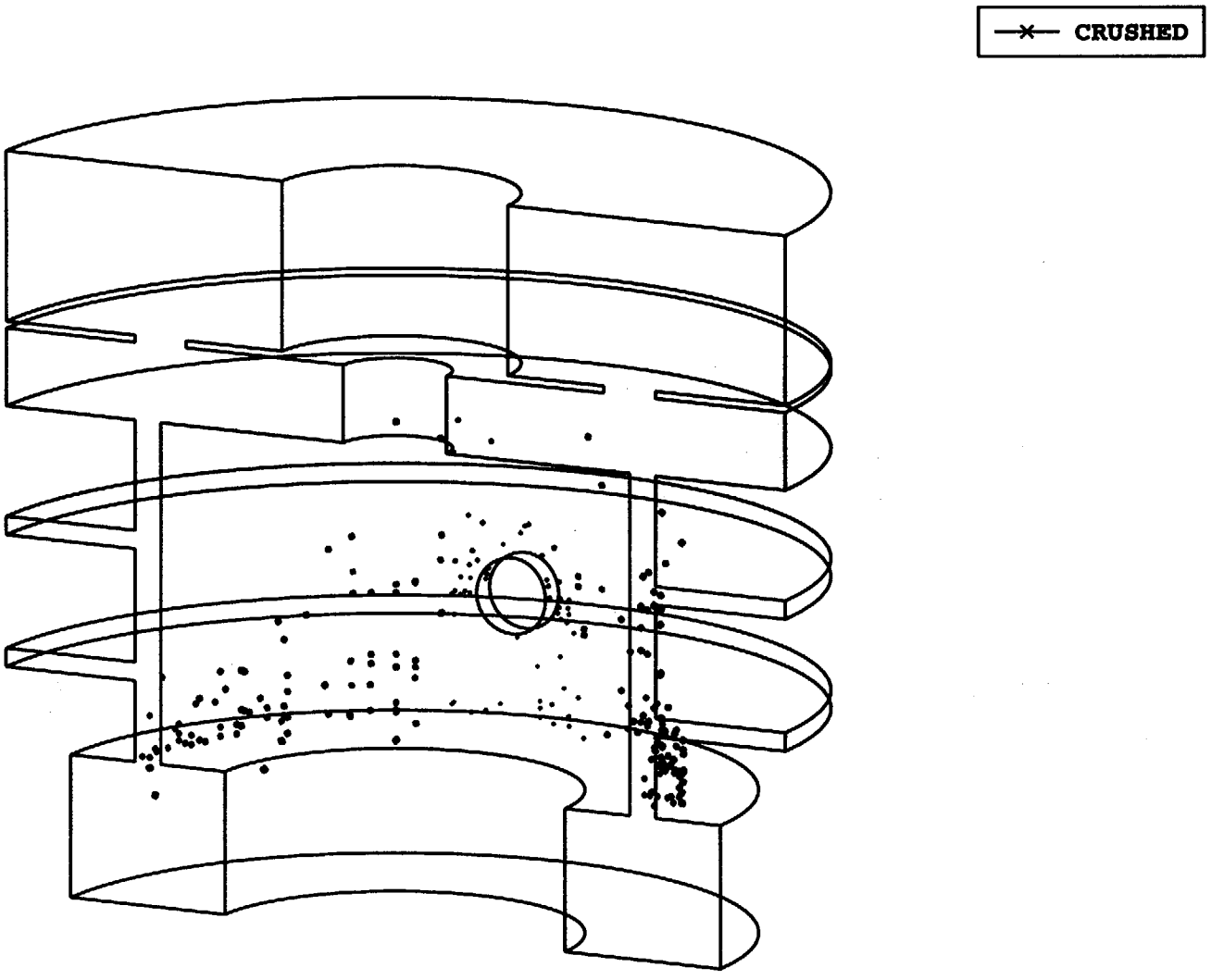

Figure 3.43 Points in compressive yield in RCCV after 4S2(H)

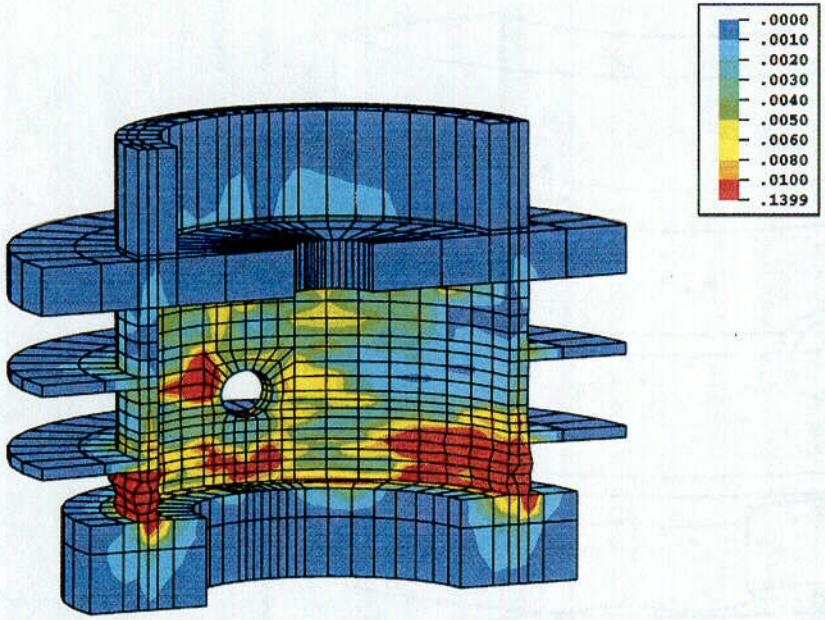

Figure 3.44 Concrete max. principal strains in RCCV after 4S2(H)

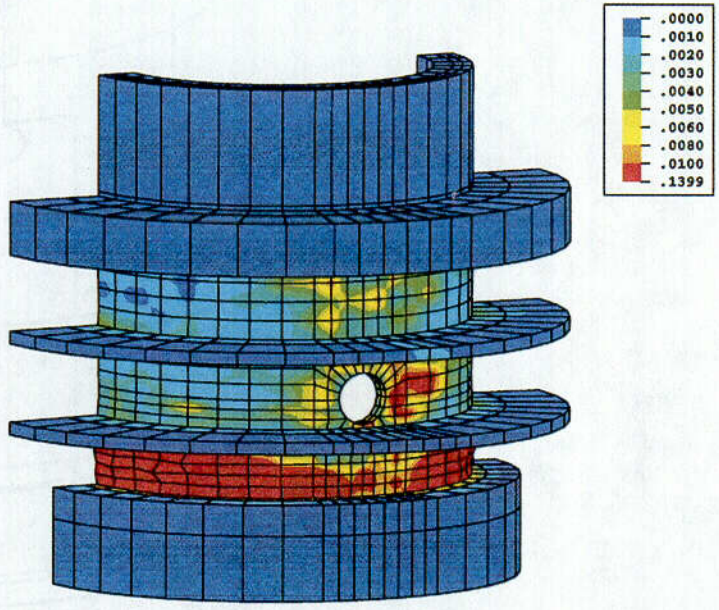

Figure 3.45 Concrete max. principal strains after 4S2(H)

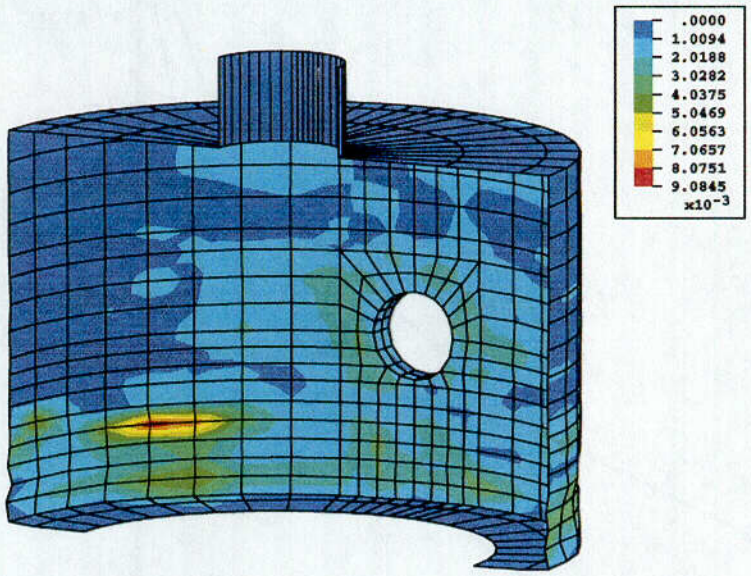

Figure 3.46 Liner max. principal strains after 4S2(H)

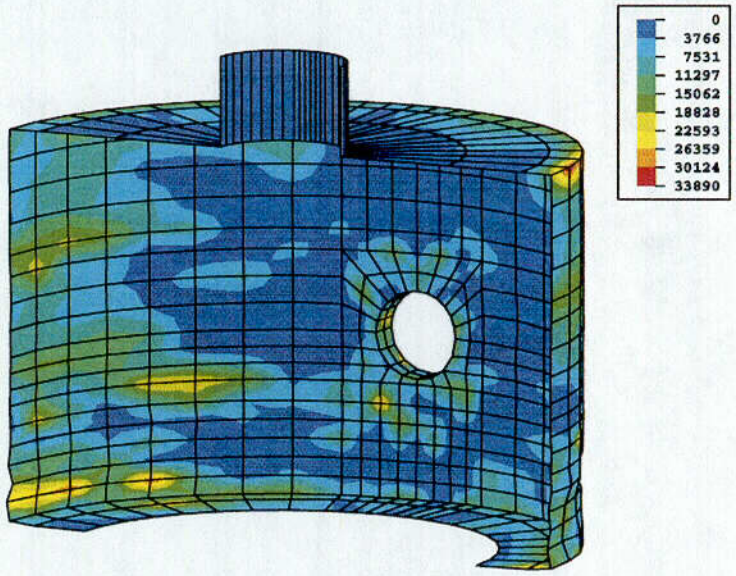

Figure 3.47 Liner max. principal stresses in RCCV after 4S2(H)

C-14

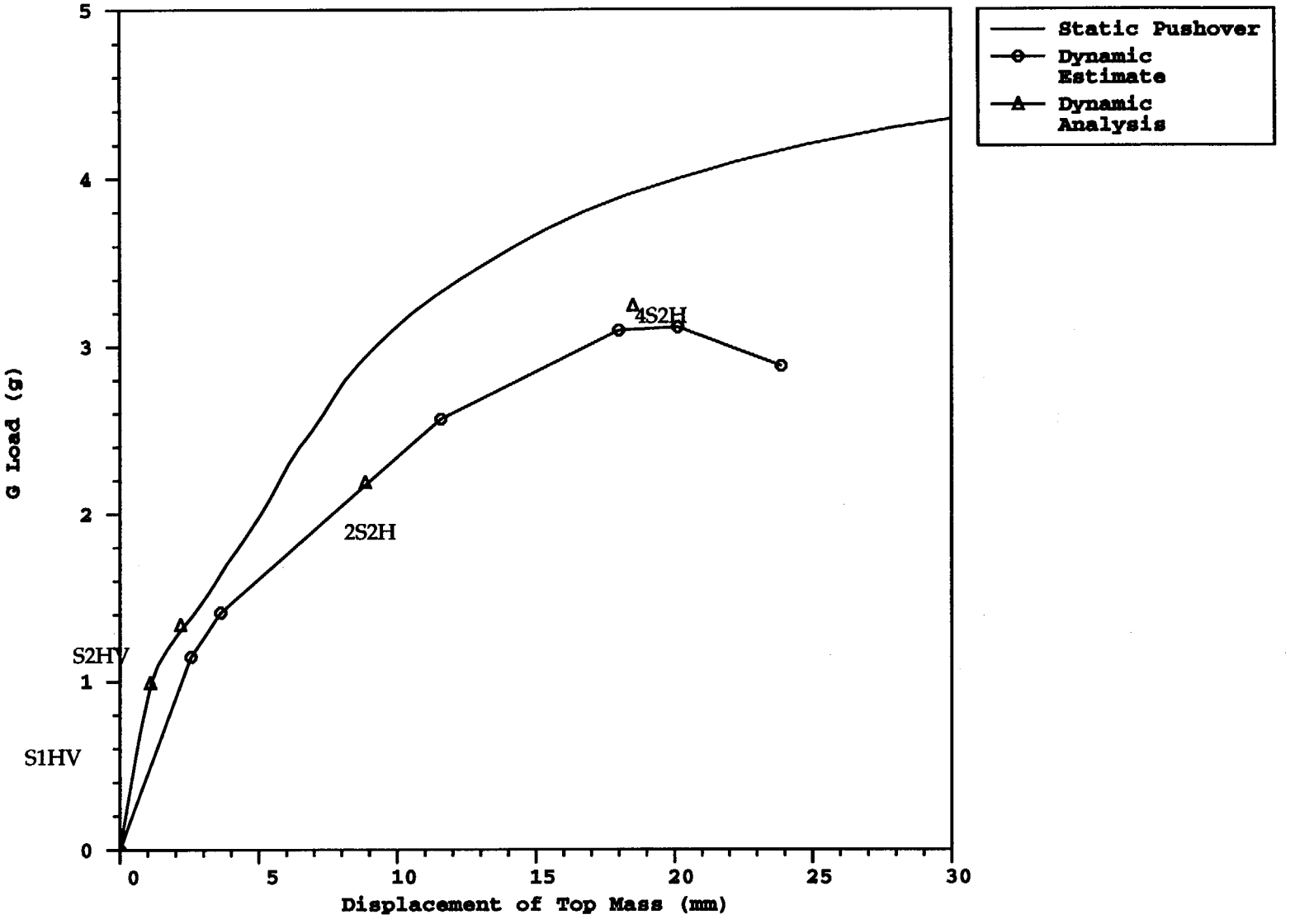

Figure 3.48 RCCV static and dynamic capacity analyses

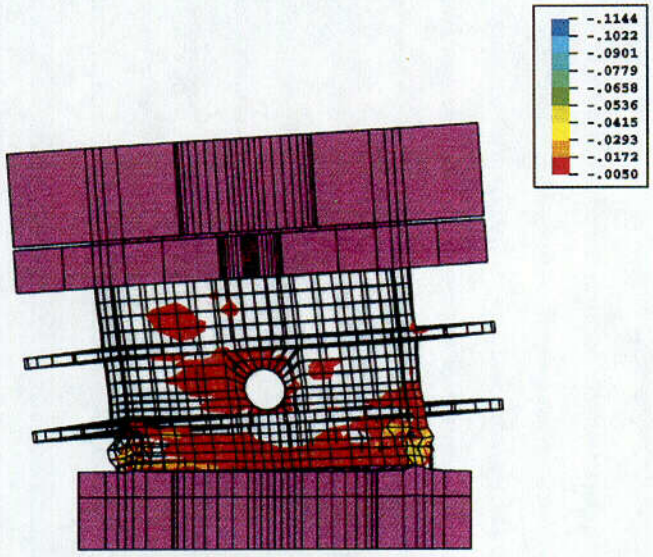

Figure 3.49 Shear strains in RCCV at 14.48 second under 4S2(H)

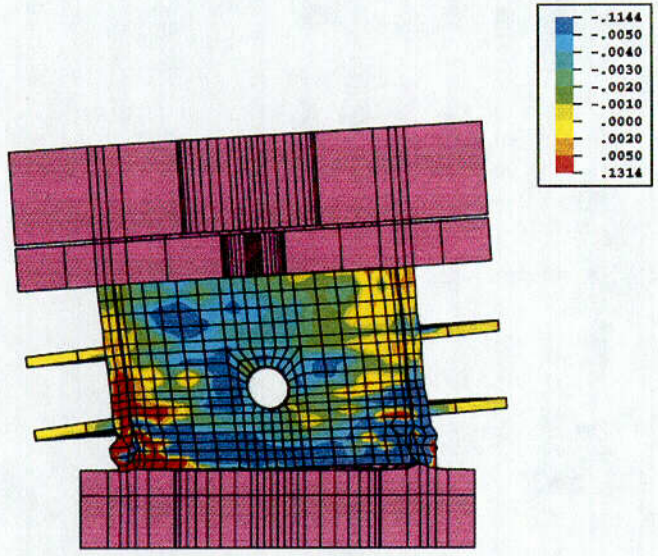

Figure 3.50 Shear strains in RCCV at 14.48 second under 4S2(H)

C-17

4. POSTTEST CALCULATIONS

4.1 Background

4.1.1 "Lessons Learned" From Tests

The RCCV analysis effort has benefited considerably from the lessons learned in the course of conducting the PCCV analysis (James et al., 1999a). However, as noted in the previous chapter, under cyclic conditions the shear stiffness of concrete in regions with a large number of cracks was still not well-understood prior to the RCCV test. The posttest analysis effort was directed at using the data from the RCCV test to calibrate the shear stiffness degradation as a function of crack size and shear cycles in the concrete analysis software.

In the PCCV model, the prestressing caused many cracks to close after they initially opened, while in the RCCV model, most of the cracks that developed remained open. After cyclic damage has accumulated, more cracks remain open in a reinforced concrete structure than for a comparable prestressed concrete structure. Correctly modeling the cyclic degradation of the shear stiffness of cracked concrete sections in reinforced concrete structures can be critical if significant shear loads exist. Therefore, the concrete material model needed to be modified to better account for cyclic degradation of the structural stiffness.

The testing sequence consisted of 15 major tests, as depicted in Figure 4.1. After each major test, the resonant frequencies were measured by subjecting the RCCV model to low-level broadband random vibrations. Frequency response functions, which are commonly referred to as transfer functions, were calculated from the measured random vibration test data, and the resonant frequencies were estimated from the transfer functions. These estimated resonant frequencies are not exact values. They can vary depending on which acceleration gages are used to calculate the frequency response functions, and on the method of selecting the resonant frequency from the transfer function. For example, frequency can be estimated to occur at the 90° phase shift, or at the peak magnitude, or by other measures. Figure 4.1 shows the approximate value of the lowest fundamental frequency of the RCCV after each major test that was performed. This figure also plots the calculated value for the analytical model after the respective test simulation.

Each of the horizontal tests identified in Figure 4.1 resulted in companion vertical and rotational (rocking) components with unexpectedly large amplitudes. Moreover, the measured basemat motion was significantly different than the intended target input motion. These effects are due to the unavoidable interaction between the RCCV model and the shake table due to the large mass of the test structure. The posttest analysis uses averages of the horizontal and vertical components of motion recorded at the top of the basemat, and calculates a rigid body rotation of the basemat based on differences in the vertical acceleration components. The horizontal, vertical, and rigid body rotation of the basemat are used as input to the posttest analyses.

Much of the analytical simulation complexities encountered in the RCCV posttest analysis stemmed from these differences between the target input motion and the actual measured motion at the control points on the basemat. Early in the test, these greater-than-target-value motions caused significant cracking and a considerable reduction in stiffness. This affected the nonlinear behavior of the structure and also caused the structure to be sensitive to small changes in the loading, particularly in the initial stages of the test sequence. This can be readily observed from the experimental record of the test model fundamental frequency vs. loading sequence depicted in Figure 4.1. This figure shows that the initial tests significantly reduced the frequency due to stiffness degradations. Later tests were much larger in magnitude, but the increased loading did not cause much additional frequency shift. This is attributed to the large extent of cracking that is induced during the design level testing. Note that frequency shift is related to the square root of the stiffness degradation; a 20% reduction in stiffness changes the frequency by 10% and a 50% change in stiffness is required to change the frequency by 30%.

The first test result worthy of note is that the initial pressure test produced cracking that changed the frequency from an initial value of 13.5 Hz to a value under 12.5 Hz. The dynamic test that followed the initial pressure test was intended to be the S1(H) target input, but the actual basemat recorded motion was equivalent to 1.3S1(H) horizontal plus significant vertical and rocking components. This initial test further reduced the fundamental frequency to a value of 9.6 Hz. The stiffness degradation continued, but at a lower rate, with each subsequent event, even for

tests with nearly equal magnitudes. Such behavior is highly symptomatic of the dependence of structural stiffness on the number of dynamic load reversals. This implies that with each test, new damage is introduced as the number of cycles increases, as long as the amplitude of the accelerations are greater than some damage threshold level. The LOCA test, which includes internal pressure, does not appear to contribute as much to the stiffness degradation. The failure level tests continue to degrade the stiffness and lower the fundamental frequency but at a somewhat reduced rate even though the magnitudes are increasing. This is attributed to the fact that in a heavily damaged structure, more and more damage is required to further reduce the frequency. Consider that prior to the 2S2(H) test, the fundamental frequency of the RCCV test model was reduced by 50%, which means that the stiffness dropped by 75%. To capture this structural behavior, the material properties that govern the dynamic response, namely shear stiffness along the crack surface, compressive stiffness normal to the crack surface, and damping, must be made to depend on the number of loading cycles.

4.1.2 Differences Between Pretest and Posttest Analyses

In the case of damping, damage-dependent viscous damping was found to play an important role in the dynamic response of the PCCV as an energy dissipating mechanism, as discussed in James et al. (1999a). This is in addition to the hysteretic damping that naturally results from the energy-dissipating cracking and plastic deformations. Similarly, the structure's shear resistance to high-amplitude dynamic loading is strongly dependent on the local deformation mechanisms at crack surfaces. The correct modeling of these mechanisms is crucial to the predictive capability of the analysis software. The complex interaction that develops at the crack surfaces under a large number of rapid load reversals poses a challenging problem of material constitutive modeling. This situation is further aggravated by the fact that material characterization experiments under high-frequency cyclic loading, which are needed to derive behavioral models, are virtually nonexistent. Nevertheless, without introducing the appropriate form of cyclic dependence in the material constitutive model, the posttest analysis effort of the RCCV would contribute very little to the current state of the art. Therefore, it became necessary to use a subset of the test records to develop cyclic dependence in the ANACAP material model for cracked material points for the three relevant constitutive properties, namely the shear modulus of cracking concrete, the viscous damping ratio, and the compression modulus of a closed crack. This development is described in some detail in Appendix C.

The dependence of these three constitutive properties on the number of cycles, cumulatively from test to test, requires that all tests identified in Figure 4.1 must be analyzed. However, because of the excessive computing demands and length of time needed to complete each analysis, only selected tests could be analyzed. These are identified in Figure 4.1. NUPEC provided test data to Sandia for the initial pressure tests, and the seismic tests of 1.1S1(H), 1.1S1(V), 1.1S1(H+V), 1.1S2(H), 1.1S2(V), 1.1S2(H+V), LOCA+1.2S1(H+V), 2S2(H), 3S2(H), 4S2(H), 5S2(H), and 9S2(H). Intermediate tests were performed for which Sandia did not get the test data. During all of the tests, including the intermediate tests, cumulative damage occurred. A subset of the actual tests performed was analyzed, with the analyses performed sequentially, so that damage calculated from previous analyses became the initial condition for subsequent analyses. To account for damage from tests that weren't analyzed, preconditioning analyses were performed as necessary. These conditioning analyses used short segments of strong motion input accelerations from appropriate tests, modified as described later in this chapter, to estimate damage that occurred from the intermediate tests. These preconditioning analyses brought the calculated and measured frequencies closer, in an attempt to simulate the test damage not simulated in the analytical model.

The addition of cyclic dependence of shear modulus, compressive modulus, and damping in the concrete material model required development and verification. The numerical methods for identifying a cycle that contributes to degradation and for establishing the dependence of the properties on cycles must be developed and implemented. The calibration and verification of cyclic degradation relative to damping must also be established. Because this development and verification must occur over the entire span of the test sequence, each test of a cyclic degradation implementation requires many sequential analytical simulations. Therefore, to stay within the project schedule, a less-refined finite element mesh was required for the posttest analyses. A coarse mesh, illustrated in Figure 4.2, was developed to significantly reduce the computer resources needed for the simulations. As illustrated, this coarse mesh model uses only one element through the wall thickness, and it significantly reduces the element discretization around the circumference of the cylindrical wall. In

addition, this model does not include the equipment hatch penetration. While this coarse model provides less refinement for local results, such as liner buckling or stress concentrations near the penetration, it is shown that the coarse model does provide adequate simulation for the overall structural response. Figure 4.3 plots a comparison between the test results, the fine mesh results, and the coarse mesh results for the horizontal displacement of the top slab during the S1(H+V) test. Figure 4.4 shows a similar comparison for the horizontal acceleration response of the top mass during the S1(H+V) test. These plots demonstrate that the coarse mesh model is sufficient for the overall structural response. It is expected that strain histories for the reinforcement and in the liner at specific gage locations may not be as good as the fine mesh since the coarse mesh will not capture local effects as well. The liner and rebar strain response can also vary significantly in local areas where concrete cracking or liner buckling develops.

4.2 Design Level Analyses

The fundamental frequency of the as-built RCCV analytical model is calculated as 15.1 Hz. This differed from the experimentally determined frequency, which was given as approximately 13.5 Hz. The higher analytical value is believed to be due to the use of a higher than actual value for the elastic modulus of the concrete. The elastic modulus was based on the ACI formula and would not represent the true modulus at origin of the stress-strain curve. In the absence of stress-strain curve test data specific to the model, the elastic modulus was adjusted to obtain a satisfactory match between the experimental and analytical frequencies.

The test sequence began by subjecting the RCCV model to a static pressure test, which, as expected, induced some cracking. The effect of the pressure-induced cracking was to reduce the experimentally determined fundamental frequency from 13.5 Hz to a value slightly below 12.5 Hz. After the pressure test, the model was subjected to the S1(H) motion, followed by a frequency measurement. The measured accelerations at the basemat deviated significantly from the target input, as discussed previously. The measured input is equivalent to 1.3S1(H) accompanied by a strong vertical and rocking components. After this 1.3S1(H) test, the experimentally determined frequency dropped to 9.6 Hz, indicating significant additional cracking.

The test structure was then further subjected to three more dynamic tests with target input motions simulating S1(H), S1(V), and S1(H+V). However, the measured base motions for these tests are equivalent to 1.1S1(H), 1.1S1(V), and 1.15S1(H+V), respectively, and also contain basemat rocking. The frequency measurements showed a continuous drop to slightly above 8 Hz after the S1(H+V) test.

The analysis plan calls for the S1(H+V) simulation as the first dynamic test to be analyzed. However, the 1.3S1(H) test caused substantial damage, and significant stiffness degradation also occurred in the following tests. This damage must be included in the analytical simulation for the S1(H+V) test. Since the measured base motion and results for the 1.3S1(H), 1.1S1(H), 1.1S1(V), and 1.15S1(H+V) were not provided to Sandia, an analytical simulation of the cumulative damage that occurred in these tests was necessary before attempting the 1.1S1(H+V) test analysis for comparison to the provided experimental data. This analytical simulation was performed with a preconditioning analyses with combined horizontal and vertical target input motions. The preconditioning analyses caused the fundamental frequency to decrease by amounts similar to those observed from the tests. The input motion used for this preconditioning analysis consisted of a combined horizontal, vertical, and rotational motion obtained by multiplying the S1(H+V) test records by the factor 1.3.

After the preconditioning analysis was applied, the RCCV model was analyzed using the 1.1S1(H+V) measured base motions, which consisted of horizontal, vertical and rotational (rocking) components, as shown in Figure 4.5. The fundamental frequency, measured and calculated at the end of the 1.1S1(H+V) test was 8 Hz. The calculated horizontal and vertical displacement histories of the top slab are shown in Figures 4.6 and 4.7, respectively, together with the measured displacement response. A similar comparison for test data and analysis results for the horizontal and vertical acceleration response of the top mass is shown in Figures 4.8 and 4.9. As these figure show, the quality of the analytical results was quite good. Comparisons of strain response in reinforcing bars and liner plate for the test data and analysis results are provided in Appendix B.

The analysis of the 1.1S2(H+V) test followed the S1(H+V) analysis. In the test sequence, intermediate tests for 1.1S2(H) and 1.1S2(V) preceded the 1.1S2(H+V) test. Again, the damage induced in the model for these intermediate tests were simulated with a preconditioning analysis prior to the

1.1S2(H+V) analysis to bring the analytical fundamental frequency down to the level present in the test model. The input motions for the S2(H+V) test simulation, which are constructed from the measured response at the basemat, are shown in Figure 4.10. The displacement results for the top slab, compared with the measured response, are shown in Figures 4.11 and 4.12 for the horizontal and vertical response, respectively. Comparisons for the acceleration response of the top mass for the S2(H+V) test are shown in Figures 4.13 and 4.14. Visual comparison of the measured and calculated time histories again indicates close agreement. The frequency dropped to 6.8 Hz with the analytical model having a slightly higher fundamental frequency. Comparison of strain response for rebars and the liner are provided in Appendix B.

It is apparent that for these levels of design basis seismic loading, the RCCV suffers substantial concrete cracking damage and the seismic response is nonlinear. This is a significant finding since in the U. S. the Operating Basis Earthquake (OBE) is typically evaluated based on linear assumptions and the OBE levels could reach those of the S1 level tests. In addition, the RCCV test model exhibited significant shifts in the fundamental frequency for the S1 level tests. Part of this frequency shift may be attributed to the 1.3S1(H) loading, which was larger by a factor of 1.3 than a 1.0S1(H) event would have been. Thus, the seismic response of an RCCV structure will depend not only on the magnitude and frequency content of the earthquake, but also on the prior seismic history of the structure.

4.3 Posttest Failure Level Analyses

After the design level tests, the test plan called for subjecting the model to increasing multiples on the S2 level magnitudes until structural failure occurs. For these tests, only horizontal input motion on the basemat was planned. However, increasing horizontal amplitudes without control of the vertical component caused substantial feedback and rocking of the RCCV test model on the shake table, resulting in rather substantial vertical acceleration input at the basemat. The final sequence of failure-level tests for the RCCV test model was 2.0S2(H), 3.0S2(H), 4.0S2(H), 5.0S2(H), and 9.0S2(H). The concrete rubblized and spalled in large areas in the wall near the basemat and around the equipment hatch penetration in the test model early in the 9.0S2(H) test.

The posttest analysis simulated the 2S2(H), 3S2(H), 5S2(H), and 9S2(H) tests. A portion of the 4S2(H) measured input record was applied to the analytical model before the simulated 5S2(H) test to account for the accumulation of damage without calculating the entire 4S2(H) test. Again, the basemat acceleration input for the analysis was constructed from the accelerometer data recorded in the respective tests for the gauges mounted on the basemat. Horizontal, vertical, and basemat rocking input, as recorded on the basemat, is used in the analytical simulation. It should be emphasized that substantial cracking damage and cyclic degradation has and continues to occur in these simulations. The RCCV test and analytical models have 50-70% stiffness reduction as evidenced by the continued decline in the fundamental frequency. In the analytical model, virtually every material integration point in the RCCV wall has cracked and most had three cracked directions at each point. The continued stiffness degradation was due to continued degradation of the shear modulus and compressive modulus (for closed cracks) with continuing crack opening and closing cycles.

The results for the 2S2(H) test simulation are shown in Figures 4.15 through 4.19 and in Appendix B. The applied input motions, constructed from the recorded motions at the top of the basemat, are depicted in Figure 4.15. Comparisons of the analysis to test results for the displacements of the top slab are shown in Figures 4.16 and 4.17. It is noted that the apparent differences in the vertical accelerations can be attributed to the cross-direction rocking which is not captured in the model because of enforcing symmetry in the analysis. Comparisons of the acceleration response of the top mass are depicted in Figures 4.18 and 4.19. These results show good agreement through the largest response peaks at 15-16 seconds. After this point, the analysis tends to overpredict the displacement and acceleration response. This can be attributed to slight differences in the structural behavior between the test model and the analytical model during the peak response at 15-16 seconds. It is hypothesized that some significant local damage occurred in the test model during this peak response that immediately degraded the stiffness resulting in a step change in the fundamental frequency. The analytical model does not capture the same magnitude of local damage and instead degrades the stiffness gradually during the remainder of the analysis. This hypothesis is based on the measured strain response in the model. Consider Figures B-40 through B-44, which show the strain response for inside and outside vertical rebar, especially at gages SIV27C and SOV27C. The measured response indicates that

yielding occurs in these bars with subsequent offset or residual strains. This would also indicate that substantial cracking damage has occurred across the concrete wall, which would degrade the RCCV stiffness. This sudden frequency change in the test model is enough to reduce the amplification of the top mass relative to the frequency of the input for the remainder of the test.

The results for the 3S2(H) test analytical simulation are given in Figures 4.20 through 4.24. Figure 4.20 identifies the horizontal, vertical, and basemat rocking components developed from the measured basemat response for the analysis input for the 3S2(H) test simulation. Figures 4.21 and 4.22 show comparisons for the horizontal and vertical displacements of the top slab for the analysis and the test data, and Figures 4.23 and 4.24 show the similar comparisons for the acceleration response of the top mass. The analysis results match the peak magnitudes and timing of the peaks reasonably well. As in the 2S2(H) simulation, the comparison is better in the first 16 seconds where the maximum response is occurring. The slightly higher response in the analysis after 16 seconds is again attributable to discrete increments of local damage occurring in the test model that is not captured in the analysis due to the coarse mesh for the posttest analytical model. Comparisons of strain results for reinforcing bars and liner plate are included in Appendix B with Figures B-59 through B.77. The vertical rebar strain in the RCCV wall at 90 and 270° (at the peak rocking points) where damage initiated in the 2S2(H) test indicates continued damage buildup. Many more peaks exceed yield during the first 16 seconds with a maximum peak near 2% strain in an outside bar. Residual strains of .8% are also in evidence, indicating substantial concrete damage. The liner response also indicates that some distress may be near in the liner with strains near yield and drift due to residual buildup.

Figures 4.25 through 4.29 provide the results of the 5S2(H) test simulation. Figure 4.25 illustrates the basemat input acceleration histories used in the analysis. Note that a subset of the measured 4S2(H) test records was used as a preconditioning run before the 5S2(H) analysis to account for damage that accumulates during this test which is not simulated. A comparison of the analysis results and test data is shown in Figures 4.26 and 4.27 for the horizontal and vertical displacement response, respectively, of the top slab for the 5S2(H) test. A similar comparison for the horizontal and vertical acceleration response of the top mass is shown in Figures 4.28 and 4.29. These figures show that the analysis has good correlation for this structural response, both in the timing and magnitudes of the response. This indicates that the analysis is doing a good job of simulating the extensive cyclic damage that is accumulating in the structure and that the cyclic dependent damping is also performing well. Again, comparisons of strain response at selected gage locations for the reinforcing bars and liner plate are provided in Appendix B as Figures B-78 through C-96. As expected, these plots indicate substantial damage is occurring in the test model and in the analytical model. Extensive plastic straining in the vertical rebar and vertical displacement offset are exhibited in the test results. Although extensive plastic straining is not shown in the selected liner gages included, some strain offset is in evidence implying nearby distress or buckling. Although this extensive damage has accumulated in this series of failure level seismic input, it is a credit to the test model that some type of structural collapse has not occurred during the 5S2(H) test. However, following such a buildup of damage, it is clear that major repairs would be required before allowing such a structure to continue in service.

Figures 4.30 and 4.31 show comparison for the horizontal and vertical displacement, respectively, for the top slab in the 9S2(H) test. Figures 4.32 and 4.33 show comparisons of the horizontal and vertical acceleration response of the top mass in the 9S2(H) test. Figure 4.30 clearly indicates the point in the test where loss of concrete integrity in the RCCV occurred. The analysis does not consider sudden material loss, but clearly predicts the correct response of the top slab and attached mass. Again the extent of damage in the model is extensive with acceleration magnitudes of 3gs and displacements of 40mm. It should also be noted that the input accelerations for the 9S2(H) test are about 3.7gs. Thus, the damage level in both the test and analytical model before the 9S2(H) test is such that the top mass is almost isolated from the basemat in shear response.

Figures 4.34 through 4.36 plot comparisons of the analysis results and test data for the indicated failure level testing. These figures plot the horizontal acceleration of the top mass versus the horizontal displacement of the top slab as a measure of the hysteretic damage accumulation. The test data is plotted in green and the analysis results are plotted in red. These figures are very informative for a number of reasons. First, the analysis shows very good correlation with the test data both in magnitudes and shape of the hysteretic loops. This means that the level and rate of damage accumulation as well as the energy dissipating mechanisms are consistent between the

analytical model and the test. Second, it is apparent that damage occurs in the design level tests as confirmed in the frequency shift measurements. However, these hysteretic bands are fairly tight and the general slope is stable indicating overall structural integrity. While some scattering began at the higher response peaks in the 2S2(H) test, the overall hysteretic band remains fairly stable. Clearly, the damage that develops during the 3S2(H) is beginning to affect the overall integrity of the structure.

Figures 4.37 and 4.38 plot contours for the shear strain during the peak response for the 3S2(H) and 5S2(H) tests, respectively. These plots set the upper contour limits so that any areas shown in dark red or dark blue have shear strains above 0.5%. These plots indicate that extensive areas of the RCCV walls have 0.5% shear strains beginning with the 3S2(H) test.

In the PCCV analysis (James et al., 1999a), this level of concrete shear strain was proposed as an analytical failure criteria for the prestressed concrete containment structure. The reinforced concrete containment model appears to be able to withstand more than 0.5% shear strain across a significant portion of the cross-section without inducing structural collapse. This is attributed to two differences in the two types of structures. First, the RCCV has substantially more reinforcement so that the dowel action of the rebar contributes additional strength. This dowel action effect is not explicitly modeled in the analysis. Second, the compressive loads present in a prestressed structure may contribute to the initiation of the concrete rubblization at this level of shear damage. While the design codes allow added shear capacities (or allowables) for compressive stress acting on shear sections, high compressive loads combined with extensive damage will contribute to brittle type failure and cause the structure to be less tolerant of cyclic damage.

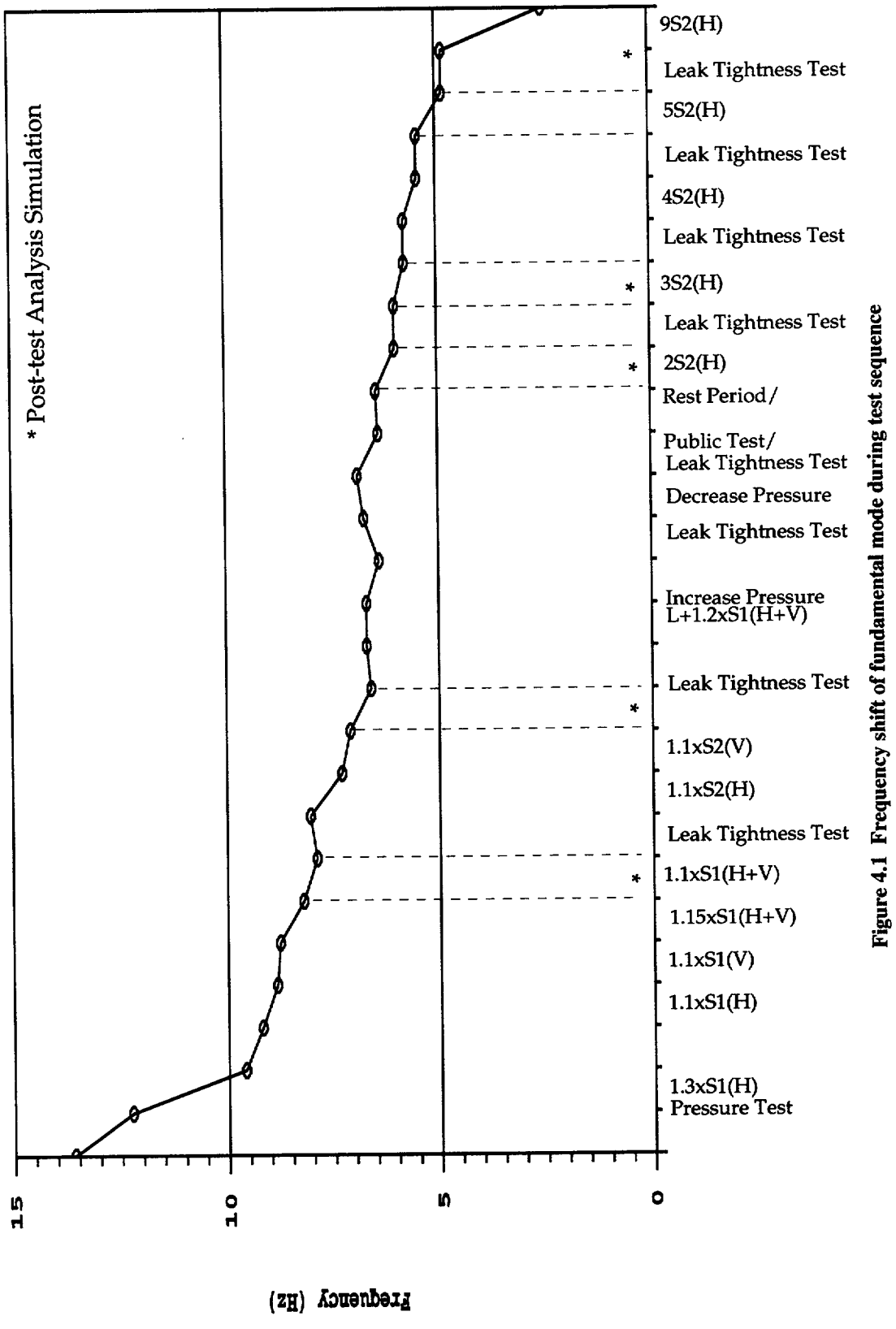

Figure 4.1 Frequency shift of fundamental mode during test sequence

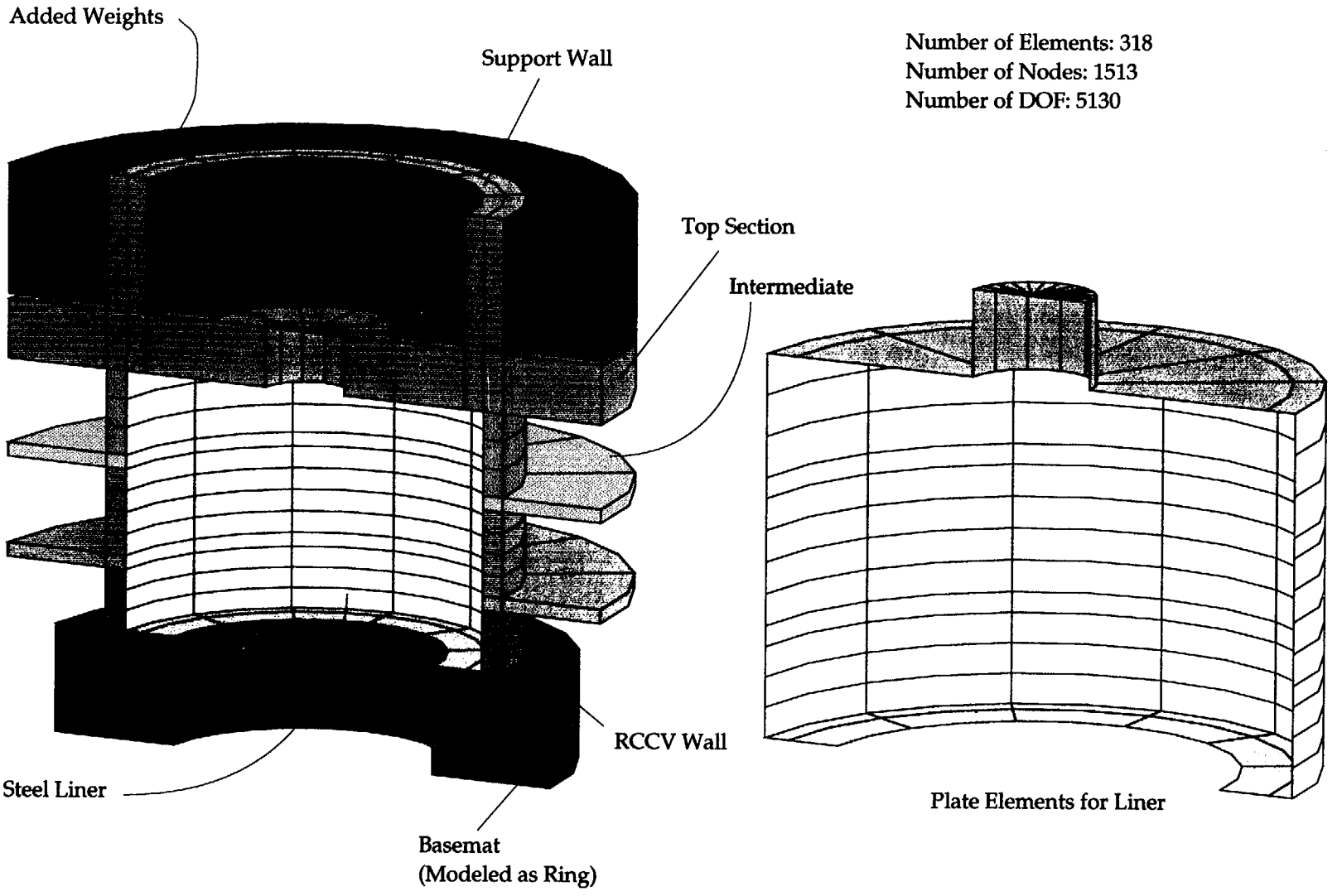

Figure 4.2. Simplified finite element model of RCCV for posttest analyses

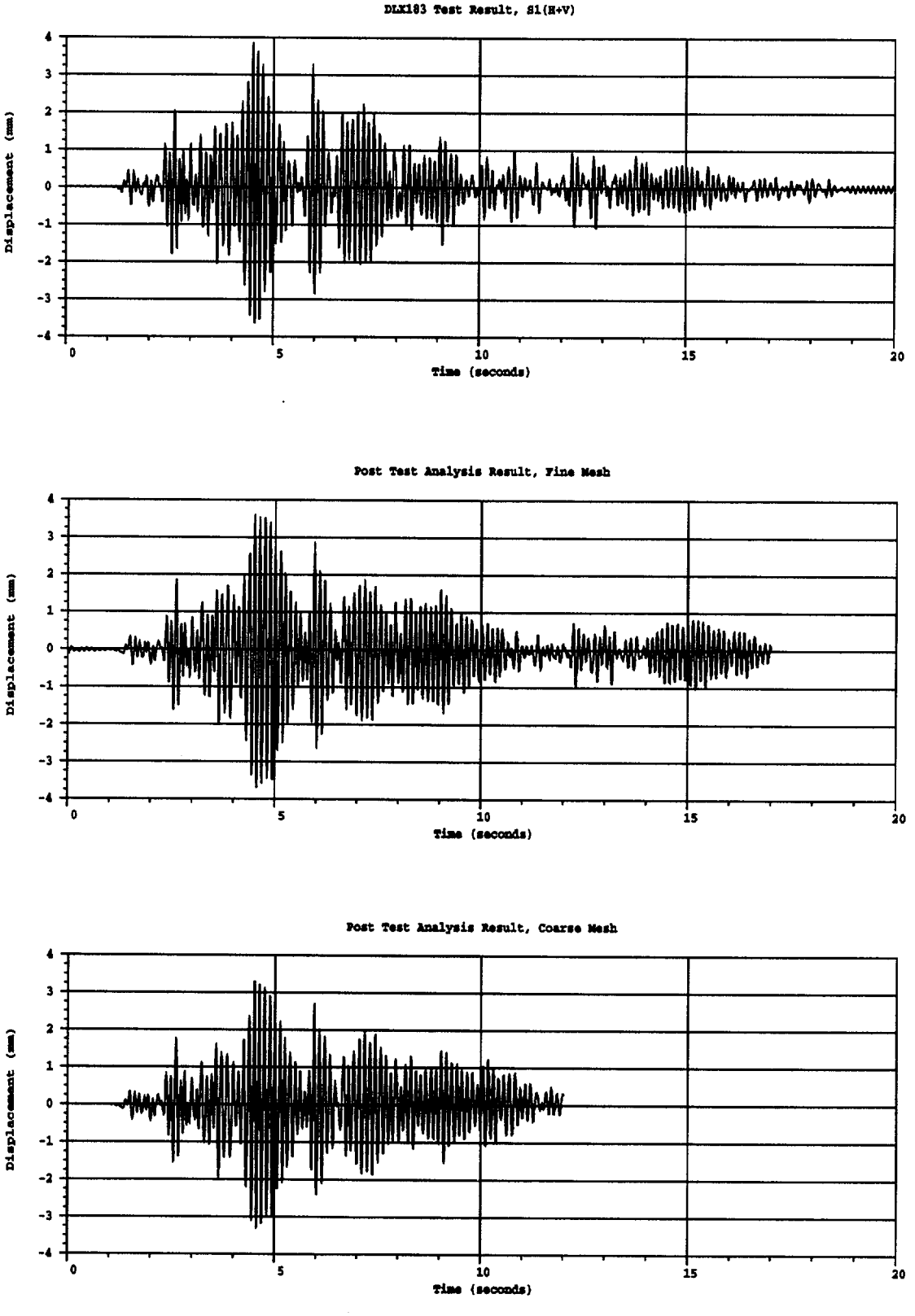

Figure 4.3 Comparison of horizontal displacements at upper slab, S1(H+V)

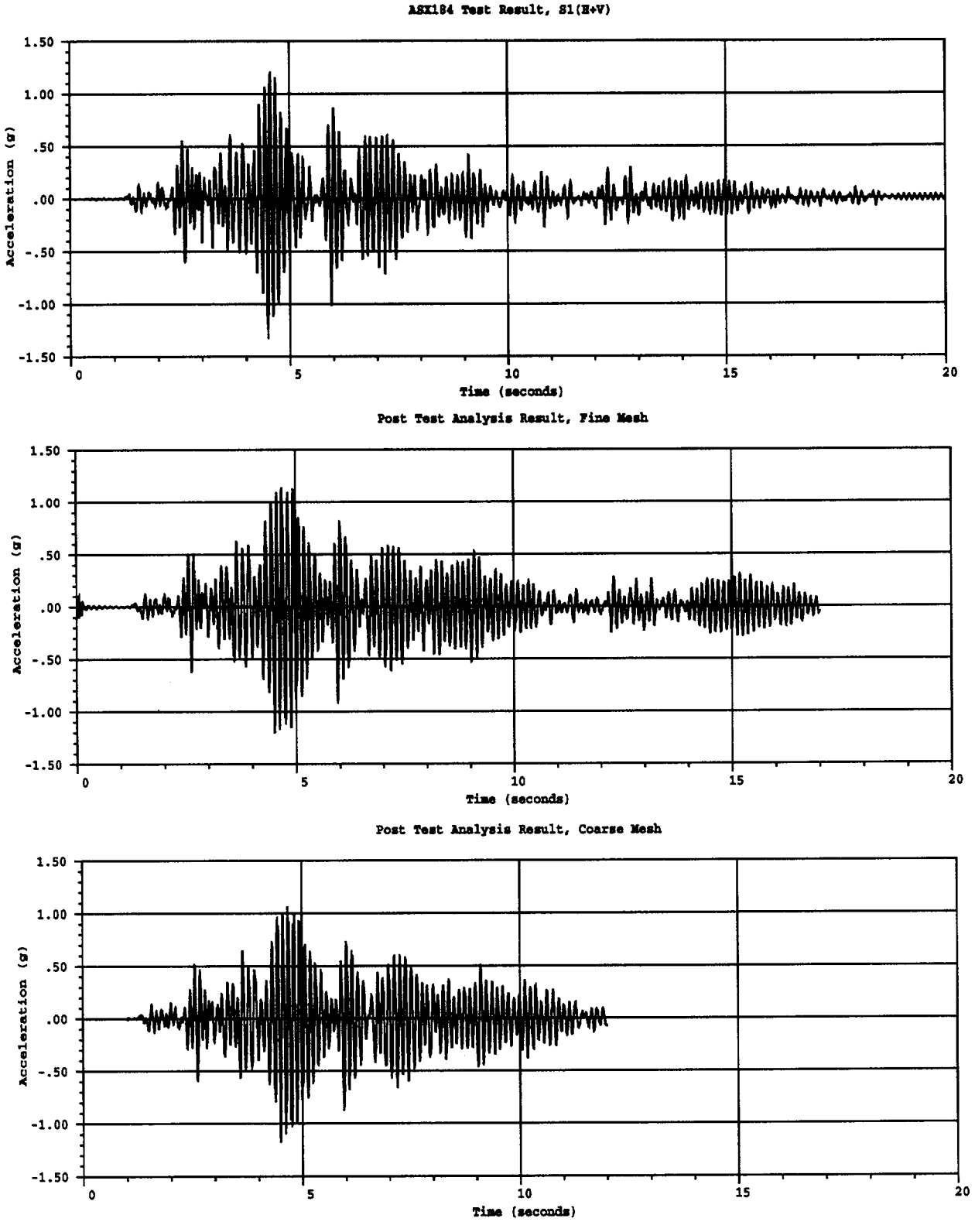

Figure 4.4 Comparison of horizontal acceleration at top mass, S1(H+V)

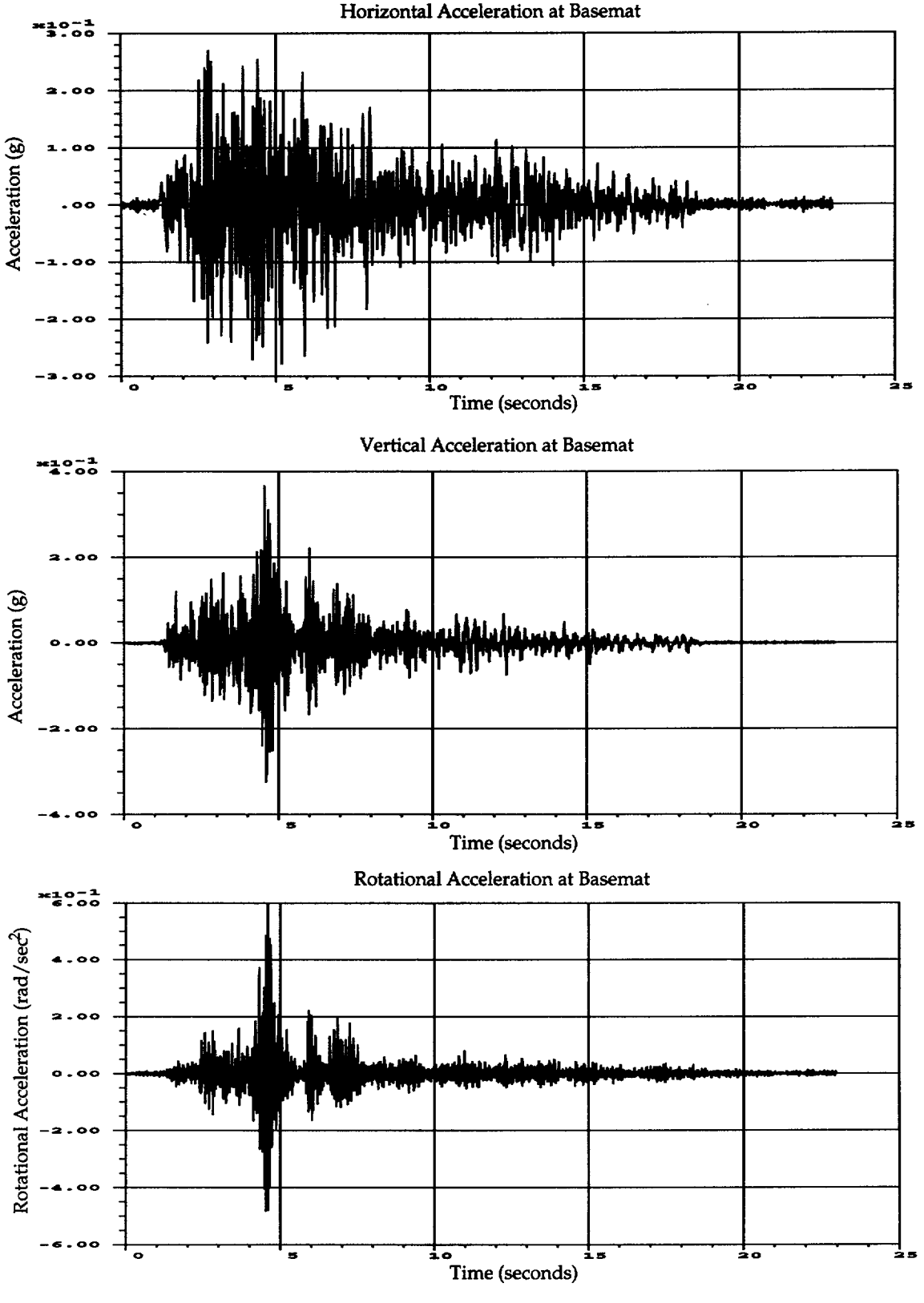

Figure 4.5. S1(H+V) time history input for posttest analysis

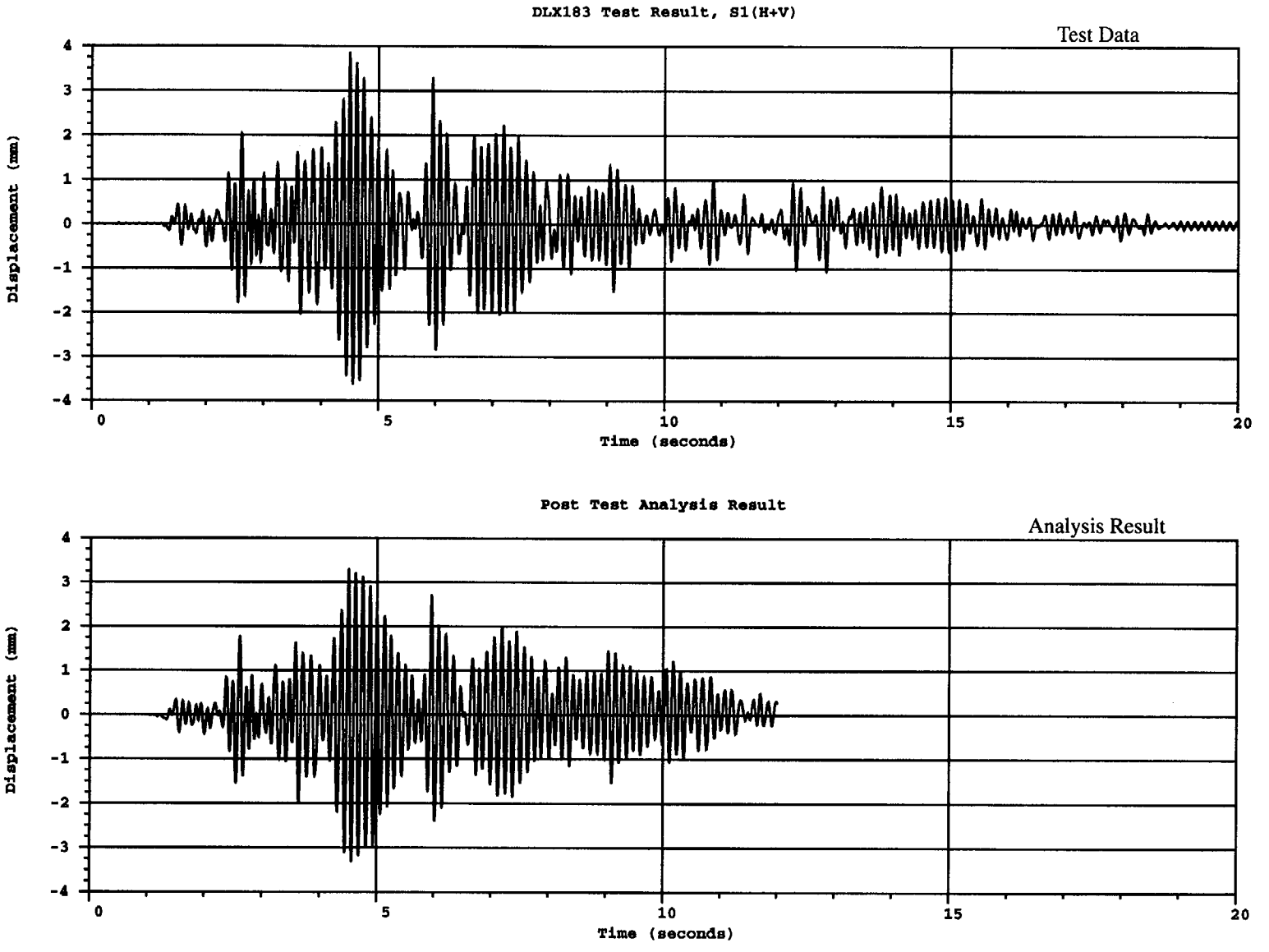

Figure 4.6 Comparison of horizontal displacement of top slab for S1(H+V) test

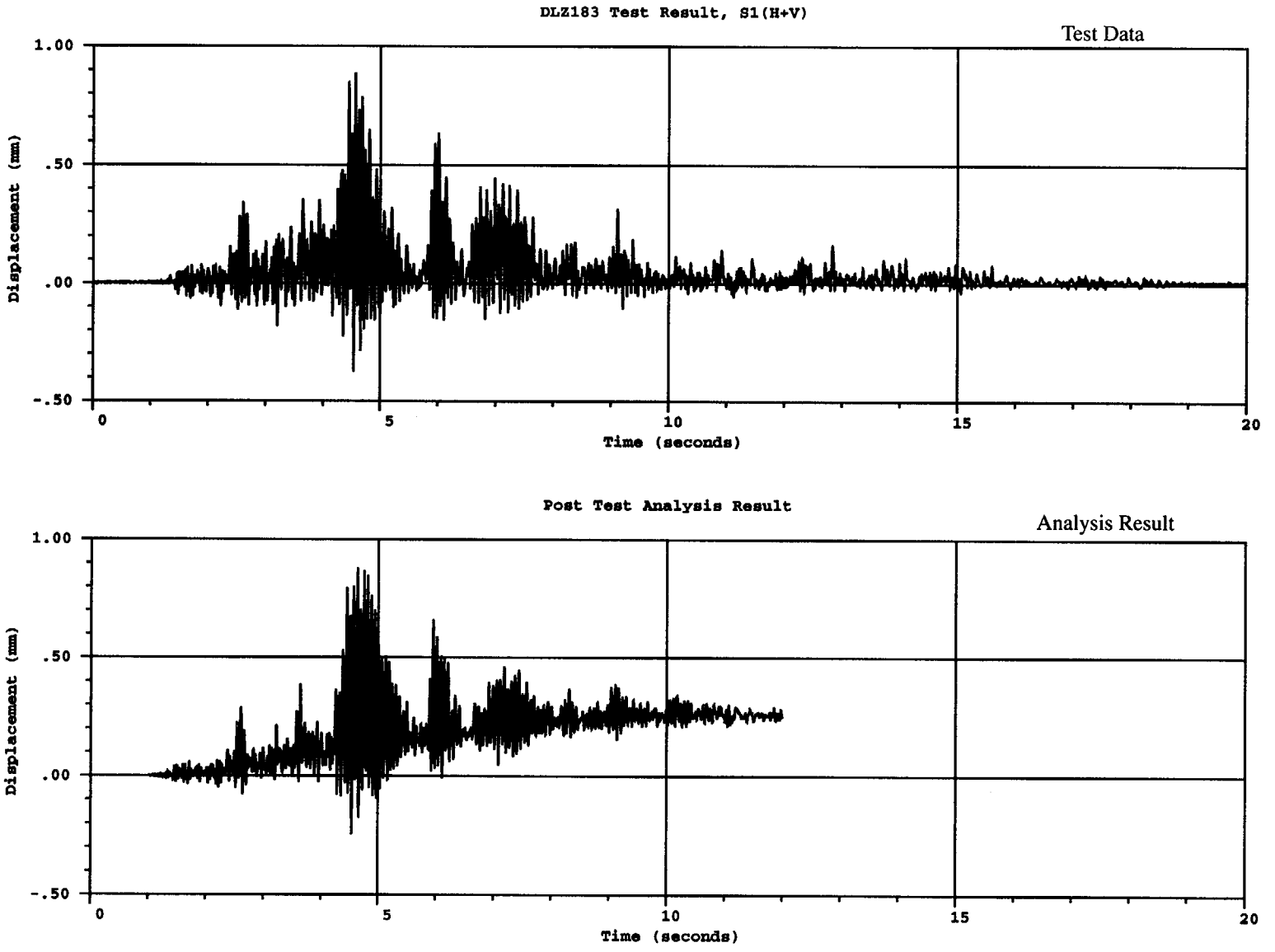

Figure 4.7 Comparison of vertical displacement of top slab for S1(H+V) test

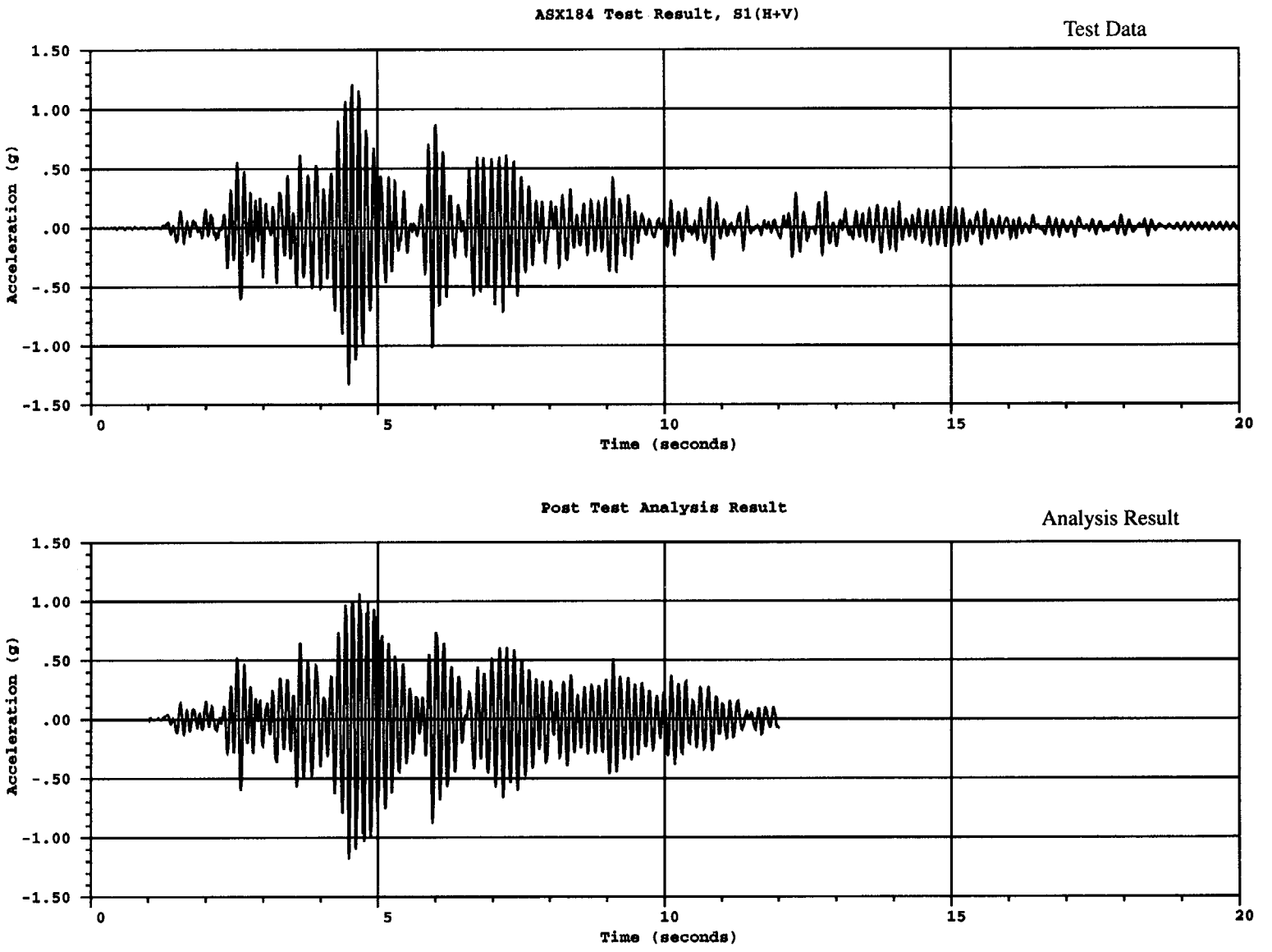

Figure 4.8 Comparison of horizontal acceleration of top mass for S1(H+V) test

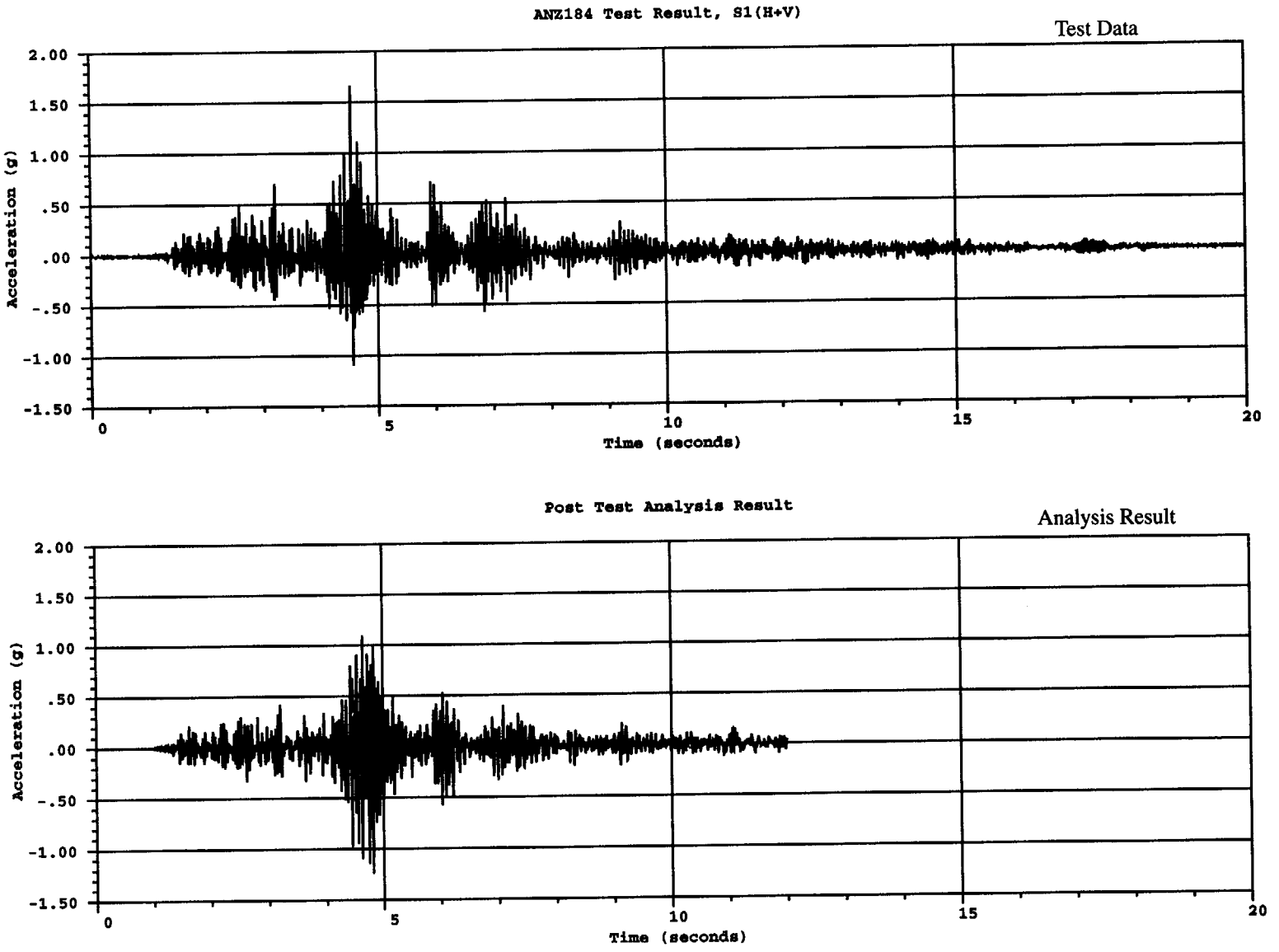

Figure 4.9 Comparison of vertical acceleration of top mass for S1(H+V) test

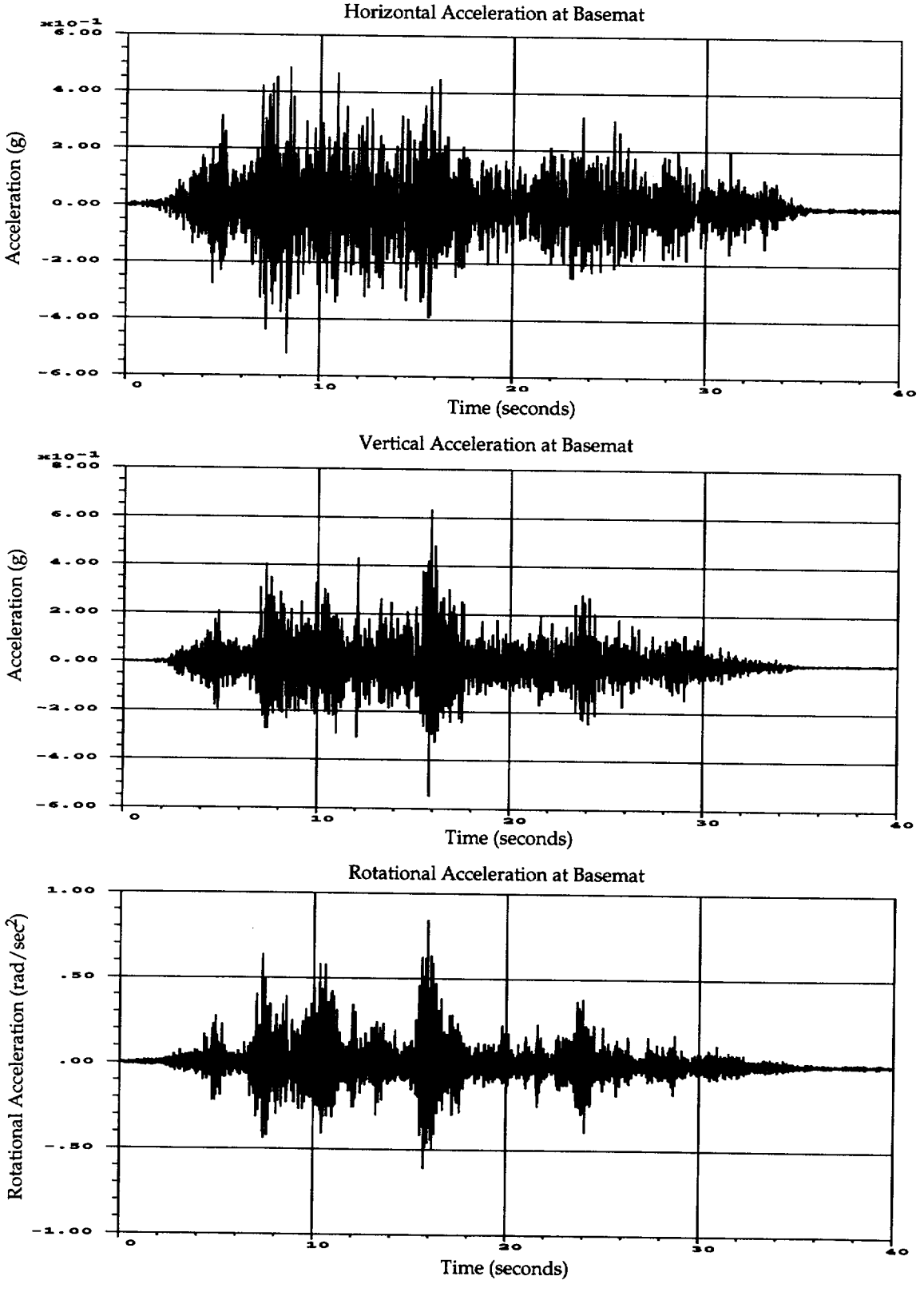

Figure 4.10. S2(H+V) time history input for posttest analysis

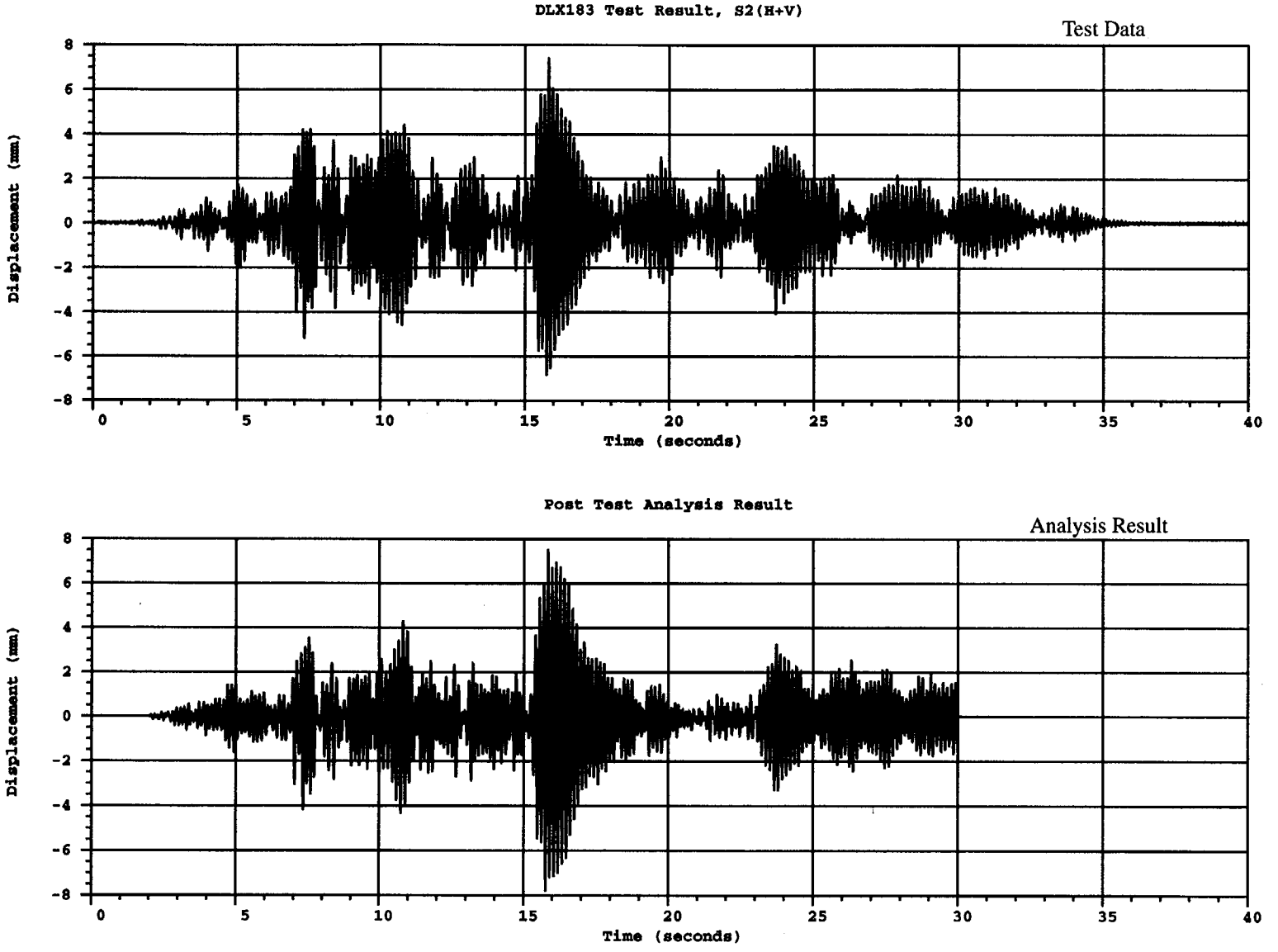

Figure 4.11 Comparison of horizontal displacement of top slab for S2(H+V) test

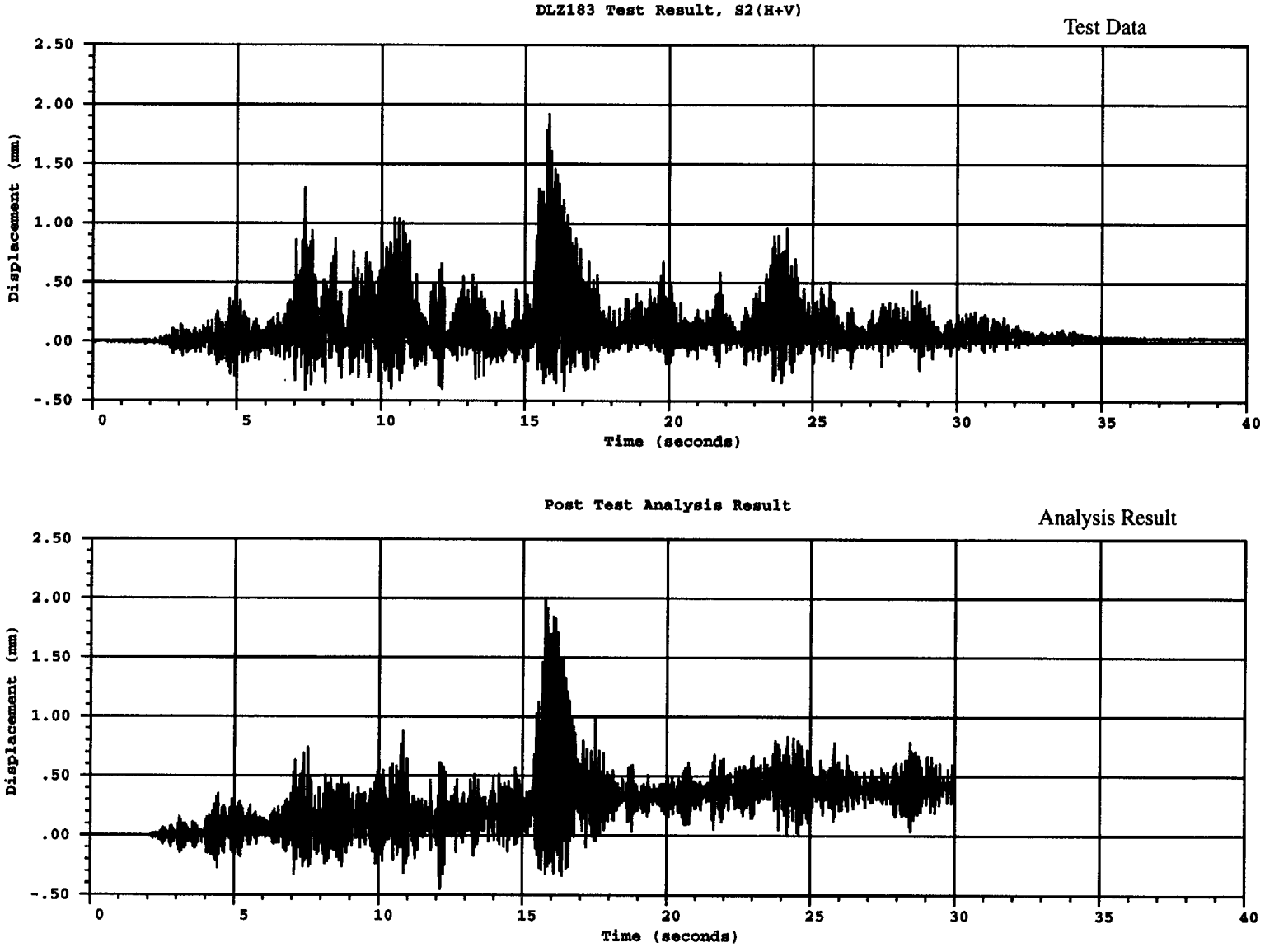

Figure 4.12 Comparison of vertical displacement of top slab for S2(H+V) test

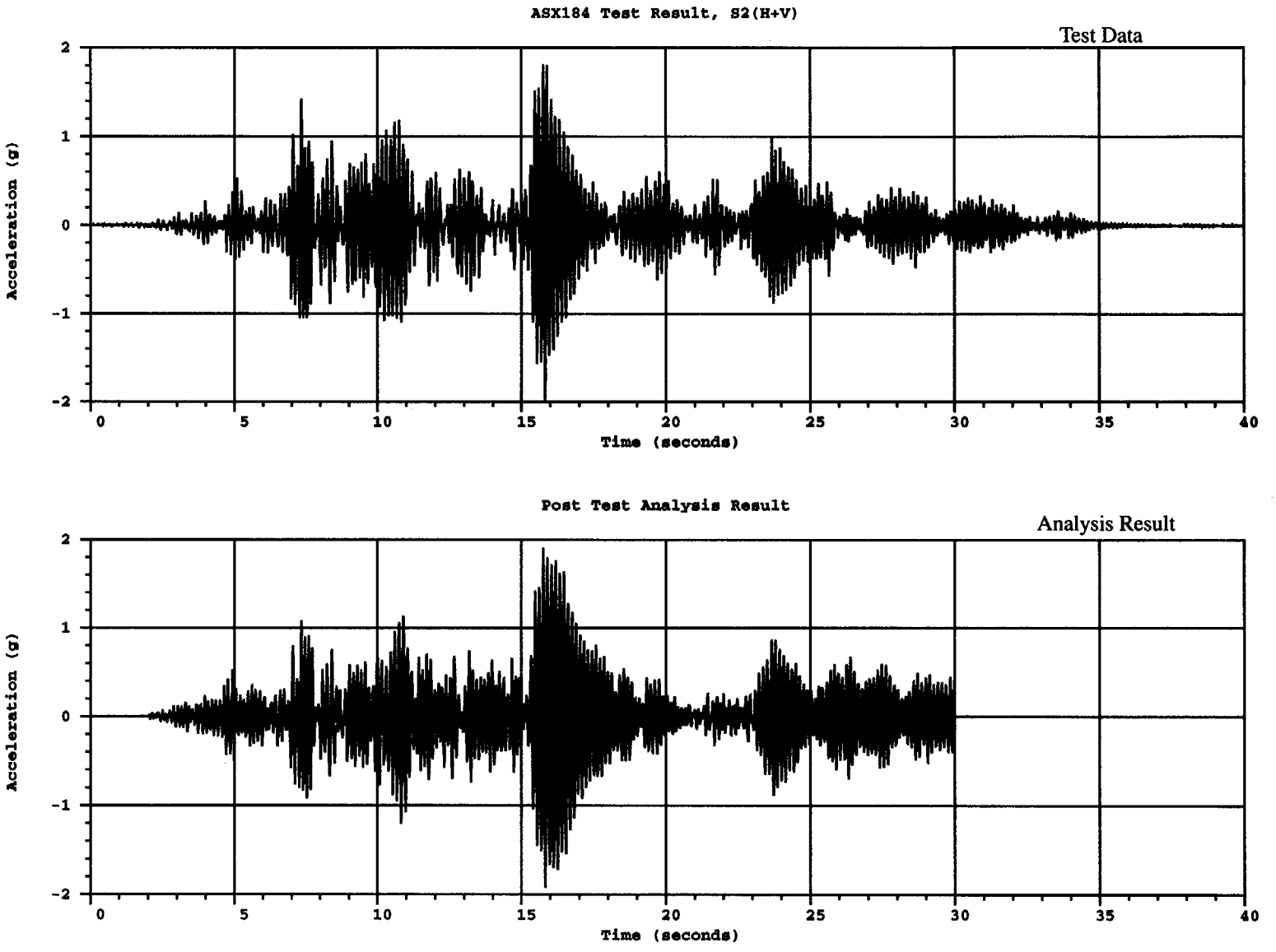

Figure 4.13 Comparison of horizontal acceleration of top mass for S2(H+V) test

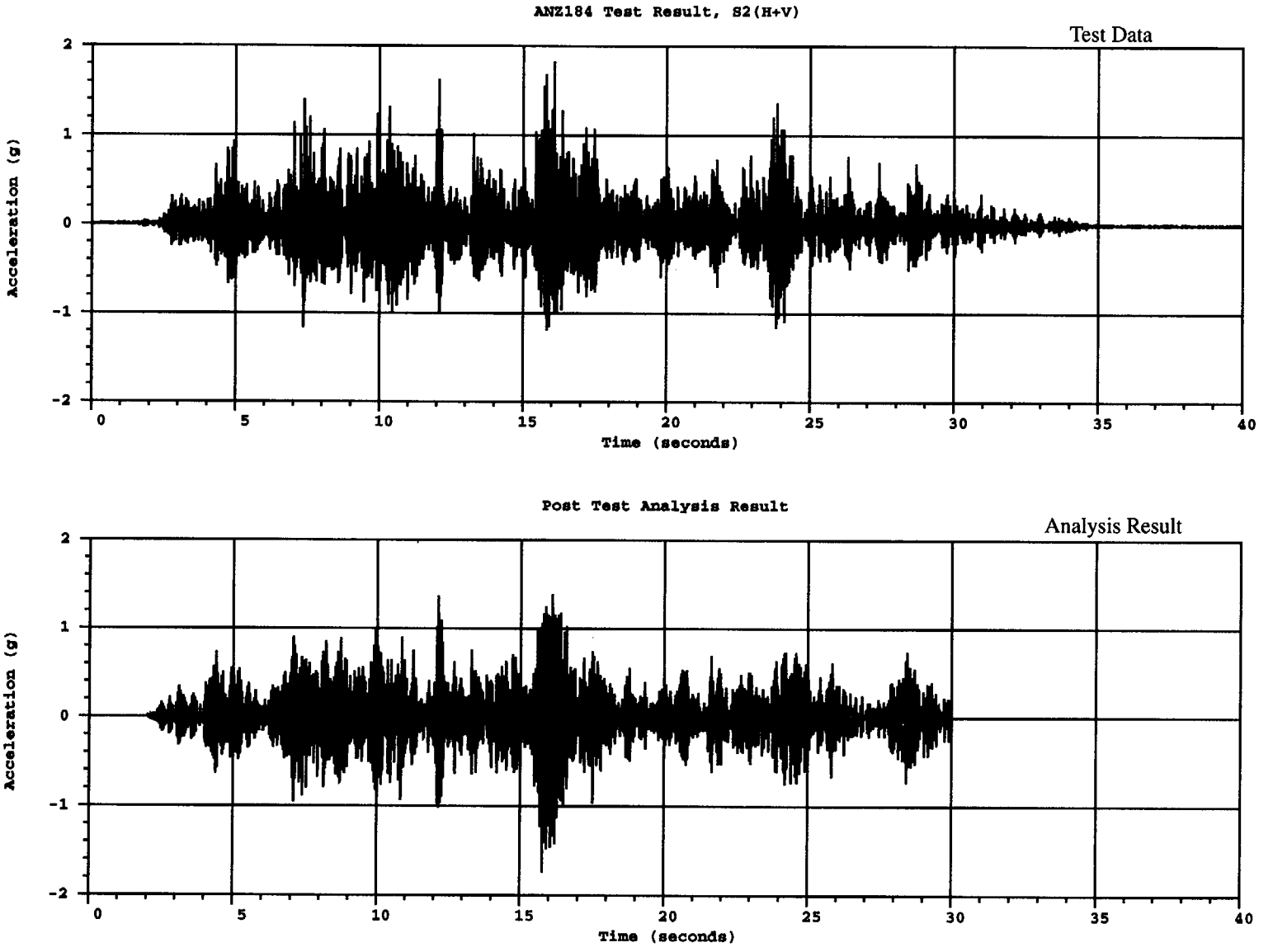

Figure 4.14 Comparison of vertical acceleration of top mass for S2(H+V) test

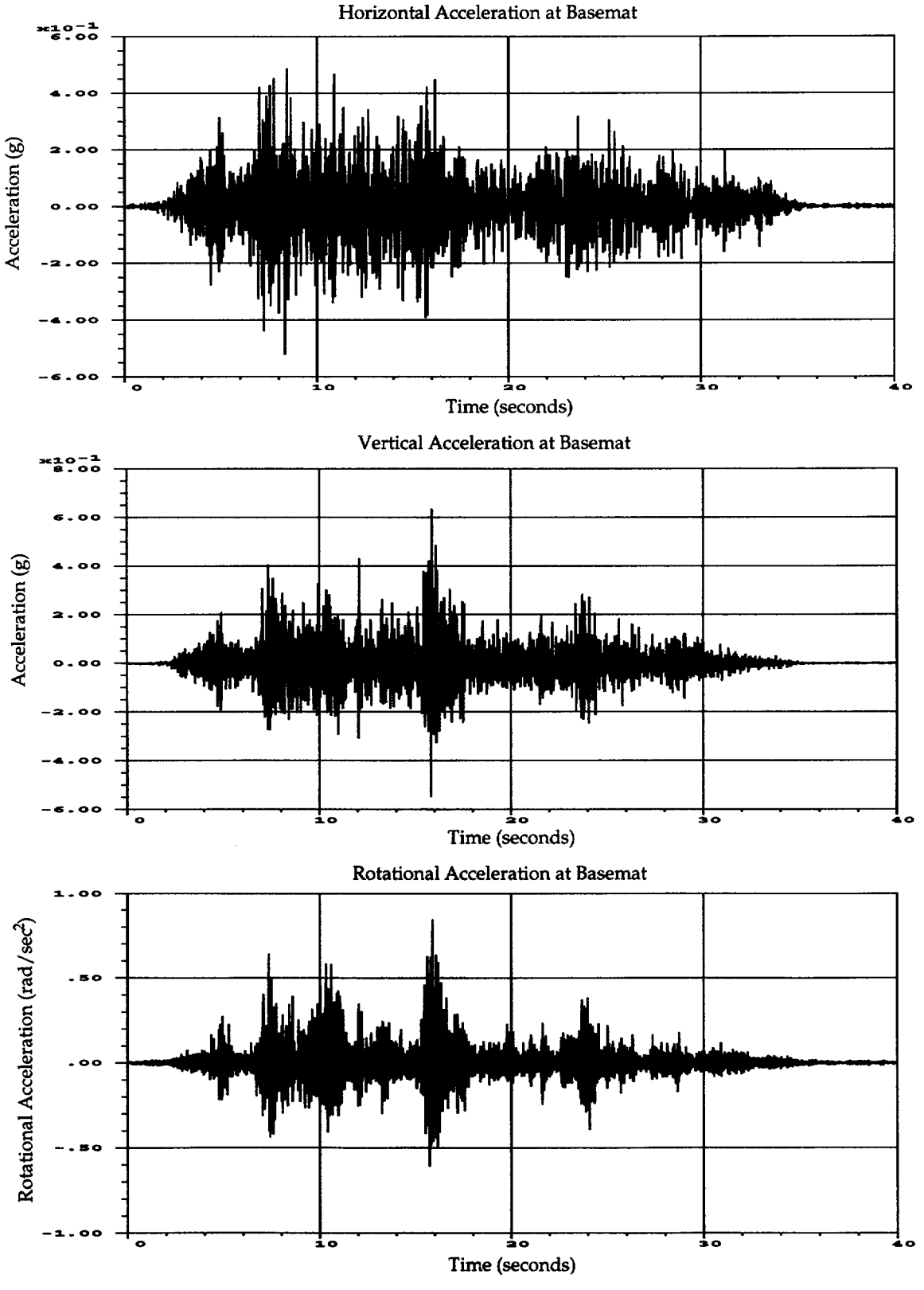

Figure 4.15. 2S2(H) time history input for posttest analysis

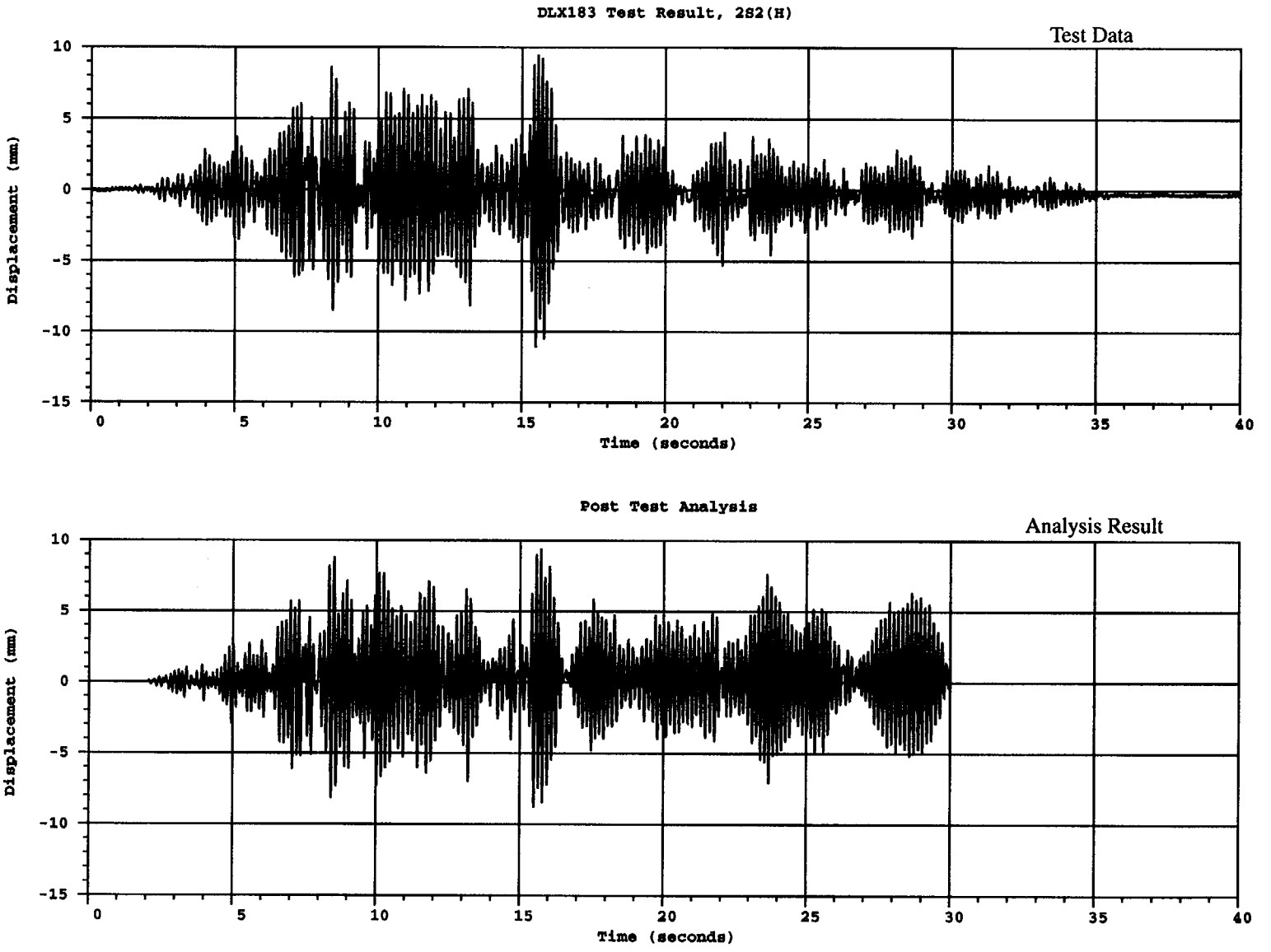

Figure 4.16 Comparison of horizontal displacement of top slab for 2S2(H) test

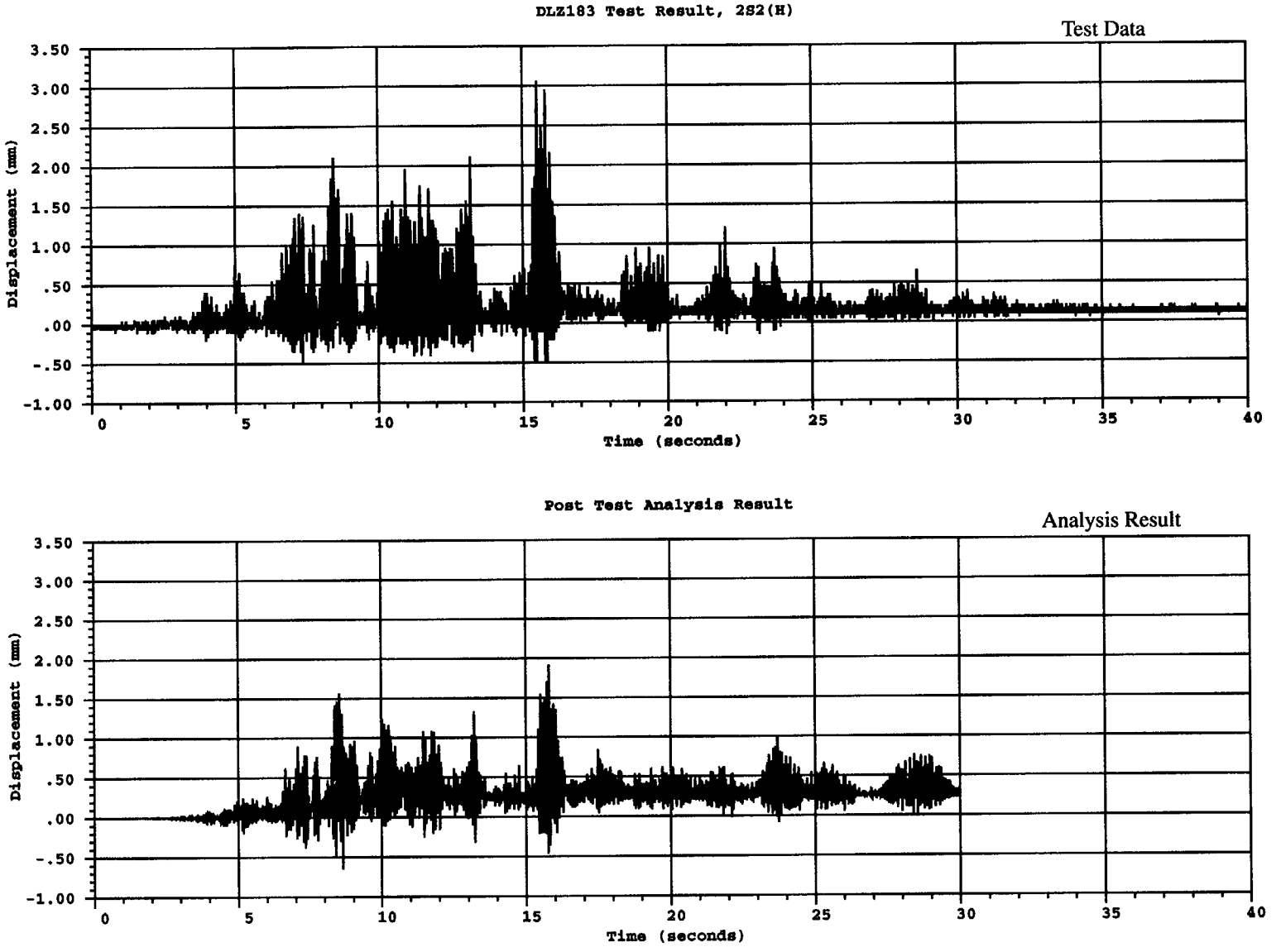

Figure 4.17 Comparison of vertical displacement of top slab for 2S2(H) test

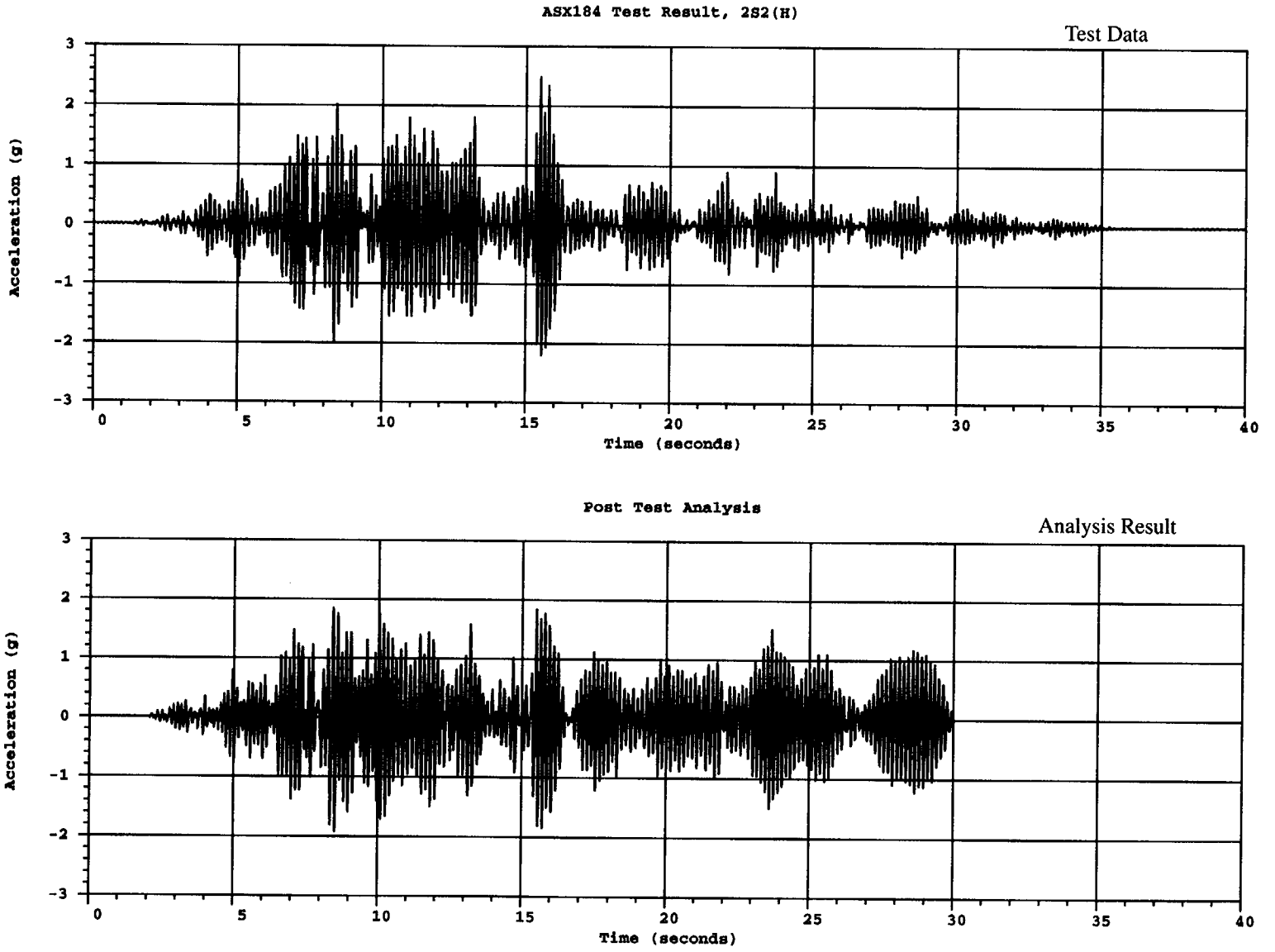

Figure 4.18 Comparison of horizontal acceleration of top mass for 2S2(H) test

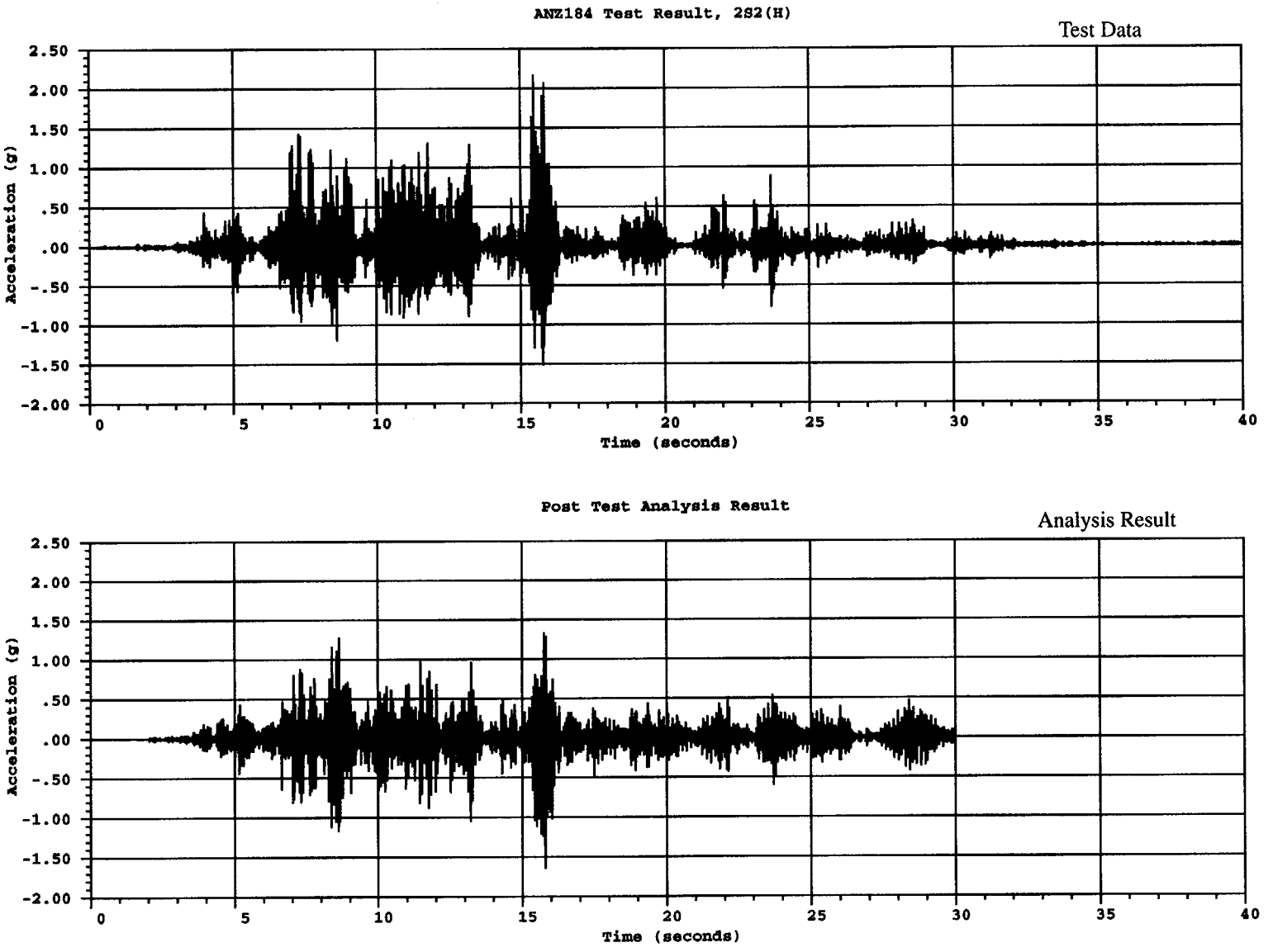

Figure 4.19 Comparison of vertical acceleration of top mass for 2S2(H) test

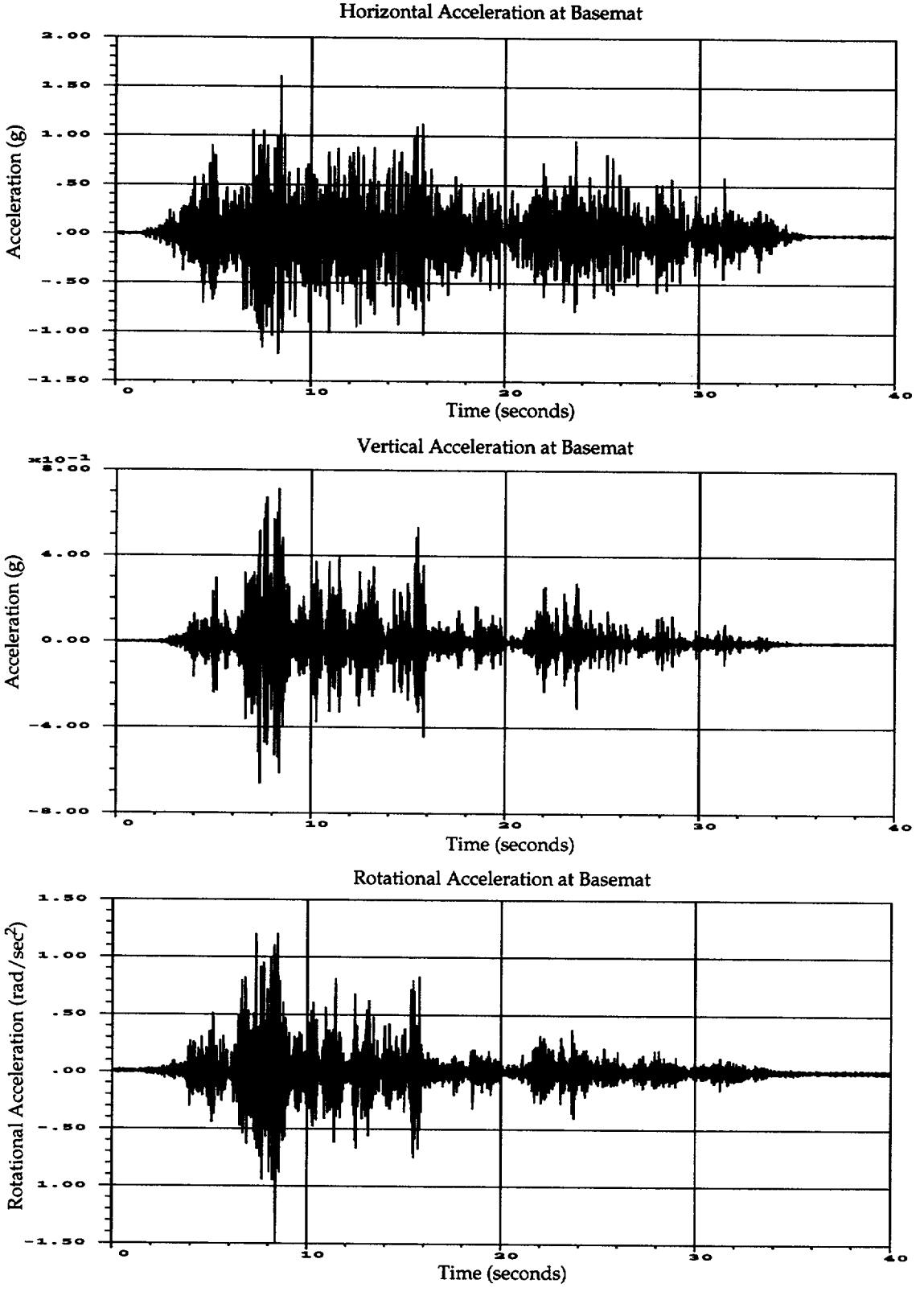

Figure 4.20. 3S2(H) time history input for posttest analysis

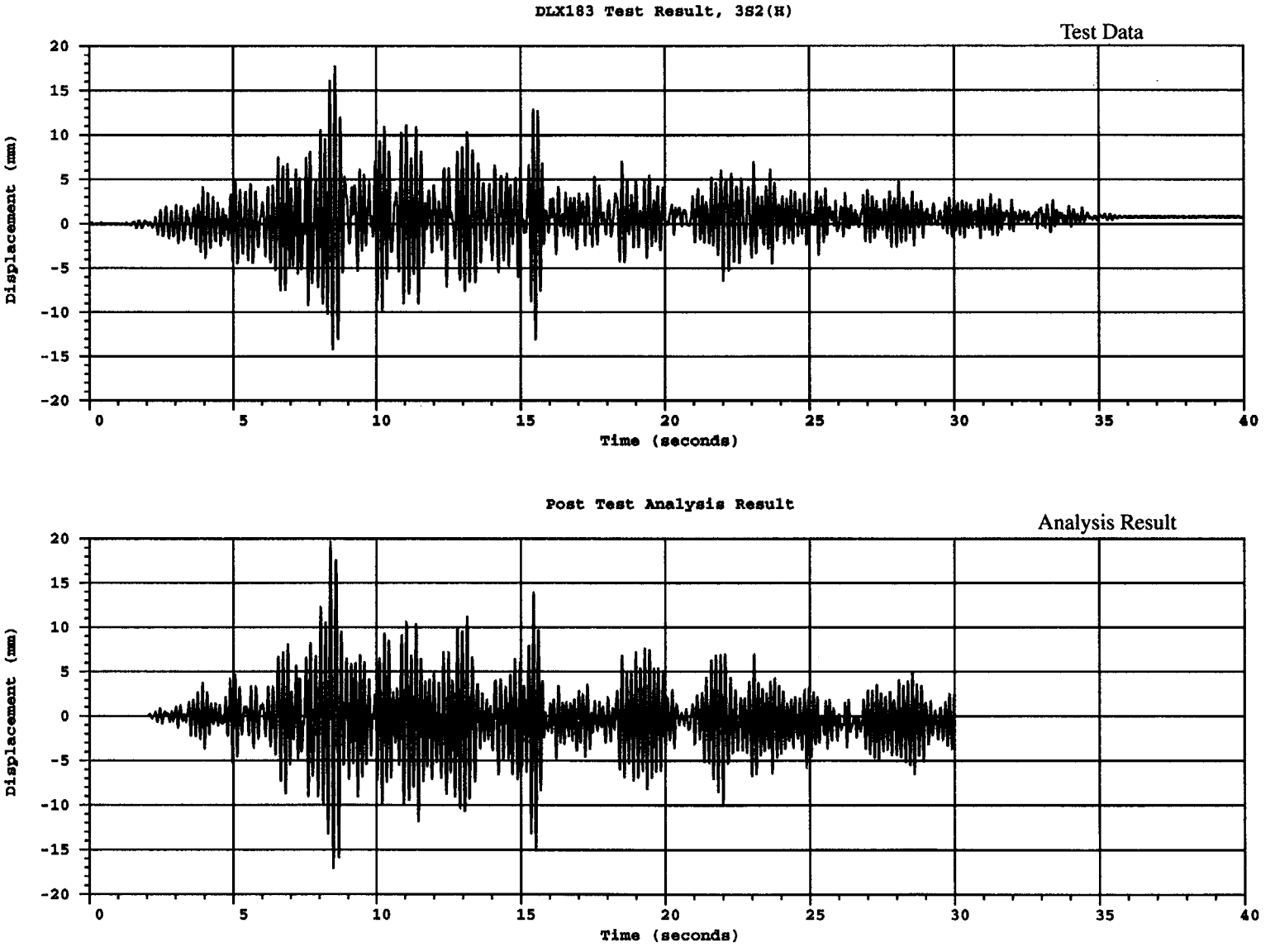

Figure 4.21 Comparison of horizontal displacement of top slab for 3S2(H) test

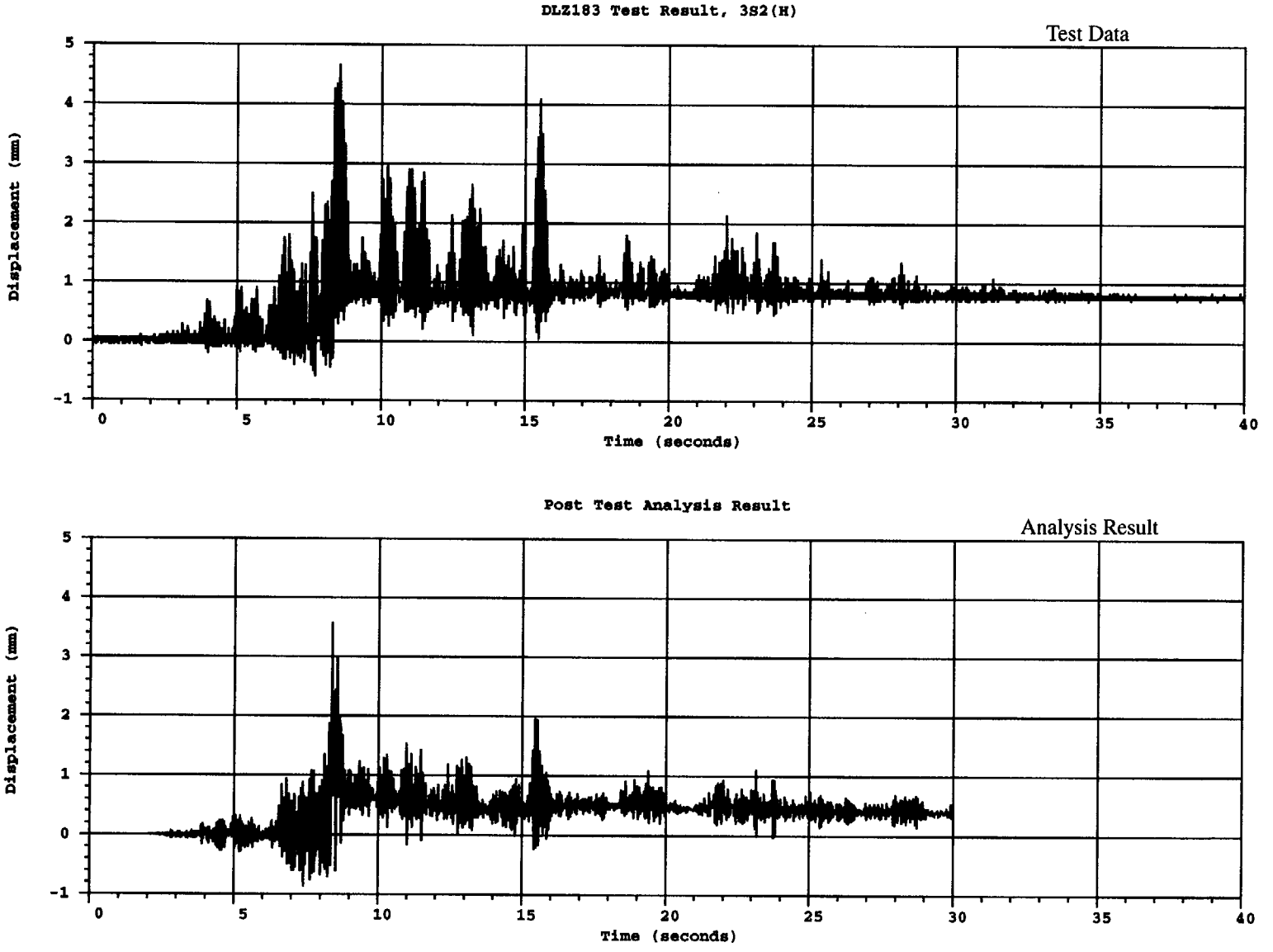

Figure 4.22 Comparison of vertical displacement of top slab for 3S2(H) test

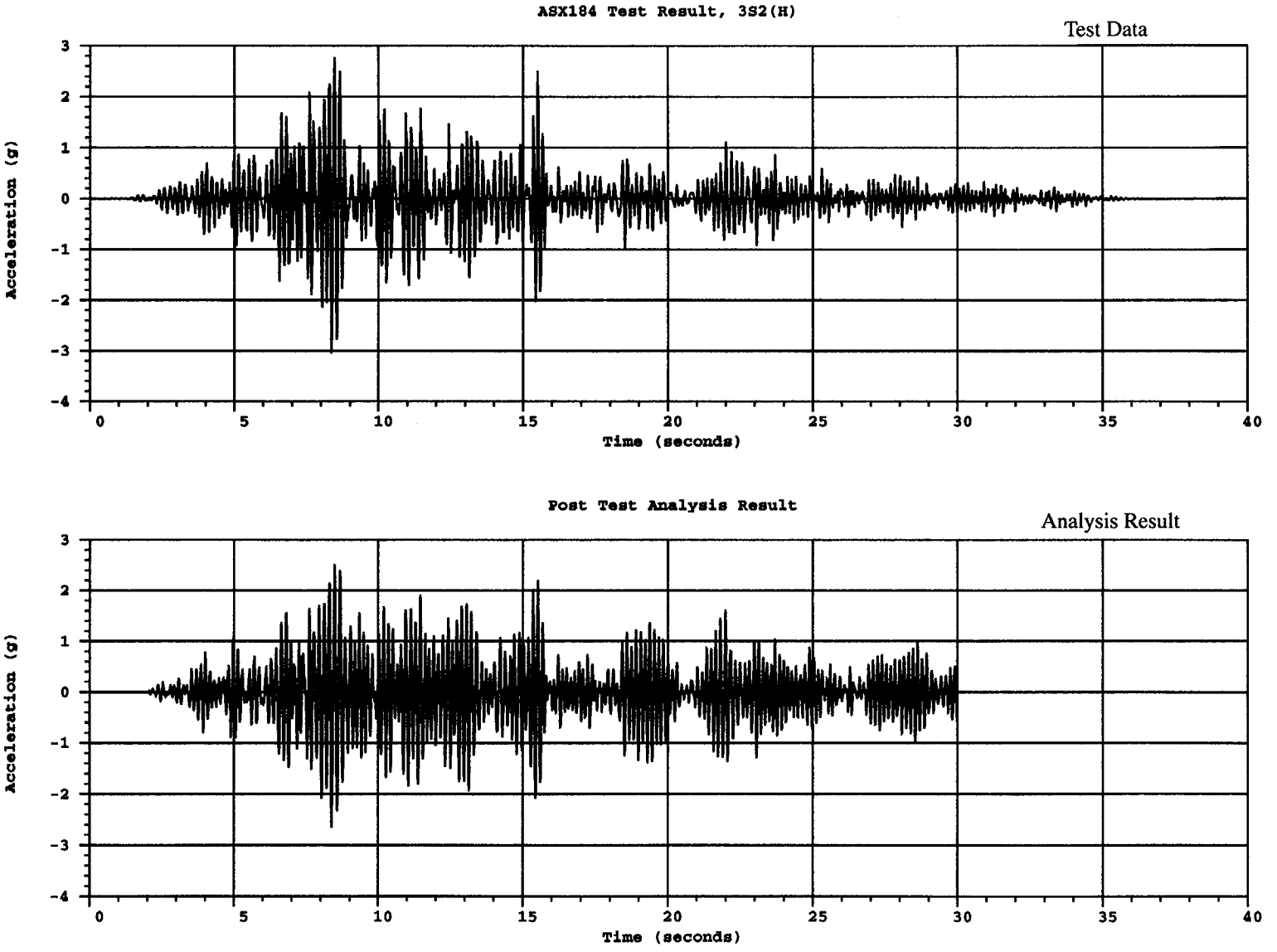

Figure 4.23 Comparison of horizontal acceleration of top mass for 3S2(H) test

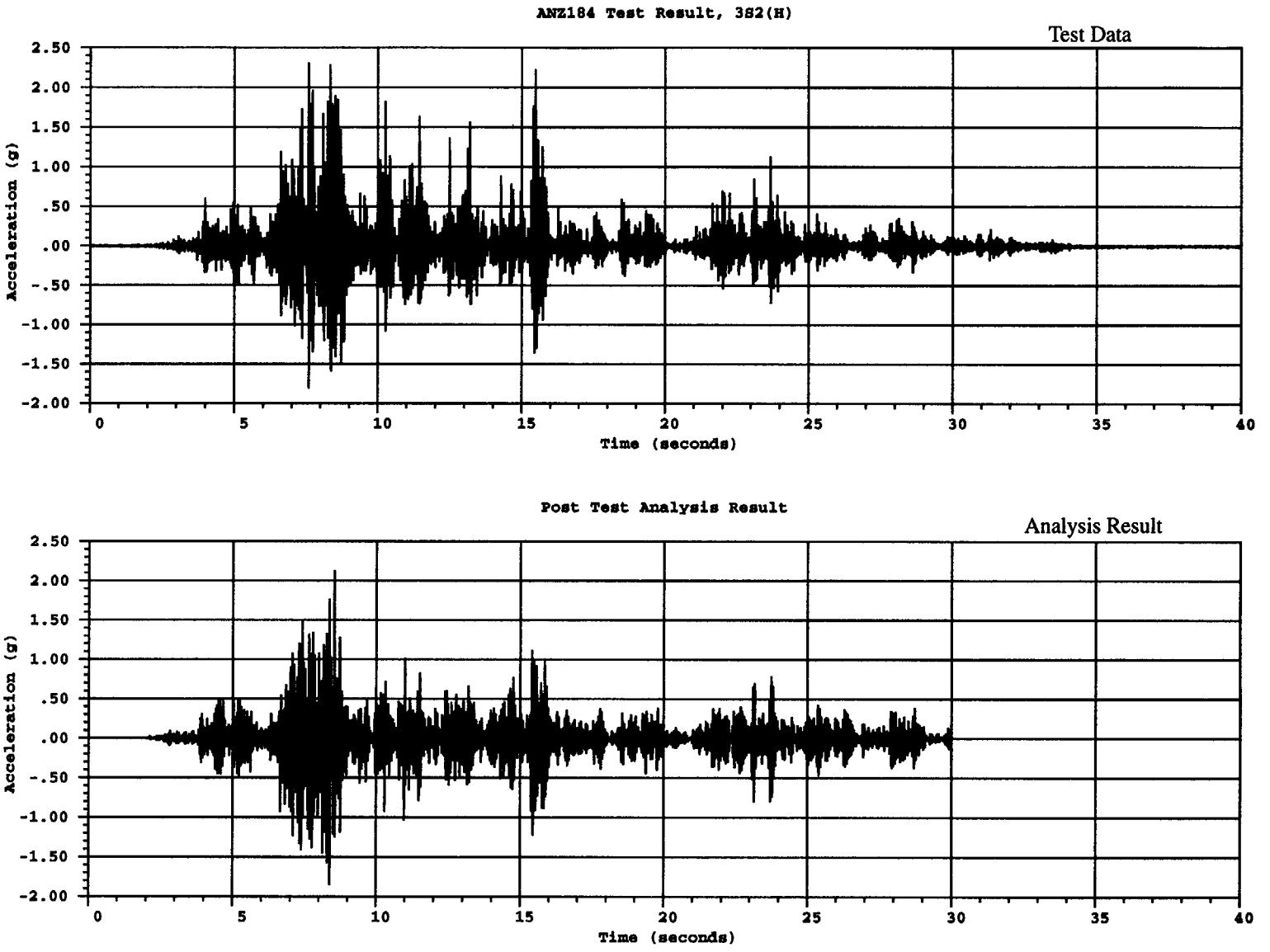

Figure 4.24 Comparison of vertical acceleration of top mass for 3S2(H) test

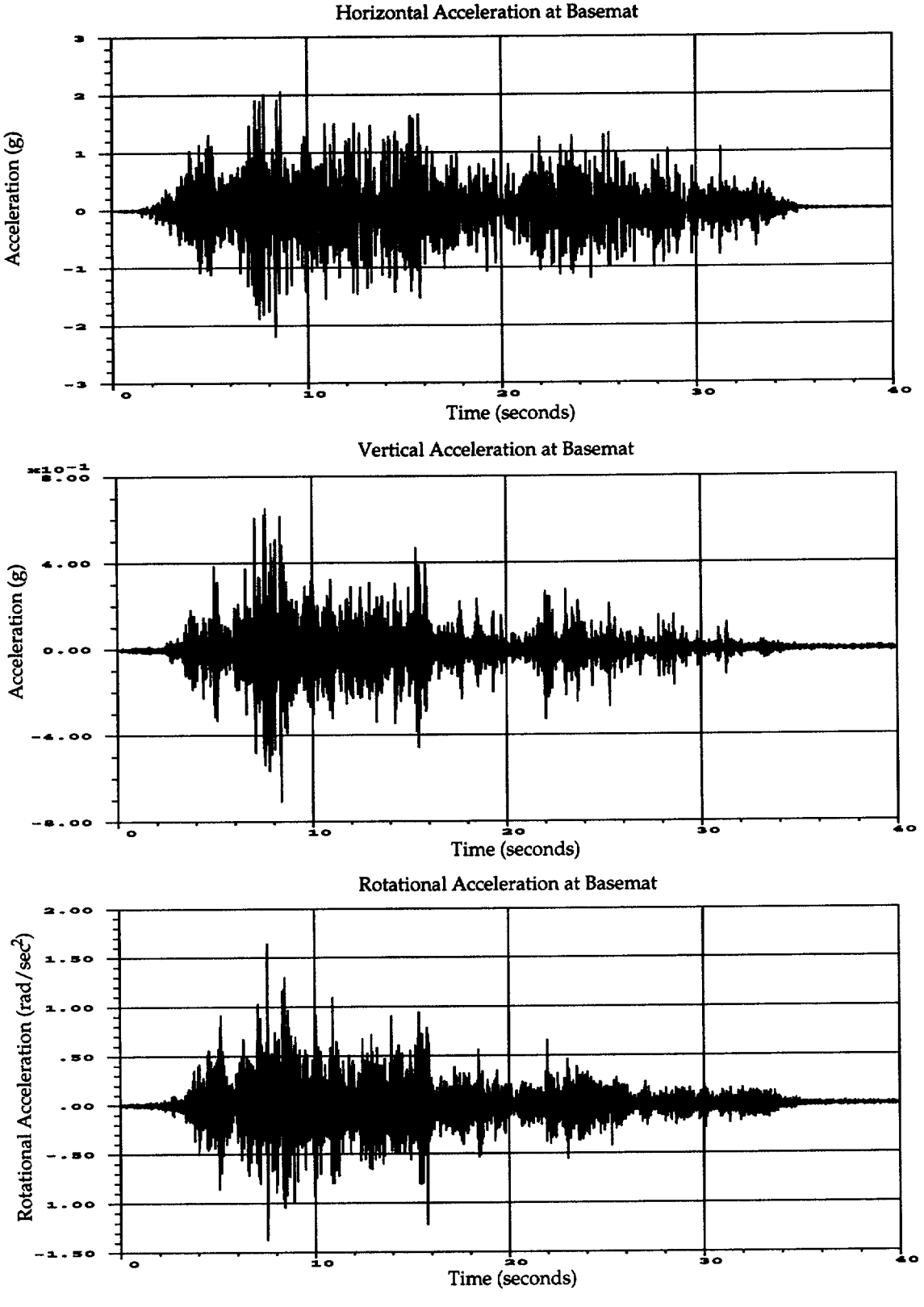

Figure 4.25. 5S2(H) time history input for posttest analysis

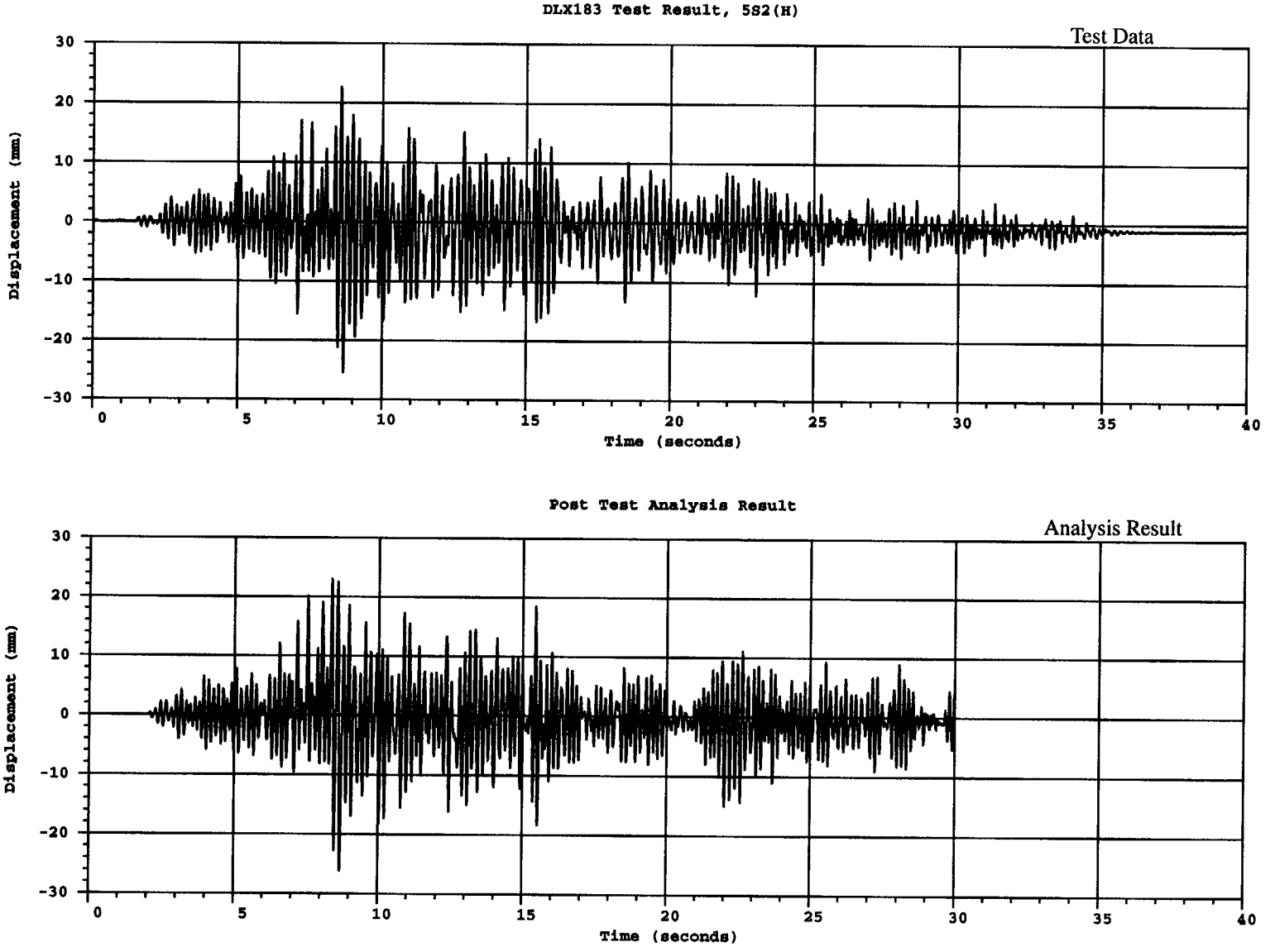

Figure 4.26 Comparison of horizontal displacement of top slab for 5S2(H) test

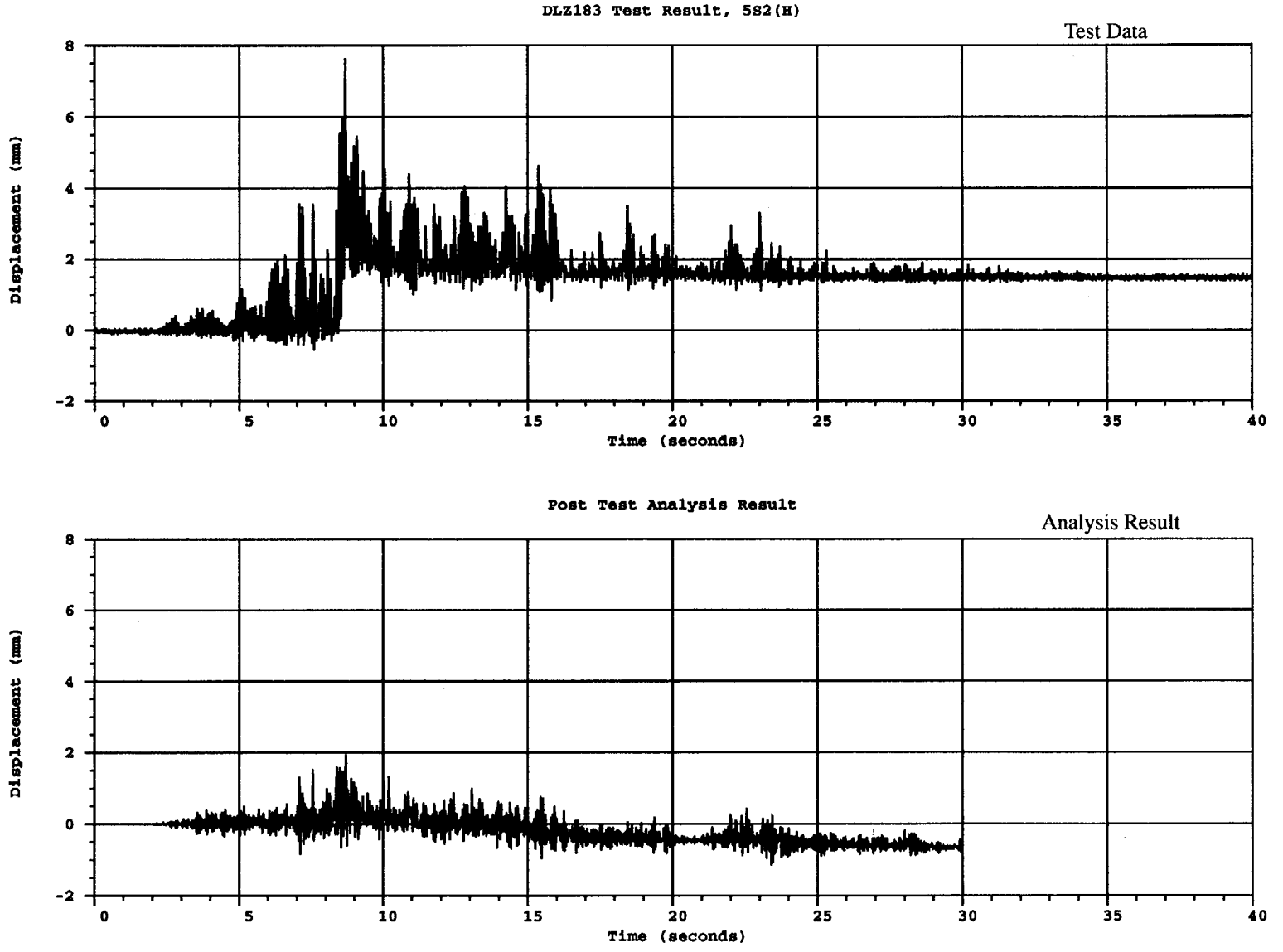

Figure 4.27 Comparison of vertical displacement of top slab for 5S2(H) test

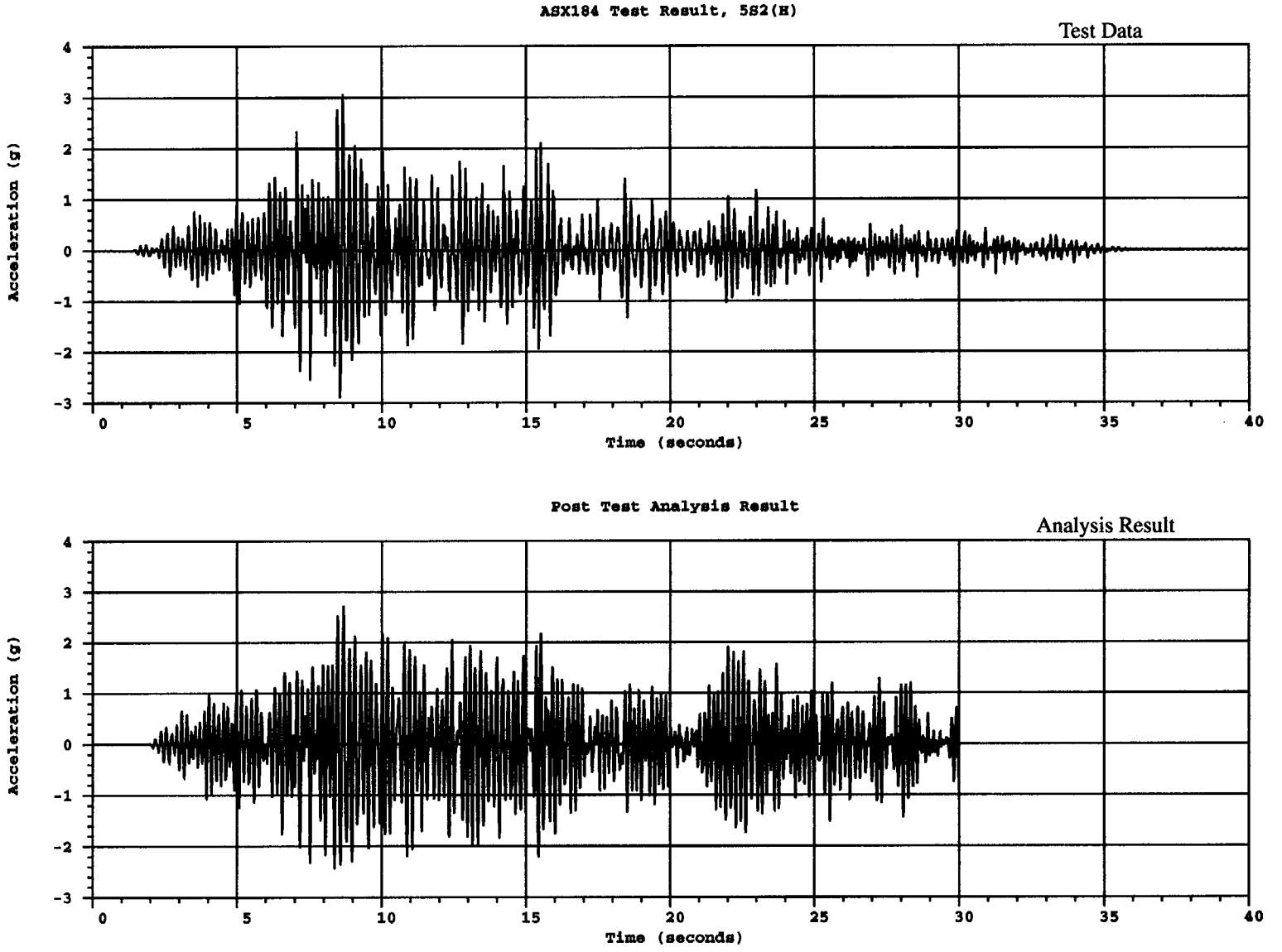

Figure 4.28 Comparison of horizontal acceleration of top mass for 5S2(H) test

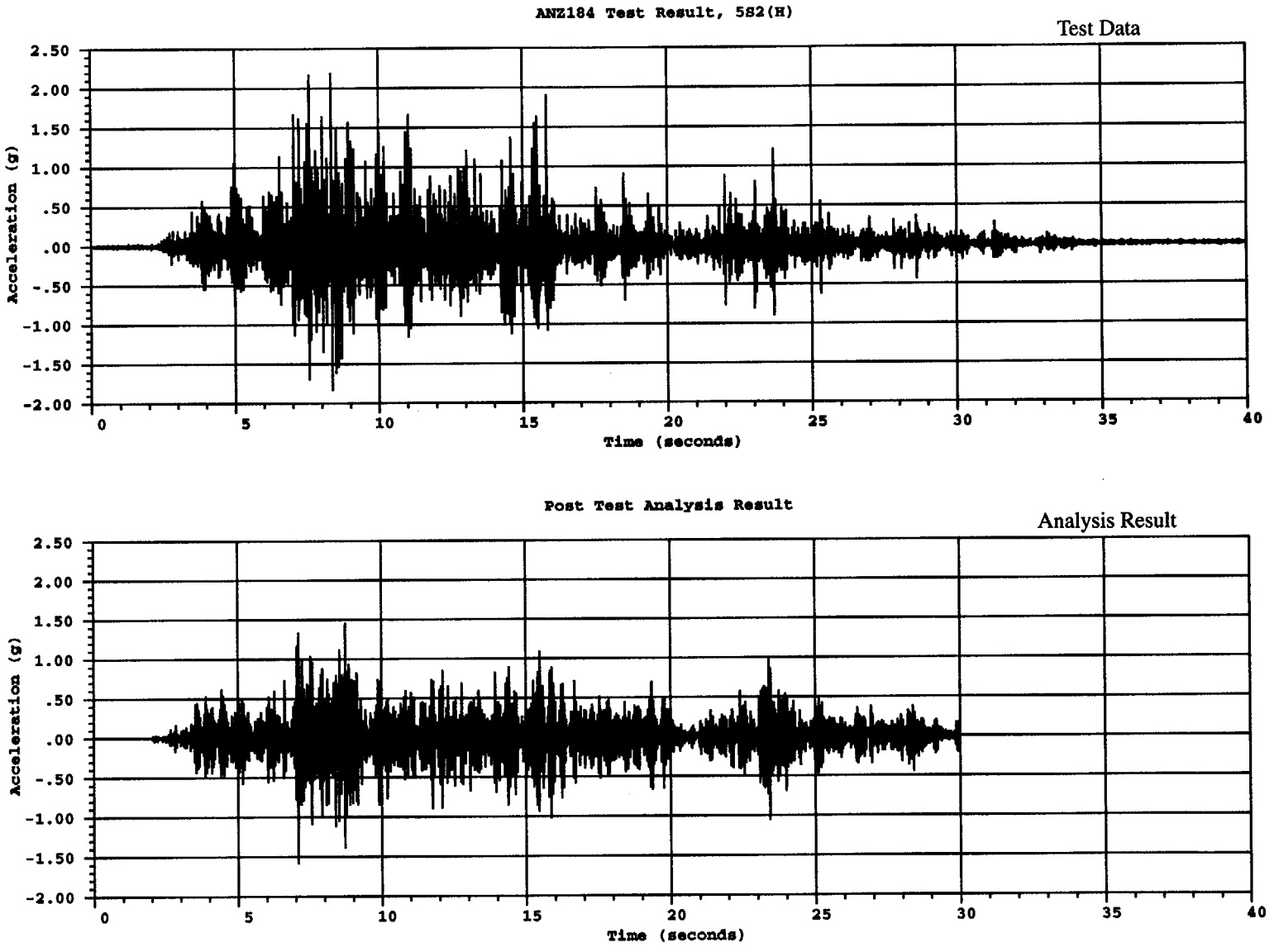

Figure 4.29 Comparison of vertical acceleration of top mass for 5S2(H) test

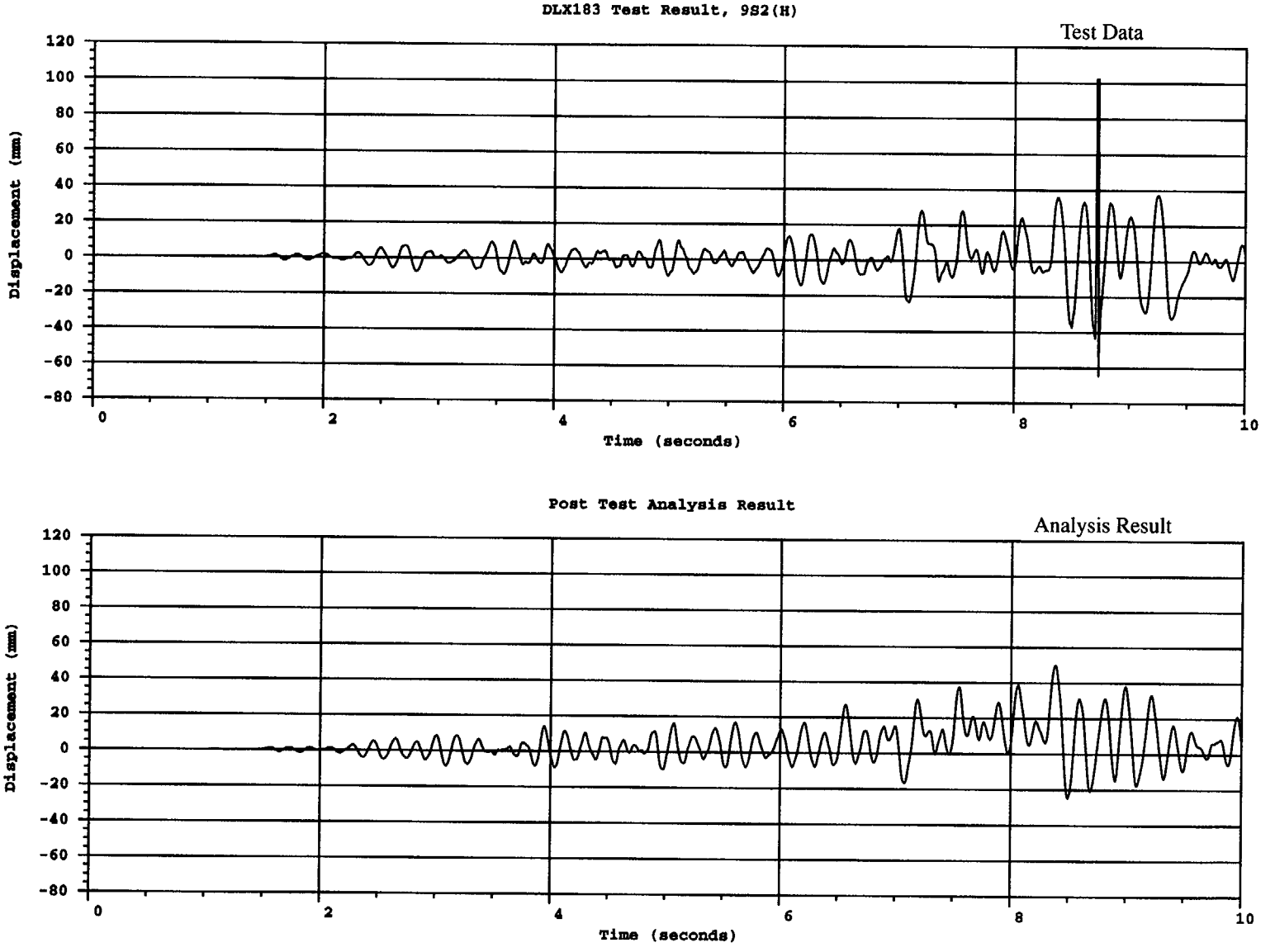

Figure 4.30 Comparison of horizontal displacement for top slab in 9S2(H) test

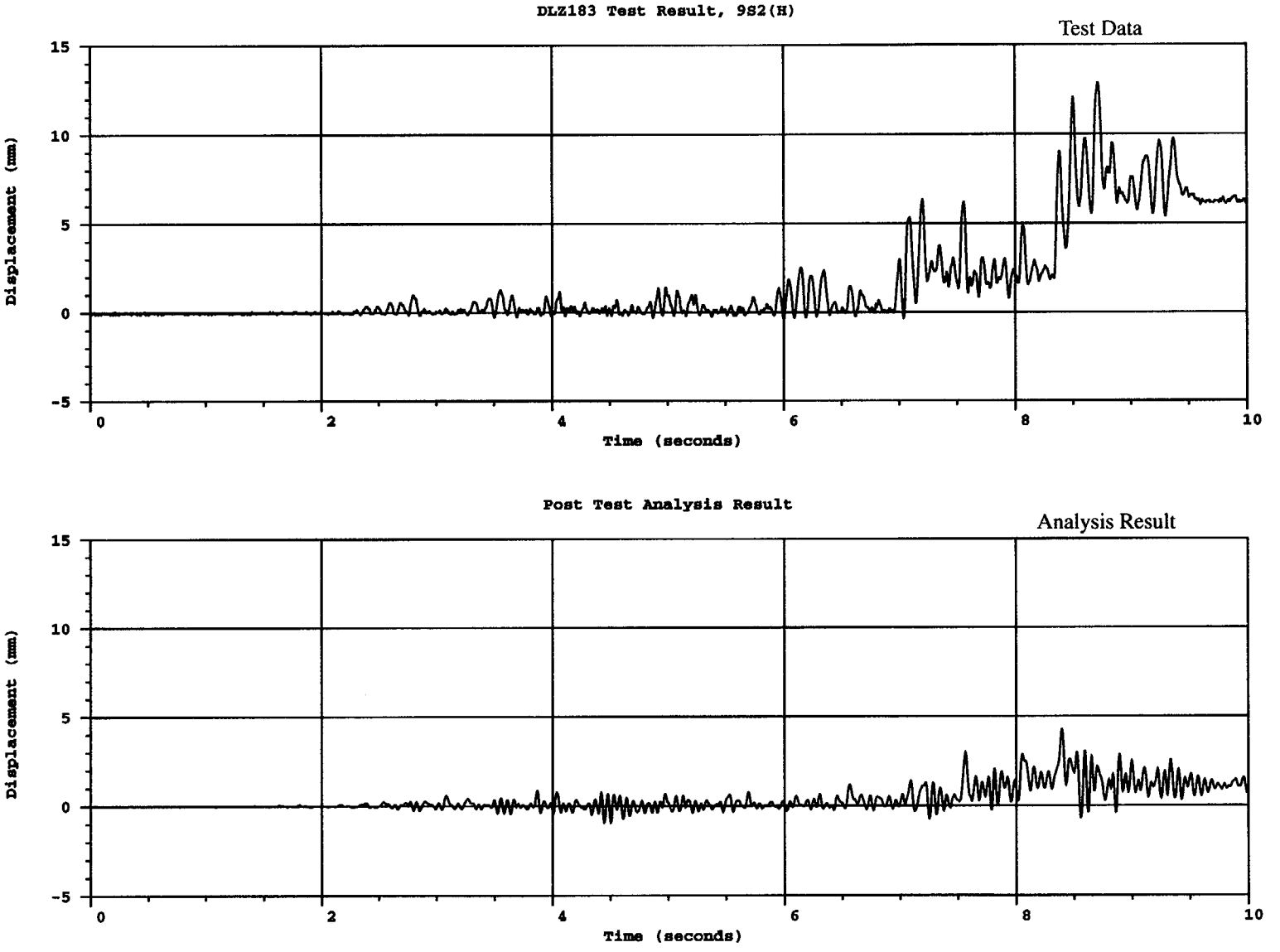

Figure 4.31 Comparison of vertical displacement for top slab in 9S2(H) test

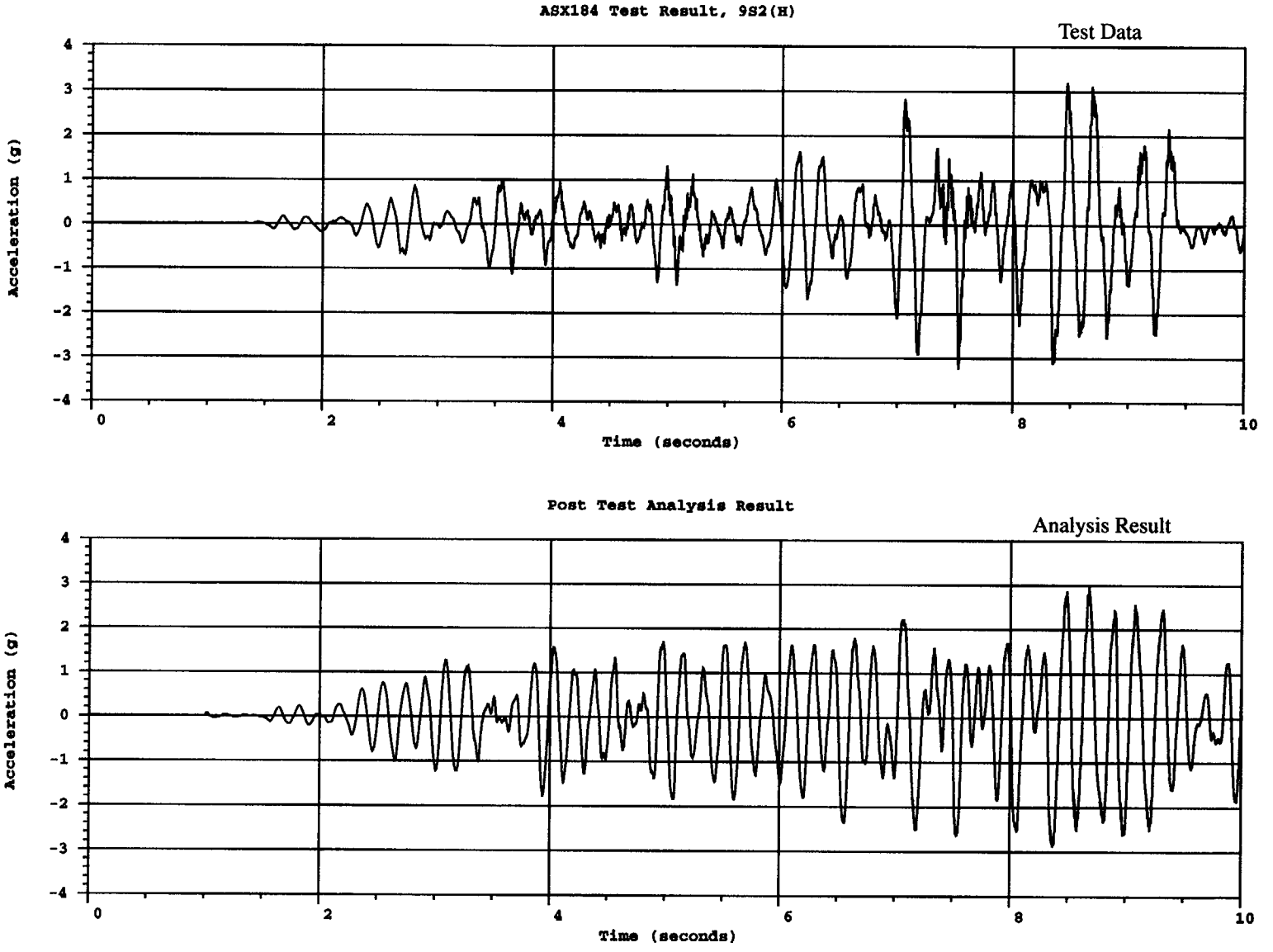

Figure 4.32 Comparison of horizontal acceleration for top mass in 9S2(H) test

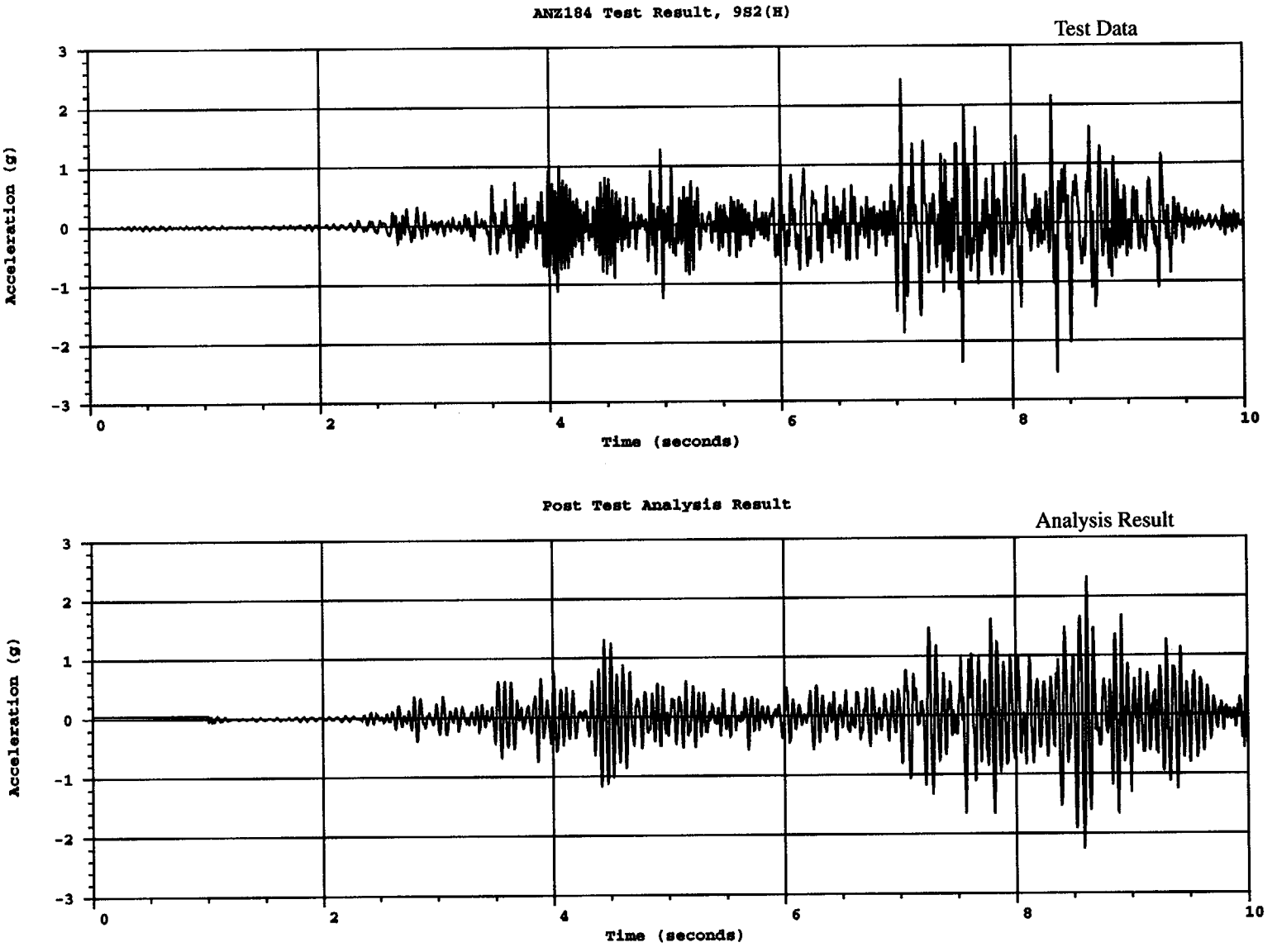

Figure 4.33 Comparison of vertical acceleration for top mass in 9S2(H) test

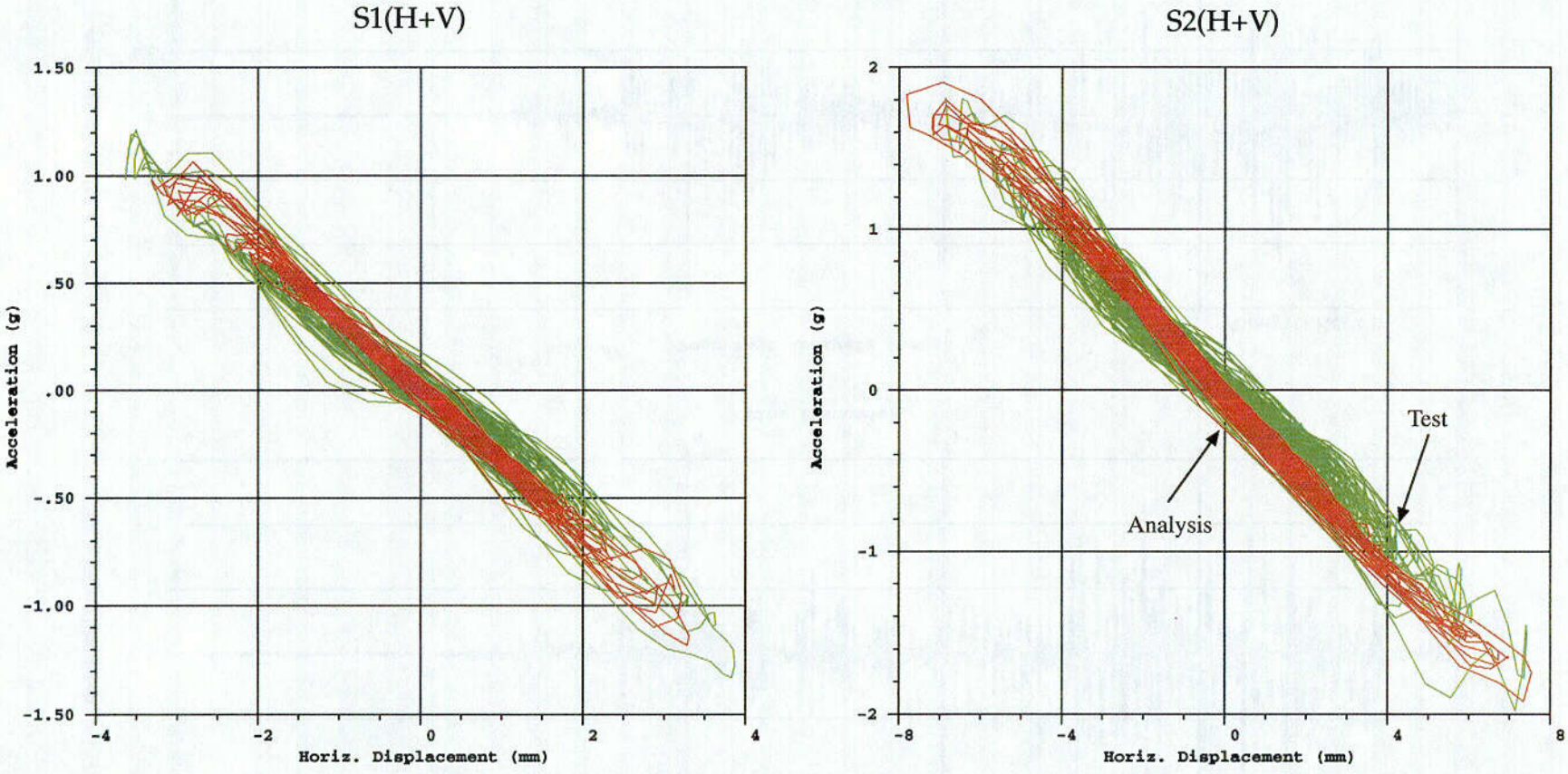

Green: Test
Red: Post-test Analysis

Figure 4.34 Comparison of acceleration at top mass vs. displacement at upper slab for S1(H+V) and S2(H+V)

C-18

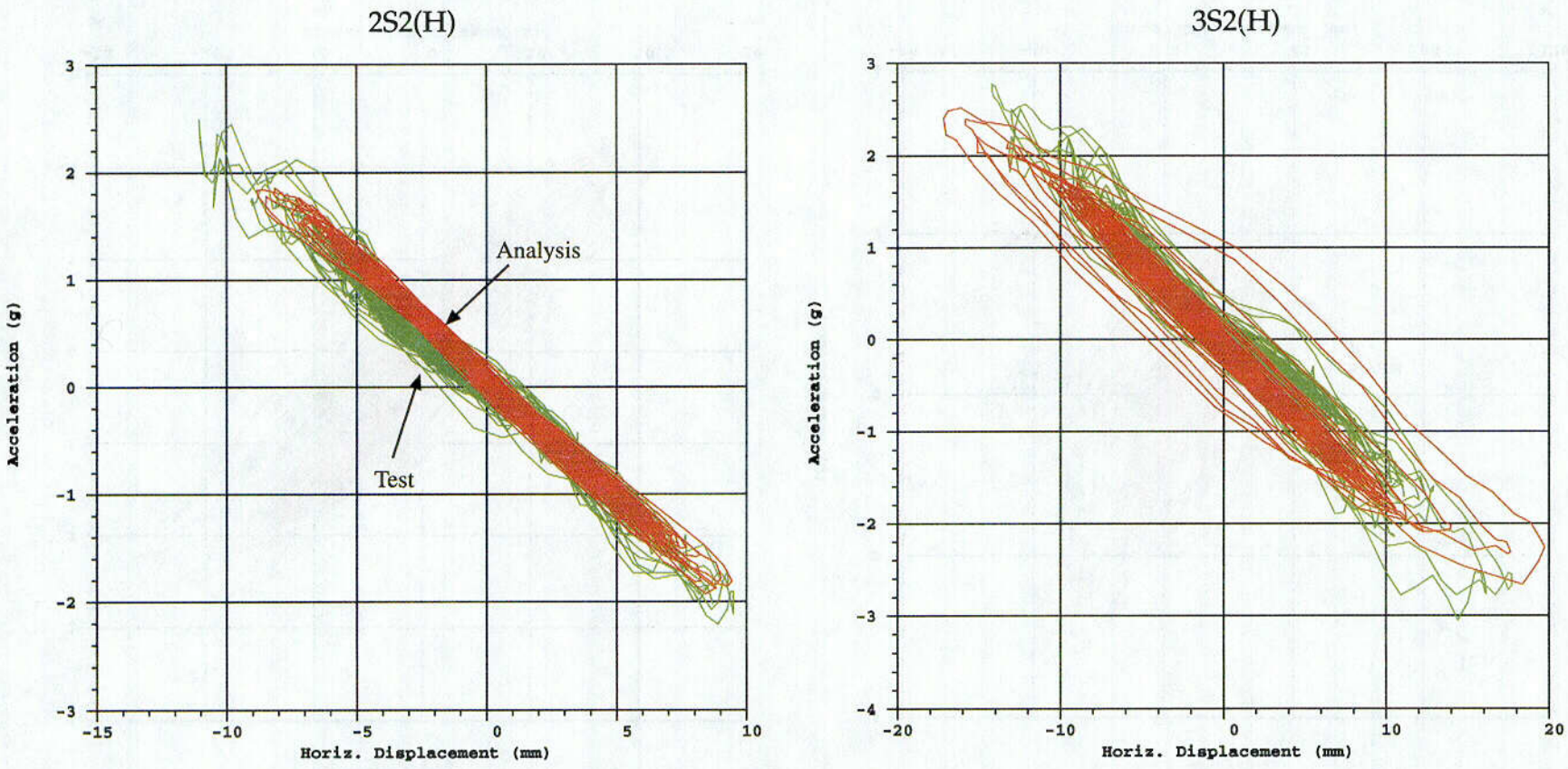

Figure 4.35 Comparison of acceleration at top mass vs. displacement at upper slab for 2S2(H) and 3S2(H)

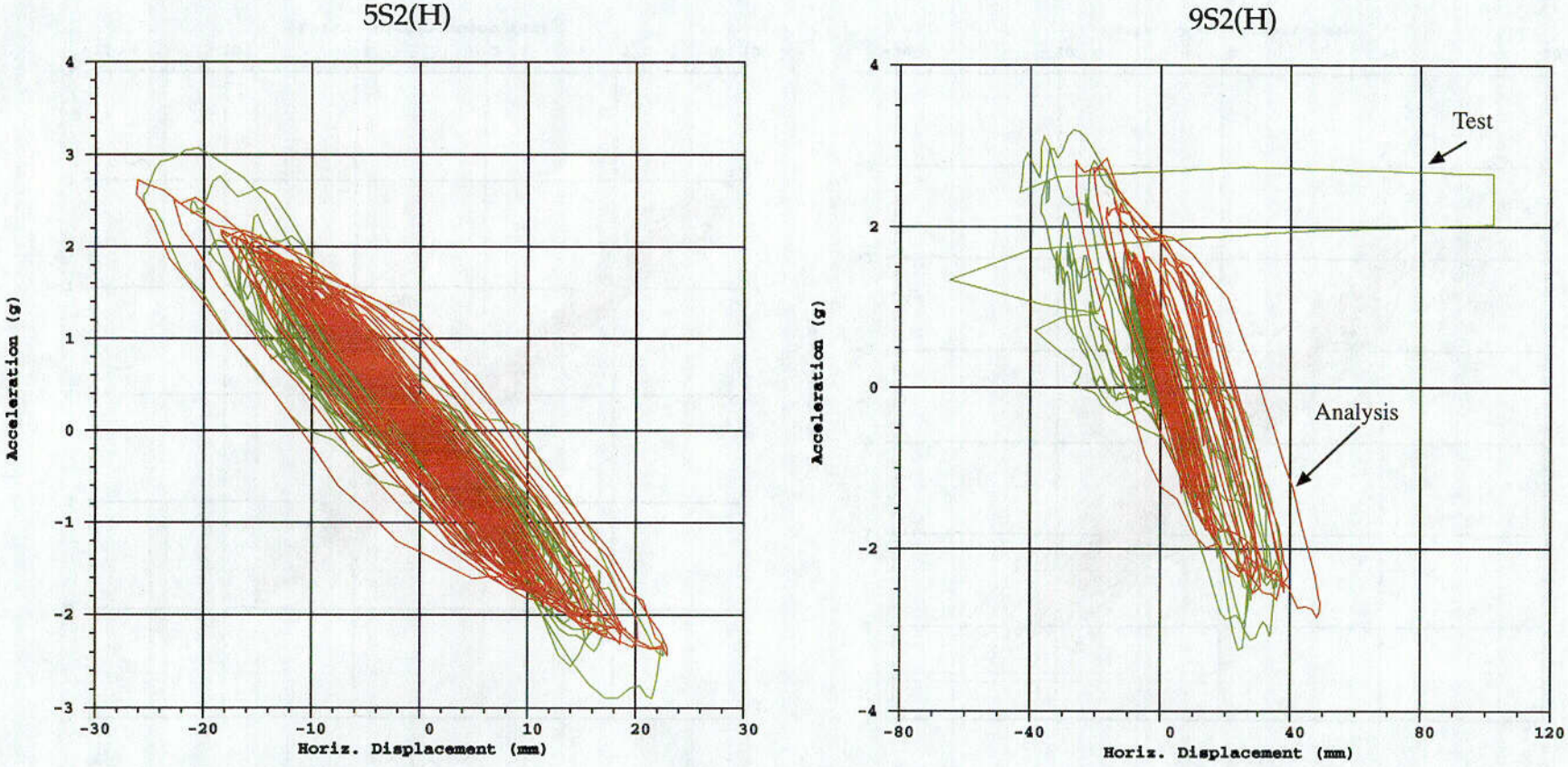

Figure 4.36 Comparison of acceleration at top mass vs. displacement at upper slab for 5S2(H) and 9S2(H)

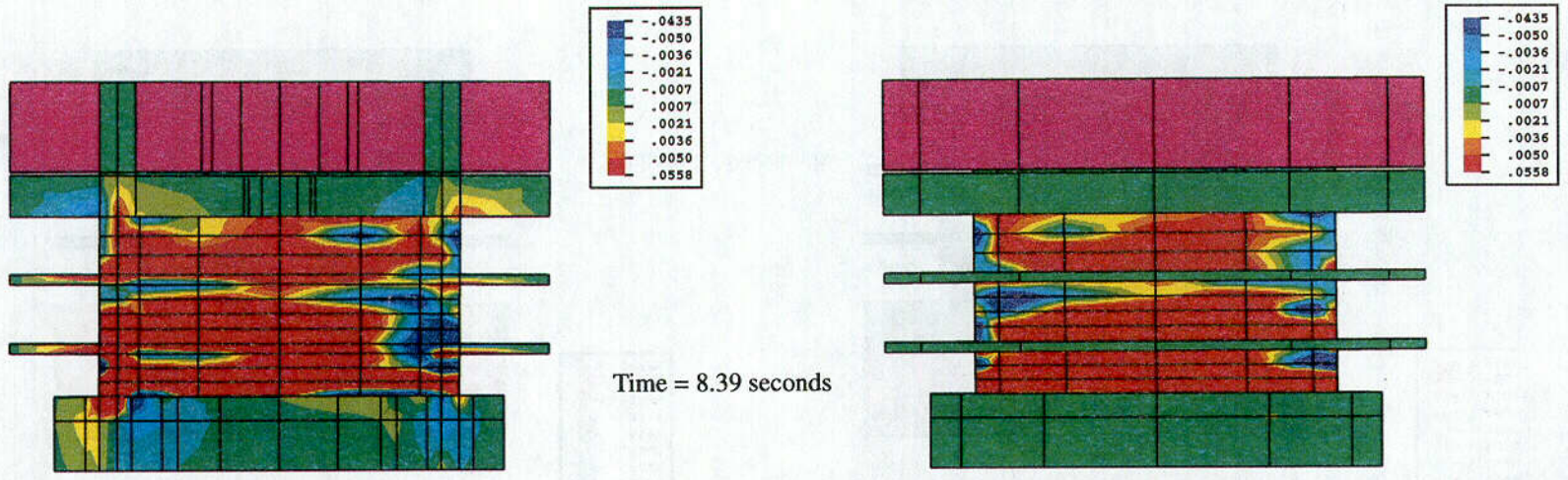

Figure 4.37 Concrete shear strain during peak response in test 3S2(H)

C-21

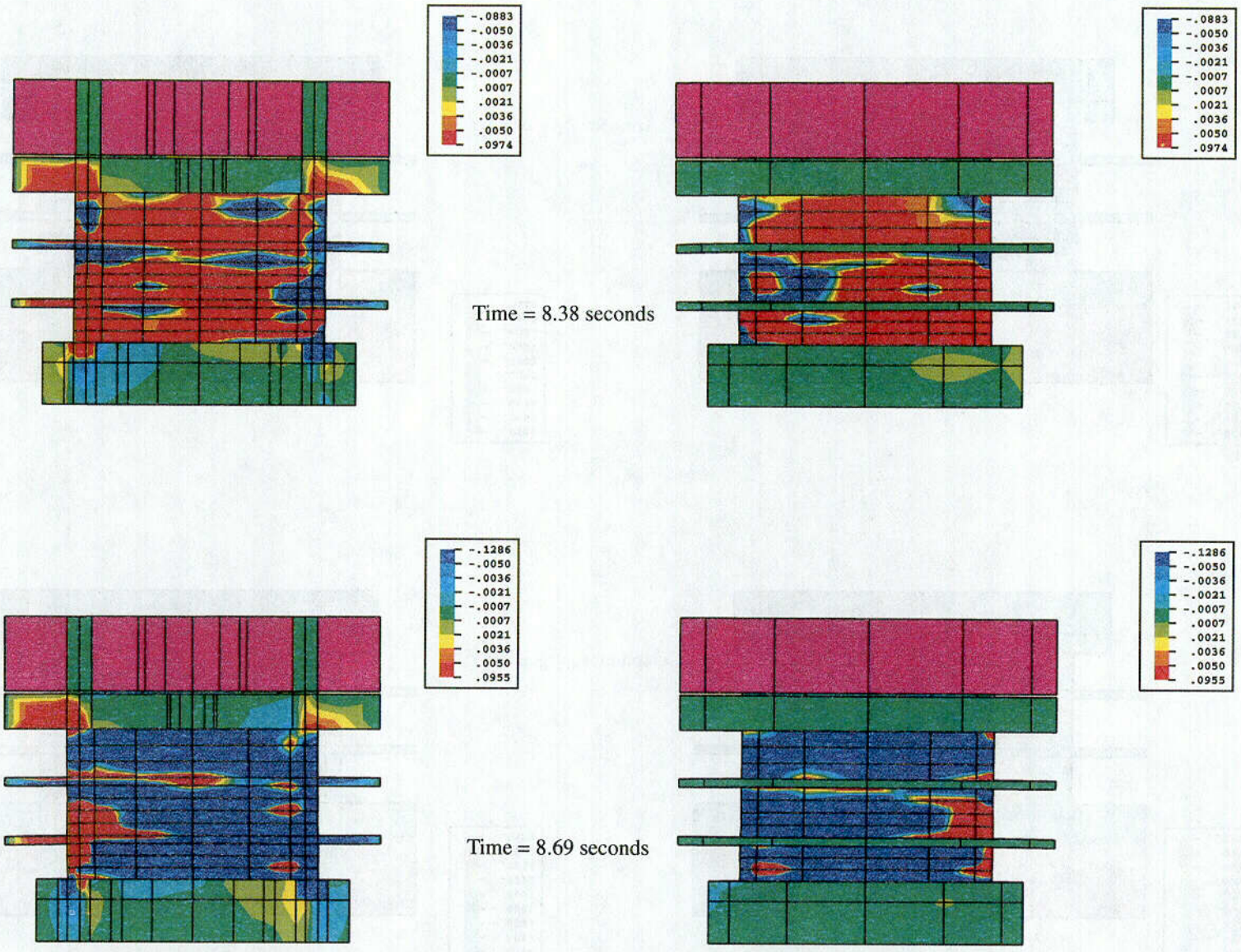

Figure 4.38 Concrete shear strain during peak response in test 5S2(H)

5. CONCLUSIONS AND RECOMMENDATIONS

5.1 Background

The NUPEC scale-model testing presents a unique opportunity to evaluate analytical methods by calculating seismic response of a model of a reinforced concrete containment vessel. Based on the test results, some very general qualitative assessments of the structural and functional integrity of a U.S. containment can be drawn. The RCCV tests consider a large-scale specimen with geometries representative of reinforced concrete containments and a broad range of seismic input from design-level test simulations through amplified motions leading to failure.

The response of the scaled test specimen is fully documented. Damage accumulates as the magnitude of seismic input increases, changes occur in the damping, and the fundamental frequency shifts. Posttest destructive examinations are also documented for levels and extent of damage through the structural sections and liner attachments.

The objective of the calculations reported herein focuses on the question, "Given a base acceleration input, can current analytical methods using detailed continuum modeling capture the seismic performance of reinforced concrete containment structures?" This section summarizes the lessons learned in this regard from the observations of the test itself, followed by a summary of the lessons learned from the analytical simulations. Final comments and recommendations are then presented.

5.2 Lessons Learned from the Testing

5.2.1 General Observations

Some very useful information can be gleaned from the test results independently of the analyses that have been reported. One observation is that, as expected, an internal design-level pressure test caused significant cracking in the concrete.

Perhaps the easiest measure of damage in the test model is the change in frequency and the change in the measured damping ratio. Before the pressure test, a low-level broad-band random vibration test was performed to measure the fundamental resonant frequency and the associated damping ratio. The measured frequency was 13.6 Hz, and the damping ratio was about 1%. After the pressure test, the low-level random vibration test was repeated, and the frequency had decreased by more than 1 Hz, while the damping ratio increased to about 1.5% damping. The cracks caused by the pressure test, but before the shaker table excitation, were mostly horizontal and vertical, and were mostly in the cylindrical section between the lower and upper ring walls (i.e., in the middle third of the vessel).

After the first S1(H) excitation, the low-level random vibration test measured a resonant frequency of about 9.5 Hz and a damping ratio of about 4.5%. After the S1(H+V) test was performed, the lowest resonant frequency had declined even further to about 8 Hz with a damping around 5%. These S1 level tests caused new horizontal and vertical cracks to appear, as well as new cracks oriented at $\pm 45°$. The 45° shear cracks were near the 0 and 180° locations, and were caused by the shear loads. The new horizontal cracks at 90 and 270° locations were caused by global bending as the containment rocked back and forth. Although the heaviest concentration of cracks was still in the middle third of the vessel, many new cracks were formed in the bottom third and top third of the vessel.

During the S2 series of tests, the lowest resonant frequency declined to about 7 Hz, and the damping approached 6%. The number of visible cracks on the concrete surface continued to increase, especially in the lower third section and the upper third section.

One very important observation about this S2 and all subsequent tests is that the energy content of the shaker table simulated earthquake is such that it excites maximum response for structures with resonant frequencies between 8 and 20 Hz. Based on response spectra curves, the input earthquake excited a smaller response for resonant frequencies below 8 Hz. Therefore, as the resonant frequency of the RCCV decreased below 8 Hz, the response acceleration of the RCCV began to decrease such that the same input time history would excite a smaller response in the structure than previous tests had. Looking at this another way, a larger earthquake time history would be required to excite the same level of response as had been measured in previous tests.

There are several other significant observations that can be made about the RCCV response during the S1 and S2 design-level series of tests. First and foremost is that the "design level" earthquakes caused significant damage to accumulate. The lowest resonant frequency

decreased from 13.6 Hz to 7 Hz, or about 50% reduction in frequency. Since frequency is equal to the square root of the stiffness (assuming the mass remains constant), this corresponds to a reduction in stiffness of about 75%.

The PCCV tests, on the other hand, experienced only minimal degradation to the stiffness during the S1 and S2 series of design-level tests. The primary difference between the PCCV and the RCCV tests is that the prestressing in the PCCV was sufficient to keep the concrete in compression and prevent significant concrete cracking from occurring during design-level tests. Therefore, the PCCV vessel experienced only a very small decrease in frequency, with an accompanying small increase in damping, while the RCCV was significantly affected.

The RCCV was also tested under simultaneous internal pressure and S1(H+V) earthquake loads. Extensive cracking had already occurred in the concrete from the previous S1 and S2 tests, and this combined test didn't cause a significant number of new cracks to develop, nor did the lowest resonant frequency or the damping ratio significantly reduce. Since damage accumulates as the tests progress, it is necessary to know which tests preceded the current test in order to understand the response. Eventually, at around 7 Hz, the model appears to reach a "saturation" point and further design level testing does not cause significant additional damage. If the tests had been performed in a different order, damage would have accumulated at different rates and locations. However, the vessel would have probably reached about the same "saturation" point, and the damage would be very similar at that point in time.

Considerable damage accumulated during the S1 and S2 "design-level" earthquakes, and the lowest fundamental frequency reduced significantly. After the S1 and S2 "design-level" tests were completed, the structure had significant cracking everywhere, but larger seismic loads didn't reduce the stiffness or frequency much more. This is attributed mainly to the reduced structural amplification that develops as the fundamental frequency of the structure shifts relative to the frequency content of the input, which does not change as the magnitudes are increased.

The seismic failure level of the vessel was determined by gradually increasing the earthquake excitations until the model failed. Although some new cracks developed under these "failure level" loads, the existing cracks also participated by absorbing energy under the cyclic loads as the cracks opened and closed.

During the 2S2(H) "failure level" event, damage continued to accumulate, but the maximum shear stresses were still below the peak shear stresses that occurred during subsequent testing. This indicates that additional reserve strength still existed, even though considerable damage was accumulating. The damping ratio, measured during low-level broad band random vibration tests before and after the 2S2(H) test, showed a damping of about 5.5 to 6.0%. However, the damping ratio during the 2S2(H) test, estimated based on transfer functions using 2S2(H) test data, showed a damping of about 7.6%. This is consistent, since the concrete cracks would open wider during the 2S2(H) test than during the low-level random vibration tests.

The 3S2(H) and larger earthquakes all resulted in peak shear stresses that were about the same magnitude, but the associated peak shear strains varied, depending on the simulated seismic event. Larger seismic accelerations caused larger shear strains. (The peak shear stresses were about the same for the 3S2(H), 4S2(H), 5S2(H), and 9S2(H) tests, but the shear strains were bigger in the higher-level excitations.) This indicates that the structure had little reserve strength left. However, the structure was able to absorb the energy of subsequent simulated earthquakes through concrete cracking, concrete crushing, steel yielding, and other cyclic dependent damage mechanisms.

Before and after the 3S2(H), 4S2(H), 5S2(H), and 9S2(H) tests, a low-level broad band random vibration test was performed, and the resonant frequencies and damping ratios of the vessel were estimated. All of the damping values during the random vibration tests ranged between about 5 and 6% damping. However, transfer functions of 3S2(H) data showed the damping during that test to be about 8.3%. Transfer functions of 4S2(H) test data show a damping ratio of 10.0%. During the 5S2(H) test, the damping was about 14.4%, and during the failure level 9S2(H) test, the damping was estimated to be 26.1%.

As damage accumulated, the effective damping level also increased, and this helped to offset the larger input acceleration levels. Also, as the tests progressed, the resonant frequency of the model decreased, and the earthquake excited a smaller response in the model. Both of these factors (the increasing amount of damping and the reduced response amplification for frequencies below 8 Hz) tended to partially offset the increase in acceleration levels.

The model, having withstood earthquake levels up to 5S2(H), indicated that a very comfortable seismic margin existed for the scaled model. The important point

is that the vessel remained structurally intact and was able to resist additional earthquake loads during the 2S2(H), 3S2(H), 4S2(H), and 5S2(H) tests. Although significant damage progressively accumulated in the model, catastrophic failure did not occur until the final 9S2(H) test.

5.2.2 Damping Performance

Damping as an energy-dissipation phenomenon is affected by local conditions and therefore must be treated accordingly in the finite element analysis. However, the damping value to be used in an analysis cannot be calculated, but rather is based on past experience and observations of similar structures. The amount of damping that exists, in either a real structure or in an analysis, significantly affects the magnitude of the structural response to the dynamic event.

For the scaled RCCV model, the observed damping ratio was about 1% until the concrete cracked early in the design-level test series. After cracking, the damping ratio was about 5%. For design earthquake level excitations, the damping stayed at about 5 to 6%. During the very large failure level tests, the apparent damping ratio became 8%, 10%, 15%, and was about 26% during the test where the structure failed. The structure does not behave in a linear manner. Cracks and other damage accumulate, which results in the hysteresis effects shown in Figures 4.34 to 4.36. Low-level vibration tests were conducted before and after each beyond-design-basis test to measure the response characteristics of the structure in the current state. At these low-levels of input motion, the scaled model had about 5% damping. The Japanese seismic design practice is to use a damping value of 5%, and the U.S. Practice is to use damping values of 4% and 7%.

Full-scale U.S. containments must address soil structure interaction issues, basemat uplift, the effect of numerous penetrations and piping connections, building-to-containment interactions, and other things that could affect the overall or "effective" damping ratio. The large lead weights that are bolted to the model, the flexibility of the shake table, and simplifications made to the model to separate the containment building from the surrounding structures may also have affected the overall damping of the model. Therefore, damping values in U.S. full-scale containments may be different than the damping values that were estimated from this test.

5.2.3 Liner Observations

Another useful piece of information that was gathered during this test concerns the functional integrity of the steel liner. The vessel was pressure tested after each major test and no significant tears or major leaks developed during the tests, even though the vessel accumulated considerable damage. It was not until the last 9S2(H) test, which caused large amounts of concrete to spall, that significant tearing of the liner occurred.

A complete concrete shear failure occurred in some sections of the cylindrical wall, and the resulting large displacements in the failed region caused the liner to tear in that area. In other areas, the concrete underwent large shear strains, and although the liner showed extensive shear buckling from plastic deformations, no significant tearing or fracture of the liner occurred. NUPEC performed tests on wall sections to investigate the effects of the mixed scaling used in their model and concluded that the mixed scaling effect was not significant for the particular containments they are evaluating.

Significant portions of the liner buckled under the large in-plane shear strains that occurred. It is important to note that the liner in the model was effective in maintaining leak-tight integrity under loads that were many times larger than those of the design earthquake.

There are many penetrations in a full-scale U.S. containment. In addition, the details of how the liner is anchored to the concrete vary between U.S. containments. These differences will affect the liner behavior in a full-scale containment. The analytical methods validated against the RCCV data can be used to assess the overall composite response of the liner and the concrete.

Buckling does not scale, and significant portions of the liner buckled under the large in-plane shear strains that occurred. Still, it is worthwhile to note that the liner in the model was extremely robust in preventing significant leaks under seismic loads that were many times larger than those of the design earthquake.

There are many penetrations in a full-scale U.S. containment. In addition, the details of how the liner is anchored to the concrete vary between U.S. containments. These differences, along with the issues discussed in the previous section, could cause the liner in a full-scale U.S. vessel to behave differently than was observed in the scaled model.

5.2.4 RCCV Integrity

The RCCV model accumulated considerable damage in the concrete and the liner, but it still maintained structural integrity and prevented significant leakage until the seismic loads were several times larger than the design requirements. The RCCV model tests have provided very good insights into the capacity and response of reinforced concrete structures during seismic events.

When performing scaled model seismic tests, mass does not scale proportionately with geometry. NUPEC selected scaling parameters of the model so that stresses and strains in the cylinder wall near the basemat would be similar to the stresses and strains that would exist in the full-scale vessel that the model represents. In a full-scale vessel, the largest shear stresses would be expected in the wall near the basemat, with the shear stresses at higher elevations decreasing in proportion to the total mass above the elevation point. Because of differences in the mass distribution, the shear stresses above the wall-basemat juncture would be different in the scaled model than in a full-scale vessel. Also, even after accounting for scale affects, there are still differences between frequencies, mode shapes, and the structural response of the scaled model and the full-scale vessel.

Failure occurred in the model at mid-height and also in the wall near the basemat, which are likely places for failure in a full-scale U.S. containment. Although a full-scale U.S. containment would likely fail near the basemat or around a large equipment hatch penetration, differences discussed in the previous sections will affect the response of a full-scale U.S. containment. Therefore, one must not predict the capacity of a full-scale U.S. containment by extrapolating the results from this scaled-model test.

Failure occurred in the model at mid-height and also in the wall near the basemat, which are likely places for failure in a full-scale U.S. containment. There are also other likely failure modes of interest in a full-scale U.S. containment, such as, around a large equipment hatch penetration. The analytical methods, which have been validated against the RCCV model test data, can now be applied to assess the complete response and failure locations of U.S. containments.

5.3 Lessons Learned from Analytical Modeling

The following observations are summarized as lessons learned from analytical modeling of reinforced concrete containment structures under seismic loading (James et al., 1999b; 2000)[d].

The static pushover capacity may not be a true indication of the seismic capacity of the structure. This conclusion is a function of both the level of the modeling used and the nature of the static pushover analysis relative to the seismic event. For the level of modeling and material characterization used herein, the structure's ultimate capacity determined in a static pushover analysis is an upper bound on the seismic capacity. The true seismic capacity is reduced because of cyclic degradation, which affects the characteristics of shear transfer across cracks and rebar bond strengths. In addition, the structure will behave differently during a static pushover analysis than it would during a seismic event. For example, if the structure responds in such a way that higher bending modes contribute to the structural response, the associated structural damage can affect the capacity of the sliding shear mechanisms that a static pushover may emphasize. Static pushover analysis is a good tool for evaluating response characteristics, and knockdown factors or reduced material capacities based on cyclic degradation could be used for estimating seismic capacities. However, the knockdown factor must be calibrated for specific models and for static pushover demands relative to seismic structural response. The latter could be tabulated as functions of modal participation relative to seismic response spectra.

Structural damping can be a critical parameter for these types of nonlinear calculations. Too little damping can develop excessive response in the analysis leading to excessive cracking. Because of the progressive nature of cracking damage, excessive cracking can lead to structural frequency shifts that may alter the general response of the structure for a given frequency content of the seismic input. On the other hand, too much damping in the analysis will underpredict the structural response and possibly inhibit cracking. Damping can be modeled in a cracking consistent manner to reduce the errors associated with using a constant damping value. There is a nominal uniform structural damping,

[d] James, R. J., L. Zhang, and Y. R. Rashid, *Seismic Proving Tests on a Reinforced Concrete Containment Vessel-Pretest Analytical Predictions*, ANA-98-0246 Report to Sandia National Labs, 1998b.

in this case about 1%, that is attributed to microcracking, voids, construction joints, and other energy dissipation mechanisms that are below the refinement of a finite element model. As concrete cracking develops, increased local damping occurs at the crack surfaces. Thus, structural damping should increase as cracks develop that is consistent with the level and extent of cracking. During periods of increased response leading to cracking, the use of a nominal level of uniform damping will over-predict cracking. On the other hand, the use of an increased uniform damping that is likely to be reached at the end of the event can inhibit cracking and underpredict the true response. In addition, especially for RCCV structures, the damping is cyclic dependent. Because the structural stiffness also degrades significantly with load cycles for the RCCV, the damping levels reached are significantly higher than for PCCV structures.

A robust and well-qualified material model is needed for these calculations. It must be robust in the sense that stable algorithms are required for extensive levels of damage. It must be well-qualified in the sense that post critical relations and interaction between all damage and failure mechanisms and resistance paths are important. For example, crack development must be followed by cyclic opening and closing and shear transfer relations. The shear stiffness along crack faces, the compressive stiffness normal to cracks, and the associated damage dependent damping must depend on the magnitude and number of load cycles.

Modeling of all structural components is important for determining ultimate capacities. However, extremely fine grids and detailed modeling of all structural connections are not necessary to establish good estimates of global response even near failure-levels of response. Evaluations of mesh density, element types, and various levels of modeling details did not show significant sensitivity for global response in the analyses. Increasing levels of modeling details are needed if local effects such as liner anchorage performance are of interest. Good estimates for general magnitudes of reinforcing steel and liner strains should be expected from these types of calculations, but local gradients may also exist because of local concrete damage. Averaged values from several nearby integration points might be considered for evaluation purposes.

Obviously, definition of the input acceleration component history is an important parameter for these analyses. In real applications, the structural response will not affect the seismic event that is loading the structure, so structural feedback is not a concern. However, all modes of structural response to a given seismic loading must be considered. For example, if basemat rocking on the foundation can develop, it should be accounted for using some type of soil structure interaction modeling. As demonstrated in the design-level simulations, basemat rocking can increase or decrease the relative response in the RCCV depending on the level and frequency of the input.

It is concluded that nonlinear, continuum-level modeling can be used for verification of design calculations for seismic response of reinforced concrete containment structures. For reinforced concrete containments, concrete cracking and damage is likely in design level events. For linear elastic analysis methods typically employed for design based calculations, the effects of cracking on stiffness and frequency shift must be addressed. Because of the progressive nature of concrete cracking, once cracking initiates it can spread and significantly alter the response from the linear assumptions. The benefit of nonlinear calculations is to provide a verification that the cracking induced during a design-level event does not lead to progressive deterioration. The design-level RCCV tests show that the cracking did not compromise the structural integrity for this case. The design-level calculations verified that cracking induced during the design-level seismic loading does not compromise the performance of the structure. A continuum-based nonlinear analysis may be a good verification that the correct frequency shift is being considered in the linear analysis.

To reduce the uncertainties about the structural seismic margin of a RCCV, these nonlinear continuum-based calculations would appear to be a useful tool. The failure-level calculations provided good correlation with test data for the RCCV scale model. The progressive levels and extent of damage can be simulated with good overall response characteristics. While the calculations could not explicitly trigger the shear failure with a numerical instability, the conditions needed for the sudden shear failure are present in the calculations at the right time and location. A proposed failure criterion for the calculations is established and can be determined currently by post-processing the calculations as they proceed.

5.4 Recommendations

5.4.1 Develop Fragility Curves for a Typical U.S. Containment

The NRC is moving towards a "risk informed, performance based" environment for U.S. nuclear power plants. Therefore, future evaluations of U.S. contain-

ment structures need to incorporate probabilistic methods that can provide important risk insights.

Parameters such as damping and material properties are not exactly known, and the variability in the assumed values can have a significant influence on predicted results. For example, the concrete shear strength varies as a function of its measured compressive strength, confining pressures, and size and location of cracks, and is not well defined.

Perhaps even more important than these parameters that cause uncertainty in predicted behavior is the fact that actual earthquake loadings are not known. For example, two earthquake records with the same peak acceleration but different frequency content could cause a structure to respond quite differently, or a design-level earthquake may be assumed to occur while the vessel is under internal design pressure caused by a LOCA.

In order to gain risk insights into U.S. containment vessels, the sensitivity of the structure to various parameters that are uncertain (e.g., damping, material properties, or seismic loading) must be understood. Although the absolute values of these parameters are uncertain, a realistic distribution of possible values can be defined, and sensitivity studies can show how these uncertainties affect the structural integrity and seismic margins of U.S. containments. These types of studies can account for significant uncertainties in the design assumptions and verify the integrity of the containment during design-level seismic events. In addition, the seismic capacity and safety margins can be predicted after accounting for uncertainties.

5.4.2 Improve Ability to Predict Leak Tightness of Liner

Somewhere between design-level integrity verification and seismic capacity evaluation is the need for evaluation of the leak-tightness of the liner during seismic events. The analyses that have been performed for the scaled model tests did not have sufficient detail to predict local liner tearing.

The liner thickness and anchorage system in the scaled model RCCV was 2.5 times the relative scale of a full-scale RCCV wall thickness, and this may have affected liner tearing. Although local tearing did not occur in the scaled model until after the structure failed in shear, differences such as liner anchorage details or thickened insert plates could result in stress concentrations and liner tears in a full-scale U.S. containment.

During static overpressurization tests on scaled reinforced concrete containment models, liner tearing has occurred under conditions of relatively low global plastic strain response in the liner (Dameron et al., 1998)[e]. This is because of strain concentrations that exist at anchorage connections or that can develop near areas of concrete damage. The pressurization tests, which were done in the 1980s, demonstrated that liner tearing leading to depressurization (leak before break) can occur for global liner strains around 1%. The liner tears occur at thickness discontinuities at penetrations and anchorages where concentration factors of 10–20 can develop.

While the liner did not develop significant tears or leaks up to structural failure for the seismic tests on the RCCV model, the question of liner integrity must be addressed for full-scale U.S. containments. Very detailed local models of penetrations and liner connections could be used to determine strain concentration factors for typical prestressed concrete containment liner configurations under dynamic loading. These tabulated strain concentration factors could then be applied to the strain response calculated from the type of global model used herein to evaluate liner integrity under seismic loads.

5.4.3 Add "Shear Shedding" Capability to Concrete Material Model

A material model for shear shedding in concrete could be developed. This model would define shear stress capacity as a function of shear strain to better simulate the shear shedding material behavior. For increasing levels of shear strain, the capacity to carry shear stress would diminish, leading to numerical failure when the structure is unable to resist the shear loads. This model is complicated by the interaction with crack opening strain, which determines the shear stiffness along the crack. Confinement and cyclic degradation effects may also need consideration. Because of the lack of material test data for shear shedding and the difficulty in developing such data, it is proposed that the material model be "reverse engineered" from the available structural test data. Such a material model could be iteratively constructed and verified against the structural shear failure in the NUPEC shear wall, PCCV, and RCCV tests, as well as other tests.

---

[e] Dameron, R. A., R. S. Dunham, Y. R. Rashid, and M. F. Sullaway, *Analysis of the Sandia One-Sixth-Scale Reinforced Concrete Containment Model,* Electric Power Research Institute, EPRI NP-6261, 1989.

6. REFERENCES

Dameron, R. A., Y. R. Rashid, and M. F. Sullaway, *Pretest Prediction Analysis and Posttest Correlation of the Sizewell-B 1:10 Scale Prestressed Concrete Containment Model Test,* U. S. Nuclear Regulator Commission, NUREG/CR-5671, 1998.

Hibbitt, D., *ABAQUS: Standard User's Manual, Version 5.6 and 5.8*. Hibbitt, Karlsson, and Sorensen, Inc., Pawtucket, R.I. 1997.

James, R. J., L. Zhang, Y. R. Rashid, and J. L. Cherry, *Seismic Analysis of a Reinforced Concrete Containment Vessel Model,* U. S. Nuclear Regulator Commission, NUREG/CR-6639, 1999a.

James, R. J., Y. R. Rashid, J. Cherry, N.C. Chokshi, S. Nakamura, "Analytical Prediction of the Seismic Response of a Reinforced Concrete Containment Vessel," *Proceedings of the 15th International Conference in Structural Mechanics in Reactor Technology,* Seoul, Korea, 1999b.

James, R. J., Y. R. Rashid, J. L. Cherry, and N. Chokshi, *Seismic Analysis of a Reinforced Concrete Containment Vessel Model,* ICONE-8, Baltimore, MD, 2000.

Raphael, J. M., "Tensile Strength of Concrete," *ACI Journal,* 81–17, March – April, 1984.

Rashid, Y.R. "Ultimate Strength Analysis of Prestressed Concrete Pressure Vessels," *Nuclear Engineering and Design,* 7, 334–344, 1968.

Sasaki, Y. S. Tsurumaki, H. Akiyama, K. Sato, and H. Eto, *Seismic Proving Test of a Prestressed Concrete Containment Vessel,* ASME/JSME Joint PVP Conference, San Diego, CA, 1998.